ARO
The Scientific Journal of Koya University
Volume 5 | Number 2 | December 2017

Aro is an open access journal got DOAJ seal and has been accepted for indexing in the Emerging Sources Citation Index (ESCI), a new edition of Web of Science™ - Clarivate Analytics (Thomson Reuters) since Feb 2016.

Issue Highlights

SYNTHESIS AND CHARACTERIZATION OF SODIUM DIPHENYLCARBAMODITHIOATE LIGAND [L] AND ITS COBALT, NICKEL, AND COPPER COMPLEXES
Page 1

A COMPARATIVE STUDY FOR STRING METRICS AND THE FEASIBILITY OF JOINING THEM AS COMBINED TEXT SIMILARITY MEASURES
Page 6

INTEGRATED USE OF GEOELECTRICAL RESISTIVITY AND GEOCHEMICAL ANALYSIS TO ASSESS THE ENVIRONMENTAL IMPACT ON SOIL AND GROUNDWATER AT ERBIL DUMPSITE, WEST OF ERBIL CITY - IRAQI KURDISTAN REGION
Page 19

FACTORS CONTROLLING THE DEVELOPMENT OF STRAIGHT VALLEYS AND STREAMS IN THE KURDISTAN REGION, NORTH AND NORTHEAST OF IRAQ
Page 32

THERMODYNAMIC EXCESS PROPERTIES AND INTERMOLECULAR INTERACTION USING FOURIER TRANSFORM INFRARED FOR THE DODECYLBENZENESULFONIC ACID-ACETONE BINARY LIQUID MIXTURE
Page 49

TWO NEW RECORDS OF ORCHID SPECIES FOR THE FLORA OF IRAQ: ANACAMPTIS PAPILIONACEA (L.) R.M. BATEMAN, PRIDGEON & M.W. CHASE AND DACTYLORHIZA ROMANA (SEBAST.) SOÓ
Page 55

THERMAL EFFECTS ON COMPRESSIVE STRENGTH OF LOCAL LIMESTONE AND CLAYSTONE
Page 61

THREE-DIMENSIONAL IMAGE SEGMENTATION USING TISSUE-LIKE P SYSTEM
Page 67

ARO DOI: 10.14500/2307-549X

KOYA UNIVERSITY

ARO-The Scientific Journal of Koya University

The Aro ("Today" in Hewramí Kurdish), is an international scientific journal published by the Koya University with p-ISSN: 2410-9355, e-ISSN: 2307-549X and DOI: 10.14500/2307-549X. Aro is a journal of original scientific research, global news, and commentary. The Aro Scientific Journal is a peer-reviewed, open access journal that publishes original research articles as well as review articles in all areas of Science.

ARO the Scientific Journal Office

Koya University, University Park
Danielle Mitterrand Boulevard, Koya KOY45
Kurdistan Region - F.R. Iraq

Tel.: +964 (0) 748 012 7423
Mobile: +964 (0) 750 187 5489
E-mail: aro.journal@koyauniversity.org
url: aro.koyauniversity.org

December - 2017 | Befranbar - 2717

ARO

The Scientific Journal of Koya University

Vol V, No 2(2017)

Contents

Aro Editorial Words ……...……... iii

Eman I. Alsalihi, Aeed S. Al-Fahdawi, Bashdar I. Meena ……..……..……...…… 01
Synthesis and Characterization of Sodium Diphenylcarbamodithioate Ligand [L] and its Cobalt, Nickel, and Copper Complexes

Safa S. Abdul-Jabbar, Loay E. George ……..……..…….…… 06
A Comparative Study for String Metrics and the Feasibility of Joining them as Combined Text Similarity Measures

Sirwa Q. Gardi …..……..……..…… 19
Integrated Use of Geoelectrical Resistivity and Geochemical Analysis to Assess the Environmental Impact on Soil and Groundwater at Erbil Dumpsite, West of Erbil
City - Iraqi Kurdistan Region

Varoujan K. Sissakian, Ahmed T. Shihab, Arsalan A. Othman ……...…… 32
Factors Controlling the Development of Straight Valleys and Streams in the Kurdistan Region, North and Northeast of Iraq

Ali A. Jazie ……..……..…… 49
Thermodynamic Excess Properties and Intermolecular Interaction Using Fourier Transform Infrared for the Dodecylbenzenesulfonic Acid-Acetone Binary Liquid Mixture

Sami M.A. Youssef, Honar S. Mahdi, Zerevan A. Mergye, Jihad I. Salim, Ahmed M.H.M. Mahmood, Errol Vela ……..…… 55
Two New Records of Orchid Species for the Flora of Iraq: Anacamptis papilionacea (L.) R.M. Bateman, Pridgeon & M.W. Chase and Dactylorhiza romana (Sebast.) Soó

Rahel K. Ibrahim, Nawzat R. Ismail, Hemn M. Omar ……..……..…… 61
Thermal Effects on Compressive Strength of Local Limestone and Claystone

Salah I. Yahya, Rafaa I. Yahya, Bisan Al-Salibi, Ghada K. Al-Khafaji, Siti Mariyam Shamsuddin ….... 67
Three-dimensional Image Segmentation using Tissue-like P System

General Information ……..……..…… 75

Guide to Author ……..……...…….. 76

Aro Reviewer/Associate Editor Application Form …….. 78

♦♦♦

DOI: 10.14500/2307-549X ARO p-ISSN: 2410-9355, e-ISSN: 2307-549X

ARO p-ISSN: 2410-9355, e-ISSN: 2307-549X DOI: 10.14500/2307-549X

ARO Editorial Words

Dear readers, Aro-the Scientific Journal of Koya University is closing its ninth issue (Vol V, No 2, 2017) after an exciting yet dynamic season of valuable inputs by our research community and supportive reviewers. Aro is publishing its 4th issue as an internationally listed Scientific Journal in Kurdistan Region of Iraq. Notably, Aro has been accepted for indexing in the Emerging Sources Citation Index (ESCI), a new edition of Web of Science™ as of Feb 2016. Content in this index is under consideration by Thomson Reuters to be accepted in the Science Citation Index Expanded™ (SCIE). Aro's individual articles are currently listed by Thomson Reuters using articles unique DOI numbers which is a historical achievement for our academic community. Aro is ending its fifth year journey in leading the quality of regional scientific publications with global impact. The editorial team has been working tirelessly to keep the novel mission and sustain Aro's future publications with greater impacts and citations. It is exciting that Aro has been awarded to DOAJ Seal listing which is an indication of a trusted high standard open access scientific work that so far haven allocated to 88 journals worldwide only. The upcoming new season will be an even more exciting period in Aro's life as Thomson Reuters will examine our journal for full permanent listing.

Despite all ongoing regional conflicts and economic downturn which still having a great impact on scientific research activities and funding of the regional universities in general and Koya University in particular, Aro is continuing to receive great numbers of well-motivated quality papers which shows its steadily growing trust among researchers in the region, demanding the increased volume of publication. Nevertheless, Aro is finding more focus in applied sciences with research values in current regional issues having International impacts.

Aro was created with long-term visions of becoming accessible to all researchers in Kurdistan and beyond, and covering a wide range of scholarly disciplines in sciences. Aro is a peer-reviewed, open access journal that publishes original scientific research, global news, letters and commentary as well as review articles in areas of natural sciences and technology. In this issue you will have access to original research papers in variety of areas, such as Physics, Biochemistry, Materials Science and Petroleum, Chemical and other fields of Engineering.

The great responses from researchers, academics and professionals in the last five years have made us to create a wider Editorial Board which serves the wider submitted scientific manuscripts. However, it is clear that having a dedicated and well organised editorial board for the journal is only one side of the coin. The other is the ability to attract submissions of quality research and scholarly work. We are thankful to all of those who put their trust in Aro and presented their original research work for publication in Vol V, No 2 (2017) of the journal, as well as, our thanks are extended to the 16 peer-reviewers from the Universities worldwide for their efforts in reviewing and enabling this issue of Aro.

Your support and feedback are invited and appreciated.

Dilan M. Rostam
Editor-in-Chief

Wali M Hamad
Executive Publisher

Dilan M. Rostam, Salah I. Yahya, Basim M. Fadhil, Fahmi F. Muhammad, Mohammed H.S. Zangana, Jorge Correia and Fouad Muhammad
Executive Editorial Board

DOI: 10.14500/2307-549X ARO p-ISSN: 2410-9355, e-ISSN: 2307-549X

Synthesis and Characterization of Sodium Diphenylcarbamodithioate Ligand [L] and its Cobalt, Nickel, and Copper Complexes

Eman I. Alsalihi[1], Aeed S. Al-Fahdawi[2] and Bashdar I. Meena[1]

[1]Department of Chemistry, Faculty of Science and Health, Koya University, Daniel Mitterrand Boulevard, Koya KOY45, Kurdistan Region - Iraq

[2]Department of Chemistry, College of Education for Women, University of Anbar, Ramadi, Anbar - Iraq

***Abstract*—A correlation of the infrared (IR) spectra of thiocarbonyl derivatives based on the literature data has been carried out. Assignments have also been made in some new systems. Sodium diphenylcarbamodithioate ligand and its monomeric complexes were synthesized at room temperature and stirring condition. The ligand and its complexes of the general formula $[M(L)_2]$ (where M=Co^{II}, Ni^{II}, and Cu^{II}) were characterized by spectroscopic methods (IR and ultraviolet-visible), elemental analysis (CHN and S) metal content, magnetic susceptibility measurement, and biological activity (an antibacterial activity of the complex was studied by agar disc diffusion method and minimum inhibitory concentration strain against *Staphylococcus aureus* and *Bacillus subtilis*). The complex exhibited significant activities against *S. aureus and B. subtilis*, thin-layer chromatography, mass spectrometry, X-ray powder diffraction, and molar conductance. Our study revealed the formation of four-coordinate square planar complexes around Co^{II}, Ni^{II}, and Cu^{II} metal ions.**

***Index Terms*—Diphenylcarbamodithioate complexes, Four-coordinate square planar complexes, Sodium diphenylcarbamodithioate ligand, Structural study.**

I. Introduction

Diphenylamine is an organic compound with the formula $(C_6H_5)_2.NH$. The compound is a derivative of aniline, consisting of an amine group bounded with two phenyl groups. The compound is a colorless solid, but commercial samples are often yellow due to oxidized impurities (Vogt and Gerulis, 2005). Diphenylamine dissolves well in many common organic solvents and is moderately soluble in water (Canady, et al., 2013). It is used mainly for its antioxidant properties. It is used as scald inhibitor for apples applied as an indoor drench treatment. Its anti-scald activity is the result of its antioxidant properties, which protect the apple skin from the oxidation products during storage scald (or "apple scald") as physical injury that manifests in brown spots after fruit is removed from cold storage (Ingle and D'Souza, 1989). Carbon disulfide (CS_2), also called carbon bisulfide, a colourless, toxic, highly volatile and flammable liquid chemical compound, large amounts of which are used in the manufacture of viscose rayon, cellophane, and carbon tetrachloride; smaller quantities are employed in solvent extraction processes or converted into other chemical products, particularly accelerators of the vulcanization of rubber or agents used in flotation processes for concentrating ores (Holleman and Wiberg, 2001). Copper$^{(II)}$ complexes have been described as a plastic metal ion because the chemistry of its complexes exhibits different coordination numbers with many kinds of irregular coordination geometries, such as tetrahedral or square planar four-coordinate, octahedral six coordinate, and square pyramidal or trigonal–bipyramidal five coordinate (Saadeh, 2013).

In this manuscript, we describe the synthesis and physical characterization of sodium diphenylcarbamodithioate ligand and its new monomeric metal complexes with a range of divalent transition metal ions (Co^{II}, Ni^{II}, and Cu^{II}), in the ratio of 1:2 metal ligands, forming new compounds of C-S and S-M new bands by condensation reaction, and it has been supported by the most important techniques.

II. Materials and Measurements

A. Materials

Chemical reagents were commercially available and used without purification. Solvents were distilled from appropriate drying agents immediately before to use.

B. Physical Measurements

Reagents were purchased from Fluka and Redial–Dehenge Chemical Co. Melting points were obtained on a

ARO-The Scientific Journal of Koya University
Volume V, No 2(2017), Article ID: ARO.10198, 5 pages
DOI: 10.14500/aro.10198
Received : 06 February 2017; Accepted 10 June 2017
Regular research paper: Published 18 July 2017
Corresponding author's e-mail: eman.ibraheem@koyauniversity.org

http://dx.doi.org/10.14500/aro.10198

Buchi SMP-20 capillary melting point apparatus and are uncorrected. Fourier transform IR (FTIR) spectra were recorded as FTIR spectrophotometer in the range 4000-400 cm^{-1}. Electronic spectra of the prepared compounds were measured in the region 200-900 nm for 10^{-3} M solutions in dimethyl sulfoxide (DMSO) and distilled water at 25°C using a Shimadzu160 spectrophotometer with 1.000±0.001 cm matched quartz cell. Elemental microanalyses were performed on a CHN analyzer. While metal contents of the complexes were determined by atomic absorption (AA) technique using a Shimadzu AA 680G AA spectrophotometer. Electrical conductivity measurements of the complexes were recorded at 25°C for 10^{-3} M solutions of the samples in DMSO and distilled water using a PW 9526 digital conductivity meter. Magnetic measurements were recorded on a Bruker BM6 instrument at 298°K following the Faraday's method.

III. Synthesis

A. Preparation of Sodium Diphenylcarbamodithioate Ligand

A suspension of finely powdered sodium hydroxide (0.15 g, 3.75 mmol) in (10 ml) absolute methanol was added dropwise with continues stirring for 24 h to a solution of diphenylamine (0.5 g, 2.95 mmol) and CS_2 (0.22 ml). The solvent was removed under reduced pressure, and the residue was dried from methanol to form a white precipitate. Yield: (74%), m.p. (66°C).

B. General Synthesis of the Complexes

Diphenylcarbamodithioate complexes were prepared by the general methods and as follows: A solution of methanol (10 ml) and nickel chloride salt (0.177 g, 0.75 mmole) was added with stirring into methanolic solution of the sodium diphenylcarbamodithioate ligand (0.2 g, 1.49 mmol) in methanol (15 ml). The mixture was allowed to stir for 2 h, and then distilled water was added, the resulted solid was filtered off, and washed with methanol and dried at room temperature to give the required diphenylcarbamodithioate complex. All the other complexes have been prepared in the ratio of 1:2 metal-ligand. Elemental analysis data, colors, and yields for the complexes are given in Table I.

IV. Results and Discussion

Sodium diphenylcarbamodithioate ligand was achieved from the reaction of diphenylamine with CS_2 in the ratio of 1:1 in alkaline medium. The general synthetic method for the preparation of the ligand and its complexes involves the reaction of the metal chloride salts with exothermic behavior according to Scheme 1. The ligand was obtained in almost a quantitative yield, and the metal complexes of the ligand with Co^{II}, Ni^{II}, and Cu^{II} metal ions were obtained in moderate yields. The compounds were characterized by elemental analysis, IR, ultraviolet-visible (UV-Vis), magnetic susceptibility, melting point, thin-layer chromatography (TLC), and conductivity measurements.

A. The IR Spectrum of the Ligand

The band at 3210 cm^{-1} due to the υ(N–H) amine group (Semalty, et al., 2010) of diphenylamine has been disappeared in the spectrum of the sodium diphenylcarbamodithioate ligand as a result of the replacement the hydrogen atom by CS_2 and forming strong vibrational coupling is operative in the case of the nitrogen containing thiocarbonyl derivatives and three bands seem to consistently appear in the regions 1386-1566 cm^{-1}, 1250-1411 cm^{-1}, and 955-1110 cm^{-1} due to the mixed vibrations, these bands, which may be tentatively designated as the $Ph_2N\text{-}CS_2$ ~ (Venkataraghavana and Raoa, 2005). On the other hand, a new bands have been formed at 1500 cm^{-1}, 1070 cm^{-1}, and 1300 cm^{-1} due to aliphatic υ(C-N)

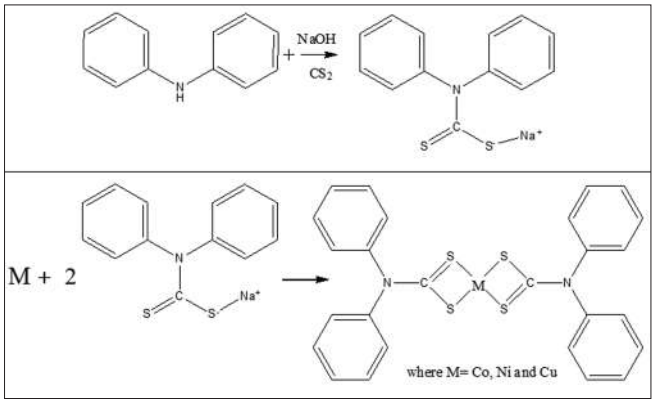

Scheme 1: Synthetic route for ligand, and general structure for suggested Co^{II}, Cu^{II}, and Ni^{II} metal ion complexes

TABLE I
The Physical Properties of the Ligand and its Metal Complexes

Molecular formula	Molecular weight	Yield%	Color	M.P.°C	Found (calc%)					ε M(Ω^{-1} cm^2mol^{-1})
					M	C	H	S	N	
[L] $C_{13}H_{10}NNaS_2$	267.35	74	White	66	8.6	58.4	3.77	23.99	5.24	-
					7.33	54.12	3.02	22.43	5.01	
$C_{26}H_{20}CoN_2S_4$	547.64	66	Yellow	170	10.76	57.02	3.68	23.42	5.12	10.6
					9.55	54.87	3	20.02	4.23	
$C_{26}H_{20}N_2NiS_4$	547.4	56	Pal yellow	103	10.72	57.05	3.68	23.43	5.12	12.9
					9.99	55.65	2.39	22.89	4.69	
$C_{26}H_{20}CuN_2S_4$	552.26	78	Orange	90	11.51	56.55	3.65	23.22	5.07	11.2
					10.79	54.12	3.03	22.23	4.77	

(Bailey, et al., 1991), υ(C-S) (Roeges, 1994), and υ(C=S) (El-Shazly, et al., 2005). Moreover, the band at 1610 cm^{-1} of υ(C=C) is still presented of the aromatic ring (Seleem, et al., 2011) (Table II).

B. The UV-Vis Spectrum of the Ligand

The UV-Vis spectra of the ligand exhibit a high intense absorption peak at 253 nm (39,525 cm^{-1}) (∈max=1420 $molar^{-1}. cm^{-1}$), assigned for (π → π*), with a shoulder peak at 302 nm (33112 cm^{-1}) (∈max=54 $molar^{-1}.cm^{-1}$) were assigned to (n → π*) transitions (Anuradha and Rajarel, 2011) (Table III).

C. The IR Spectrum of the Complexes

An important bands of all the formed complexes at 1110 cm^{-1}, 1131 cm^{-1}, and 1120 cm^{-1} attributed to υ(C-S), and the bands at 1210 cm^{-1}, 1231 cm^{-1}, and 1220 cm^{-1} assigned to υ(C=S) for (Co^{II}, Ni^{II} and Cu^{II}) ion complexes, respectively (Al-Fahdawi and Al-Salihi, 2015), which are shifted to lower frequency as a result of the coordination with metal ions. Moreover, the new bands at 440 cm^{-1}, 450 cm^{-1}, and 477 cm^{-1} have been formed are attributed to υ(M-S) of (Co^{II}, Ni^{II}, and Cu^{II}) ion complexes, respectively (Al-Fahdawi, et al., 2014; Beer et al. 2003; and Bensebaa, et al., 1999) (Table II).

D. The UV-Vis Spectra of the Complexes

The UV-Vis spectra of Co^{II}, Ni^{II}, and Cu^{II} complexes showed two intense peaks in the range 243 nm (41,152 cm^{-1}) (∈max=1243 $molar^{-1}. cm^{-1}$), 222 nm (45,045 cm^{-1}) (∈max=765 $molar^{-1}. cm^{-1}$), and 249 nm (40,160 cm^{-1}) (∈max=1567 $molar^{-1}. cm^{-1}$) range assigned to the ligand field for Co^{II}, Ni^{II}, and Cu^{II} metal ions, respectively (Griffith, et al., 2011). Other peaks at 366 nm (27,322 cm^{-1}) (∈max=65 $molar^{-1}. cm^{-1}$), 310 nm (32,258 cm^{-1}) (∈max=100 $molar^{-1}.cm^{-1}$), and 300 nm (33,333 cm^{-1}) (∈max=81 $molar^{-1}. cm^{-1}$) range assigned to the charge transfer transition for Co^{II}, Ni^{II}, and Cu^{II}, respectively (Amy, et al., 2011). The third peak detected in the visible region for same complexes at 560 nm (17,857 cm^{-1}) (∈max=50 $molar^{-1}. cm^{-1}$), 534 nm (18,726 cm^{-1}) (∈max=90 $molar^{-1}. cm^{-1}$), and 555 nm (18,018 cm^{-1}) (∈max=204 $molar^{-1}.cm^{-1}$) is due to $^4T_1g_{(F)} \rightarrow {}^4A_2g_{(p)}$, $^1A_2g \rightarrow {}^1A_1g$, and $^2A_1g \rightarrow {}^2B_1g$ transitions indicating square planar structure (Manishankar, et al., 2001) around Co^{II}, Ni^{II}, and Cu^{II} metal complexes (Table III).

E. Molar Conductance

The molar conductance of the Co^{II}, Ni^{II}, and Cu^{II} metal ion complexes indicates non-electrolytic nature in DMSO solutions (Kai, et al., 2009) (Table I).

F. Magnetic Moment

The magnetic moment (2.2, 1.9, and 2.1 B.M) value of the Co^{II}, Ni^{II}, and Cu^{II} ion complexes, respectively, as well as the other analytical data Table III is in agreement with suggested structure of square planar geometry for the three complexes in the solid state (Uppadin, et al., 2001; Al-Jeboori, et al., 2010). TLC measurement for the derivative ligands [L] and

TABLE II
FTIR Spectra for the Ligand and its Complexes

Compound	ν(N-H)	ν(X-N)	ν(X=Σ)	ν(X-Σ)	ν(M-Σ)
Diphenylamine	3210	1550	-	-	-
[L] $C_{13}H_{10}NNaS_2$	-	1500	1300	1170	-
$C_{26}H_{20}CoN_2S_4$	-	1355	1220	1110	440
$C_{26}H_{20}N_2NiS_4$	-	1362	1231	1131	450
$C_{26}H_{20}CuN_2S_4$	-	1359	1220	1120	477

FTIR: Fourier transform infrared

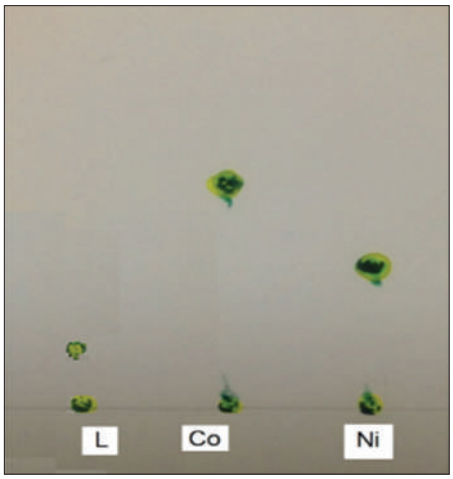

Fig. 1. The thin-layer chromatography measurements for the [L] ligand and its Co^{II} and Ni^{II} metal ion complexes

TABLE III
The Electronic Spectral Data for the Ligand and its Complexes

Compound	Band position λ_{nm}	Wave number (cm^{-1})	ε_{max} ($dm^3 mol^{-1} cm^{-1}$)	Assignment	Magnetic Moment (B.M)	Suggested Configuration
[L]	253	39525	1420	π → π*	-	-
$C_{13}H_{10}NNaS_2$	302	33112	54	n → π*		
$C_{26}H_{20}CoN_2S_4$	243	41152	1234	π → π*	2.2 paramagnetic	Square planar
	366	27322	65	Ch.T		
	560	17857	50	$^4T_{1g}$ (F)→$^4A_{2g\,(p)}$		
$C_{26}H_{20}N_2NiS_4$	222	45045	765	π →π*	1.9 diamagnetic	Square planar
	310	32258	100	Ch.T		
	534	18726	90	$^1A_{2g} \rightarrow {}^1A_{1g}$		
$C_{26}H_{20}CuN_2S_4$	249	40160	1567	π →π*	2.1 diamagnetic	Square planar
	300	33333	81	Ch.T		
	555	18018	204	$^2A_{1g} \rightarrow {}^2B_{1g}$		

http://dx.doi.org/10.14500/aro.10198

TABLE IV
THE TLC MEASUREMENTS FOR THE [L] LIGAND AND ITS Co^{II} AND Ni^{II} COMPLEXES

Compound	Range of R_f (mm)
[L] $C_{13}H_{10}NNaS_2$	0.4
$C_{26}H_{20}CoN_2S_4$	3.5
$C_{26}H_{20}N_2NiS_4$	2.5

TLC: Thin-layer chromatography

its complexes were performed with Co^{II} and Ni^{II} are showed in Fig. 1. The appearance of new spots with different Rf compared with the Rf of the ligand Table IV for Co^{II} and Ni^{II} indicated the formation of the complexes. Since the spots positions belong to Co^{II} and Ni^{II} ion complexes are differ from the positions of the ligands spot. The biological activity of the [L] ligand and its Co^{II}, Cu^{II}, and Ni^{II} complexes was tested on two types of pathogenic bacteria using inhibition method (Anacona, 2006; Tauber and Nau, 2008; Petra, et al., 2005; Sultana and Arayne, 2007). The two types of bacteria were Gram-positive *Staphylococcus aureus* and *Bacillus subtilis*. The ligand [L] showed inhibition diameter against the two types of bacterial after 24 h, and this inhibition diameter was increased after 48 h (Fig. 2). Furthermore, experimental results indicated that the complexes show more activity than the ligand under similar experimental conditions with the same kinds of bacteria. The X-ray powder diffraction (XRD) pattern of Co^{II} complex shows well-defined crystalline peaks indicating that the sample is 25% crystalline in nature (Dokken, et al., 2009). An XRD powder diffraction pattern of copper complex has been given in Fig. 3 of different scale particles are well coincident with each other, and it means that different forms of complexes have the same structure (Guillemet-Fritsch, et al., 2006). The sample has been dried and then scanned in the 2θ range of 10-80° confirming square planar geometry around Co ion complex (Kavitha and Lakshm, 2017; Zheng, et al., 2017). The mass spectrum shows the base peak at 267 related to the molecular weight of the ligand. Moreover, all the other fragmentations are compatible with the value of the fragments of the ligand as shown in Fig. 4. The proposed molecular structure of the [L] ligand and its Ni^{II} complex according to Chemoffice program displays geometrical shape of the complexes is square planer (Fig. 5a and b).

V. CONCLUSION

The reaction of diphenylamine with CS_2 in alkaline solution gives the required sodium diphenylcarbamodithioate ligand. The reaction of this ligand with metal chloride salts resulted in the formation of the required diphenylcarbamodithioate complexes with the square planar geometry around Co^{II}, Cu^{II}, and Ni^{II} ion complexes. Physical, chemical, and spectroscopic methods were used to investigate the mode of bonding and overall structure of the complexes. Co^{II}, Cu^{II}, and Ni^{II} complexes of sodium diphenylcarbamodithioate ligand have been synthesized and characterized by elemental analyses and spectroscopic techniques. The XRD of the (Co^{II}, Ni^{II}, and Cu^{II}) ion complex revealed that the complexes are 25% crystalline. The FTIR measurements, UV-Vis and mass spectrum for the ligand and its complexes reveal the exact peak for each of the compounds functional groups. Moreover, the aims of this study are to:

1. The formation of new complexes by the reaction between diphenylamine and CS_2 with Co^{II}, Ni^{II}, and Cu^{II} metal ions
2. Determine the best some metal complexes for activating the multiple bonds in C-S_2, C-S, and S-M
3. Syntheses of new ligand with CS_2
4. Studding the characteristic properties of the sodium diphenylcarbamodithioate ligand and its complexes.

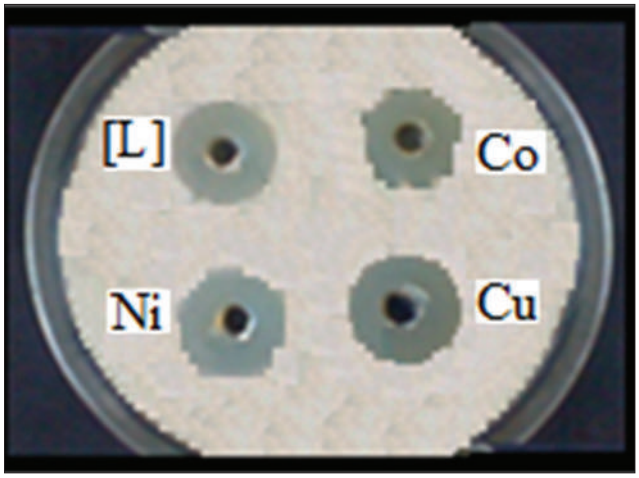

Fig. 2. The biological activity of the [L] ligand and its Co^{II}, Cu^{II}, and Ni^{II} metal ion complexes after 48 h

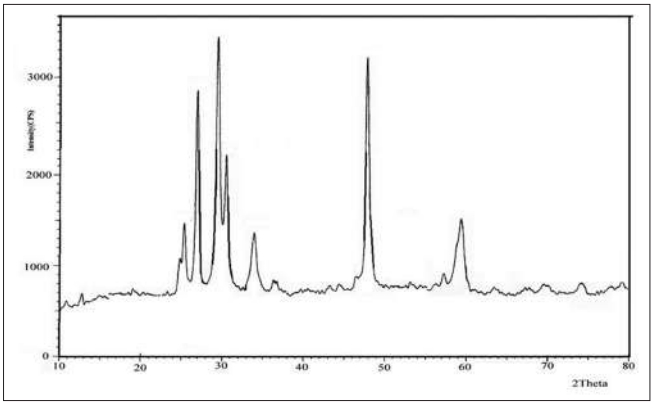

Fig. 3. The X-ray powder diffraction pattern for Co^{II} complex

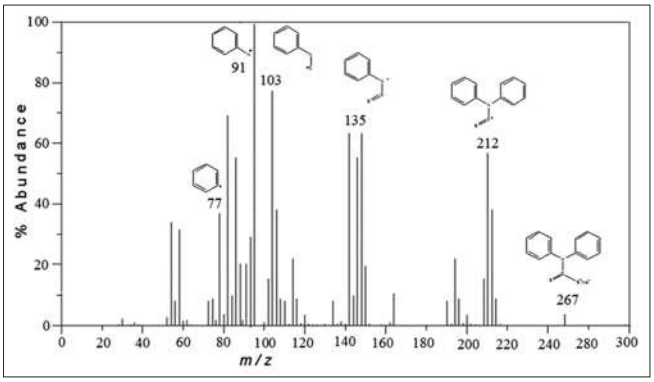

Fig. 4. The mass spectrum for the ligand

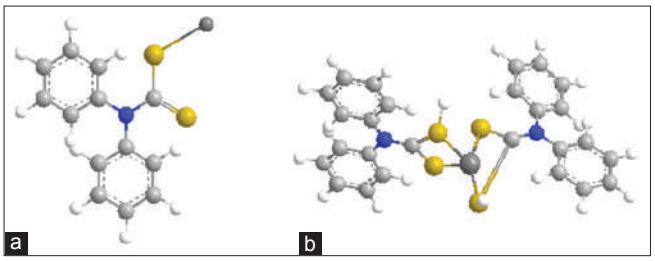

Fig. 5. (a and b) The proposed molecular structure of [L] and Ni^{n} complex according to Chemoffice program

A. Prospective Studies

1. Preparing new complexes with other transition elements
2. Modern industries rely heavily on sulfuric materials because of their real effectiveness in many fields, so it can be used in industry and health field as well.

References

Al-Fahdawi, A.S., Al-Kafajy, H.A., Al-Jeboori, M.J. and Potgieter, H., 2014. New bimetallic bisdithiocarbameta-based macrocyclic complex; Preparation and spectral characterization. *Chem-Xpress*, 4(3), pp.262-267.

Al-Fahdawi, A.S. and Al-Salihi, I.I., 2015. Preparation of Tris (diphenyl methanol) binding by hydrogen bonds through the application of microwave techniques. *International Journal of Current Research in Biosciences and Plant Biology*, 2(7), pp.1-9.

Al-Jeboori, M.J., Al-Tawel, H.H. and Mahmood, R., 2010. New metal complexes of N2S2 tetradentate ligands: Synthesis and spectral studies. *Inorganica Chimica Acta,* 363(6), pp.1301-1305.

Amy, L., Pochodylo, R.L., LaDuca, 2011. A layered grid divalent cobalt coordination polymer constructed from ferromagnetically coupled linear trimeric units. Inorganic Chemistry Communications, 14, pp.722-726

Anacona, J.R. and Patiño, C., 2006. Metalloantibiotics: Synthesis and antibacterial activity of ceftazidime metal complexes. *Journal of Coordination Chemistry*, 54, pp.355-365.

Anuradha, K. and Rajarel, R., 2011. Synthesis, spectral characterization and biological activity of new symmetrical macrocyclic binuclear Schiff base complexes. *International Journal of Pharmacy and Technology*, 3(2), pp.2217.

Bailey, J.H.E., Drake, J.E., and Wong, M.L.Y., 1991. WONG Department of Chemistry and Biochemistry, University of Windsor, Windsor, Ont., Canada N9B 3P4. Preparation and characterization of a series of bromodiphenyl(N,N-dialkyldithiocarbamato)tellurium(IV) compounds where R = Me, Et, i-Pr, Bu, and of chlorodiphenyl(N,N-dibutyldithiocarbamato)tellurium(IV) and diphenylbis(N, N-dibutyldithiocarbamato)tellurium(IV). Crystal structure of Ph2TeBr[S2CNEt2] and Ph2Te[S2CNBu2I2, http://www.nrcresearchpress.com/doi/pdfplus/10.1139/v91-280. [Last received on 1991 Apr 18].

Beer, P.D., Cowley, A.R., Jeffery, J.C., Paul, R.L. and Wong, W.W.H., 2003. Self-assembled xanthate-transition metal polyether macrocycles and cryptands. *Polyhedron,* 22(5), pp.795-801.

Bensebaa, F., Zhou, Y., Brolo, A.G., Irish, D. E., Deslandes, Y., Kruus, E. and Ellis, T.H., 1999. Raman characterization of metal-alkanethiolates. *Spectrochimica Acta Part A-Molecular and Biomolecular Spectroscopy,* 55(6), pp.1229.

Canady, R., Richard, L., Greg, P., Margaret, W., Heidi, B., Steven, H., Brent, K., Ji-Eun, L., Craig, L. and Joseph, S., 2013. Determining the applicability of threshold of toxicological concern approaches to substances found in foods. *Critical Reviews in Food Science and Nutrition*, 53 (12), pp.239-1249.

Dokken, K.M., Parsons, J.G., McClure, J. and Gardea-Torresdey, J.L. 2009. Synthesis and structural analysis of copper(II) cysteine complexes. *Inorganica Chimica Acta*, 362, pp.395-401.

El-Shazly, R.M., Al-Hazmi, G.A., Ghazy, S.E., El-Shahawi, M.S. and El-Asmy, A.A., 2005. Spectroscopic, thermal and electrochemical studies on some nickel (II) thiosemicarbazone complexes. *Spectrochimica Acta A*, 61, pp.243.

Griffith, D.M., Szocs, B., Keogh, T., Suponitsky, K.Y., Farkas, E., Buglyo, P. and Marmion, C.J., 2011. Suberoylanilide hydroxamic acid, a potent histone deacetylase inhibitor; its X-ray crystal structure and solid state and solution studies of its Zn(II), Ni(II), Cu(II) and Fe(III) complexes. *Journal of Inorganic Biochemistry*, 105, pp.763-769.

Guillemet-Fritsch, S., Lebey, T., Boulos, M. and Durand, B., 2006, Dielectric properties of CaCu3Ti4O12 based multiphased ceramics. *Journal of the European Ceramic Society*, 26, pp.1245-1257.

Holleman, A.F. and Wiberg, E., 2001. *Inorganic Chemistry*. Academic Press, San Diego.

Ingle, M., and D'Souza, M.C., 1989. *Physiology and control of superficial scald of apples: A review.* Horticultural Science, 24(28), pp.31.

Kai, Y., Gu, Z., Ji, R. and Lou, L.S., 2009. Heterogeneous chiral Mn(111) salen catalysts for the epoxidation of unfunvtionalized olefins immobilized on mesoporous materials with different pore sizes. *Tetrahedron,* 65, pp.305-311.

Kavitha, N. and Lakshm, P.V.A., 2017. Synthesis, characterization and thermogravimetric analysis of $Co^{(II)}$, $Ni^{(II)}$, $Cu^{(II)}$ and $Zn^{(II)}$ complexes supported by ONNO tetradentdate Schiff base ligand derived from hydrazine benzoxazine. *Journal of Saudi Chemical Society*, 21 Suppl 1, pp.S457-S466.

Manishankar, P., Sarpudeen, A. and Viswanathan, S., 2001. Electroanalysis of dapsone, an anti-leprotic drug. *Journal of Pharmaceutical and Biomedical Analysis,* 26, pp. 873-881.

Petra, D., Tatjano, Z. and Boriset, P., 2005. Mixed-valence Cu(II)/Cu(I) complex of quinolone ciprofloxacin isolated by a hydrothermal reaction in the presence of l-histidine: Comparison of biological activities of various copper-ciprofloxacin compounds. *Journal of Inorganic Biochemistry*, 2, pp.432-442.

Roeges, N.G.P., 1994. *A Guide to the Complete Interpretation of the Infrared Spectra of Organic Structures*. Wiley, New York.

Saadeh, S.M., 2013. Synthesis, characterization and biological properties of Co(II), Ni(II),Cu(II) and Zn(II) complexes with an SNO functionalized ligand. *Arabian Journal of Chemistry*, 6, pp.191-196.

Seleem, H.S., El-Inany, G.A., El-Shetary, B.A. and Mousa, M.A., 2011. The ligational behavior of an isatinic quinolyl hydrazone towards copper(II)-ions. *Chemistry Central Journal*, 5, pp.20.

Semalty, A., Semalty, M. and Rawat, M.S., 2010. Development and characterization of aspirin-phospholipid complex for improved drug delivery. *International Journal of Pharmaceutical Science and Nano Technology*, 3, pp.940-947.

Sultana, N. and Arayne, M.S., 2007. *In vitro* activity of cefadroxil, cephalexin, cefatrizine and cefpirome in presence of essential and trace elements. *Pakistan Journal of Pharmaceutical Sciences*, 20(4), pp.305-310.

Tauber, S.C. and Nau, R., 2008. Immunomodulatory properties of antibiotics. *Current Molecular Pharmacology*, 1, pp.68.

Uppadin, L.H., Weeks, J.M. and Beer, P.D., 2001. Metal-directed self-assembly of terphenyl based dithiocarbamate ligands. *Journal of the Chemical Society Dalton Transactions,* 22, pp.3367-3372.

Venkataraghavana, R. and Raoa, C.N.R., 2005. The C=S stretching frequency and the "-N-C=S bands" in the infrared. Spectrochimica Acta *A,* 18(4), pp.541-547.

Vogt, P.F. and Gerulis, J.J., 2005. Amines, aromatic. In*: Ullmann's Encyclopedia of Industrial Chemistry*. Wiley-VCH, Weinheim.

Zheng, Z., Junwei, X., Sisi, Y., Yangli, C., Yan, W., Zhuo, C. and Chunlin, N., 2017. Two organic cation salts containing tetra(isothiocyanate)cobaltate(II): Synthesis, crystal structures, spectroscopic, optical and magnetic properties. *Crystals*, 7(3), pp.92.

 http://dx.doi.org/10.14500/aro.10180

A Comparative Study for String Metrics and the Feasibility of Joining them as Combined Text Similarity Measures

Safa S. Abdul-Jabbar[1] and Loay E. George[2]

[1]Computer Department, College of Science for Women,
University of Baghdad, Baghdad, Iraq

[2]Computer Department, College of Science,
University of Baghdad, Baghdad, Iraq

***Abstract*–This paper aims to introduce an optimized Damerau–Levenshtein and dice-coefficients using enumeration operations (ODADNEN) for providing fast string similarity measure with maintaining the results accuracy; searching to find specific words within a large text is a hard job which takes a lot of time and efforts. The string similarity measure plays a critical role in many searching problems. In this paper, different experiments were conducted to handle some spelling mistakes. An enhanced algorithm for string similarity assessment was proposed. This algorithm is a combined set of well-known algorithms with some improvements (e.g. the dice-coefficient was modified to deal with numbers instead of characters using certain conditions). These algorithms were adopted after conducting on a number of experimental tests to check its suitability. The ODADNN algorithm was tested using real data; its performance was compared with the original similarity measure. The results indicated that the most convincing measure is the proposed hybrid measure, which uses the Damerau–Levenshtein and dice-distance based on n-gram of each word to handle; also, it requires less processing time in comparison with the standard algorithms. Furthermore, it provides efficient results to assess the similarity between two words without the need to restrict the word length.**

***Index Terms*–Word classification, Word clustering, String distance, String matching operation, and String similarity metric.**

I. Introduction

To find the similarity ratio between strings, many comparing operations should be used, this subject considered as a basic task in natural language processing (NLP), as well as other disciplines such as computational biology. In NLP, the sequences of symbols are composed of a number of sentences, consisting of words. In the first approximation (such as applications in speech recognition), sentences are considered to be more similar to the more words they share and the reordering is no consideration. While in the second approximation (such as Grammar induction), the reordering of single words and blocks between two sentences can be expected (Leusch, et al., 2003; Mohri, 2003).

Many applications require string search with errors possibility. These applications should use a matching function to the user entry (which may contain an incorrect spelling) in the database. This operation should be done in milliseconds (Fenz, et al., 2012).

The problem underlying the searching operation, measuring the similarity or dissimilarity of two strings, had been a powerful topic of research for over five decades, ranging from early operations to modern machine learning and data analysis. Each method uses different aspects and characteristics of the data (Rieck and Wressnegger, 2016).

Various similarity measures were proposed for use in various fields: Damerau and Levenshtein introduced a method named Damerau–Levenshtein that used as a string metric between two strings. By counting the minimum number of operations needed to transform one string to the other, through measuring the substitution operations of a single character besides the insertion, deletion, or transposition operation of two adjacent characters (provided by the Levenshtein distance) (Damerau, 1964). These measures are based on probabilistic modeling for a particular applied instance. For example, in error correction of noisy sentences (Kashiap and Oommen, 1984; Oommen, 1987) and in recognition tasks (Marzal and Vidal, 1993; Bunke and Bühler, 1992; Cortelazzo, et al., 1996; Cortelazzo, et al., 1994; Peng and Chen, 1997); Winkler had proposed an enhancement to the Jaro metric based on the observation that spelling errors may occur commonly at the end of a string (Winkler, 1999). While the N-gram techniques can determine the similarity between strings from given text sequence by computing the similarity, on the basis of the distance between each character in the compared two strings. This distance is computed by dividing the number of similar grams by the maximal number of n-grams (Alberto, et al, 2010).

ARO-The Scientific Journal of Koya University
Volume V, No 2(2017), Article ID: ARO.10198, 13 pages
DOI: 10.14500/aro.10180
Received 03 December 2016; Accepted 09 September 2017
Regular research paper: Published 21 October 2017
Corresponding author's e-mail: safasami1988@scbaghdad.edu.iq

Sehgal, et al. (2006) compared three string similarity measures on a data integration task; they referred that edit distance is better than Jaccard and Jaro-Winkler when mapping between two sets of place names in Afghanistan. Martins (2011) used machine learning to classify gazetteer records as duplicates or non-duplicates and compared the importance of several feature types, including eight string similarity measures. The experimental results show that using feature vectors which combined from (place names, semantic relations, place types, and geospatial footprints) leads to an increase in the results accuracy. Wang, et al. (2014) proposed a new hybrid similarity metrics, called "fuzzy token matching based similarity," which extends token-based similarity functions (e.g., Jaccard similarity and Cosine similarity) by allowing the fuzzy match between two tokens. They considered as new signature schemes and develop effective techniques to improve the performance.

Different measures of distance or similarity are convenient for different types of analysis:

1- String Similarity: Defines a similarity between two strings (0 means strings are completely different, 1 means strings are identical) like Sorensen–Dice coefficient (Dice, 1945).
2- String Distance: Defines a distance between two strings (0 means strings are identical), like Damerau–Levenshtein. The maximum distance value depends on each algorithm (Sellers, 1980; Hall and Dowling, 1980).

In this paper, many measures were implemented to make a decision about which one was more suitable to use. The implemented algorithms are listed in Table I. While in Table II, the comparison of different similarity metric methods was described in the context of their advantages and weak points.

These methods can be merged to provide fast retrieval systems, using the symbols enumeration operation for handling the string operations as a sequence of numbers instead of a sequence of characters to reduce the hidden cost of the string operations; this will reduce the memory, time, and CPU consumption.

Table I
The Studied String Metric Methods

Method name	Type
Levenshtein	Distance
Damerau–Levenshtein	Distance
Longest common subsequence	Distance
Jaro–Winkler	Similarity measures
N-Gram	Distance
Dice coefficient	Similarity measures
Matching coefficient	Similarity measures
Overlap coefficient	Similarity measures

II. Materials and Methods

In this paper, many different metrics were explored to decide which one is suitable for string-matching purpose depending on the elapsed time with respect to the result accuracy. Furthermore, a set of hybrid algorithms was made up using several existing measures with a simple modification. According to the conducted comparisons between eight string distance/similarity for evaluating them in terms of the consumed time; a brief summary of each one is presented in this section.

The experiments for these algorithms were involved with words of length (1-16) characters only. The conducted statistical analysis of the used datasets showed that approximately 99% of the overall words in each dataset are available in this range of word length; as depicted in Table III.

The number of comparisons for each given word will be reduced using a specific threshold based on the word length. The process of selecting the threshold was treated as follows:

- For words that have length ≤5, the threshold=1) the comparison operations were made with only words that have the length equal ±1 to the length of the given word).
- For words that have length ≥6, the threshold=2) the comparison operations were made with words that have the length equal ±2 to the length of the given word).

Which means the types that are processed in the proposed system are limited in two types: Words with length ≤5 have the possibility of one error only, whereas words with length >5 allow errors with two letters as the maximum probability. Then, to get the best system performance, the proposed system used the integrated number of similarity measures which

Table II
Comparison of Different Similarity metrics methods

Method name	Advantage	Disadvantage
Levenshtein and Damerau–Levenshtein	Gives the best result in case of short string and it is fast and best suited for strings similarity (Pradhan, et al., 2015; Patel, 2016)	In case of long string cost of Levenshtein distance is same as the length of string and considered it is not order of sequence of characters while comparing (Pradhan, et al., 2015; Patel, 2016)
Longest common subsequence	-	Uses the recursion approach which uses stack that takes lots of space (Pradhan, et al., 2015)
Jaro–Winkler	Gives better result in case of hybrid method (Pradhan, et al., 2015)	If the data size is too much large, then Jaro distance similarity not gives efficient results (Pradhan, et al., 2015)
N-gram	Similarity technique is high (Pradhan, et al., 2015)	They are not suitable at multilingual environment, and the accuracy is very less (Pande, et al., 2013; Pradhan, et al., 2015)
Dice coefficient	Obtain satisfactory results and used to consider the sizes of the two words and the similarity score will be normalized into [0,1] (Pradhan, et al., 2015)	-
Matching coefficient	Very simple vector-based approach which simply counts the number of similar terms (dimensions) (Gomaa and Fahmy, 2013)	If one of these dimensions is zero, this method cannot work efficiently (Gomaa and Fahmy, 2013)
Overlap coefficient	Similar to the Dice's coefficient, but considers two strings a full match if one is a subset of the other (Gomaa and Fahmy, 2013)	-

Table III
The Words Count within the Considered 4 Datasets of Complete Words whose Lengths bounded between [1,16] Characters

Dataset#	No. of words in the overall dataset	No. of words from 1 to 16 char.
Dataset 1	530421873 (%100)	529051745 (%99.74)
Dataset 2	63948272 (%100)	63944562 (%99.99)
Dataset 3	246650908 (%100)	246598321 (%99.97)
Dataset 4	3455357163 (%100)	3452403297 (%99.88)

have proven successful through experiments. These combined measures were used for measuring the string distance between pairs of strings. The considered measures are:

- Dice coefficient and N-gram (DN).
- Dice coefficient, N-gram, and Damerau–Levenshtein (DADN).
- Damerau–Levenshtein and longest common subsequence (DAL).

A. DN Measure

It is obtained by integrating the N-gram measure with the dice-coefficient measure to increase the similarity results accuracy. Algorithm (1) illustrates the implementation steps for DN.

Algorithm (1): DN Algorithm

Objectives: Measuring the similarity between two given strings.
Input: Variable number of input words ($string_1$), Text File.
Output: Integer value, words List contain the same number of input words, which is the most similar words from files.

```
Step1:
  String [] s1 → string1.Split(' ')  //Read the given string
                                     and split it to words array
                                     using the space delimiter
  Double len → 0, Double total_len → 0
  Double temp → -1, Int g→0
Step2:
  StreamReader sr →new StreamReader(ss)
//Read                                          the   file
content
  line = sr.ReadToEnd();
  string[] words = line.Split(' ');  //Split the file content in
                                     to words using the space delimiter
  For i = 0 to s1.Length-1 step 1 do
    For j = 0 to words.Length-1 step 1 do
      If (((s1[i].Length >= 1) & (s1[i].Length <= 5)) &
      ((s1[i].Length <= words[j].Length + 1) && (s1[i].
      Length >= words[j].Length-1))) then//For words
      that have length0-5 the threshold of error is 1 char.
      temp → DiceCoefficient(s1[i], words[j])
      If (len == 0) then len=temp, g = j
      Else If (temp > len) then len = temp, g = j
      End If
  Else If (((s1[i].Length >= 6) & (s1[i].Length <= 18)) &
  ((s1[i].Length <= words[j].Length + 2) & (s1 [i].Length >=
  words[j].Length - 2))) then//For words that more than 5
  characters the threshold of error is 2 char.
  temp → DiceCoefficient(s1[i], words[j])
      If (len == 0) then len=temp, g = j
      Else If (temp > len) then len = temp, g = j
      End If
    End If
    temp →0
  End For
  total_len = total_len + len//For collect distance of all
                                  words in the given string
  list1.Items.Add(words[g]);
  len → -1, temp → -1
  End for
Step3:
  Int Result_Distance= total_len/s1.Length
End;
```

```
Function1: Double DiceCoefficient(string stOne, string stTwo)//
    For strings instead of char comparing using words of two
    characters
  List<string> nx, ny; string temp = ""
  For i = 0 to stOne.Length – 2 step 1 do
      temp = "" + stOne[i] + stOne[i + 1]: nx.Add(temp)
  End For
  For j = 0 to stTwo.Length – 2 step 1 do
      temp = "" + stTwo[j] + stTwo[j + 1]: ny.Add(temp)
  End For
  If (stOne.Length == 1)//For handling words with one
  character
      temp = "" + stone, nx.Add(temp)
  End if
  If (stTwo.Length == 1)//For handling words with one
  character
      temp = "" + stTwo, ny.Add(temp)
  End if
  HashSet<string> intersection = new HashSet<string>(nx)
  intersection.IntersectWith(ny), double dbOne =
  intersection.Count//Determine the intersection between
  words
Return (2 * dbOne/(nx.Count + ny.Count))
```

B. DADN Measure

It is obtained by integrating the previous mentioned DN algorithm with Damerau–Levenshtein distance measure to increase the result accuracy; this integration aimed to take the advantage of Damerau–Levenshtein efficacy and speed. Then, handling the situation of equal single character movement results with a DN measure to decide which string is more similar to a given one. Algorithm (2) illustrates the implemented steps for DADN.

Algorithm (2): DADN Algorithm

Objectives: Measuring the similarity between two given strings.
Input: Variable number of input words ($string_1$), Text File.

Output: Integer value, List of words contains the same number of input words, which is the most similar words from files.

Step1:
String [] s_1 → $string_1$.Split(' ')//Read the given string and split it to words array using the space delimiter
Double len → 0, **Double** total_len → 0//Define the variables
Double temp → -1, **Int** g →0
DamerauLevensteinMetric da=newDamerauLevenstein Metric()//Define the object da as class of Damerau Levenste in Metric
Step2:
StreamReader sr →**new** StreamReader(ss), line = sr.ReadToEnd()//Read the file content
String[] words = line.Split(' ')//Split the file content in to words using the space delimiter
For i = 0 **to** s_1.Length-1 **step** 1 **do**
For j = 0 **to** words.Length-1 **step** 1 **do**
If ((s_1[i].Length >=1) & (s_1[i].Length<=5)) & ((s_1[i].Length<=words[j].Length+1) & (s_1 [i].Length>=words[j].Length - 1))) **then**//
For words that have length 0-5 the threshold of error is 1 character
temp → da.GetDistance(s1[i], words[j], 100)
If (len == 0) **then** len → temp, g → j
If (temp < len) **then** len → temp, g → j
else If ((temp==len) & (j!=g) & (len!=0)) **then**
Double one → DiceCoefficient(s1[i], words[g]), **Double** two → DiceCoefficient(s1[i], words[j])
If (one > two) **then** g = j
End If
else If ((s_1[i].Length>=6) & (s_1[i].Length<=18)) & ((s_1[i].Length<=words[j].Length+2) & (s_1 [i].Length >= words[j].Length - 2))) **then**//For words that have more than 5 char. the threshold of error is 2 char.
temp → da.GetDistance(s1[i], words[j], 100)
If (len == 0) **then** len=temp, g = j
If (temp < len) **then** len = temp, g = j
else If ((temp == len) & (j!= g) & (len != 0)) **then**
Double one → DiceCoefficient(s1[i], words[g]), **Double** two → DiceCoefficient(s1[i], words[j])
If (one > two) **then** g = j
End If
End If
temp →0
End For
total_len = total_len + len//For collect distance of all words in the given string
list1.Items.Add(words[g]), len → -1, temp → -1
End for
Step3:
Int Result_Distance= total_len/s_1.Length
End;

Function1: Double DiceCoefficient(string stOne, string stTwo)// The Same Function Steps (used to compare between two strings using Dice-Coefficient and N-gram) as in Algorithm(1)
Class DamerauLevensteinMetric
Const Int DEFAULT_LENGTH → 255
Int [] currentRow, previousRow, transpositionRow//Define the variables
Double GetDistance(**String** first, **String** second, **Int** max)//Max is the threshold of movements number
Int maxLength → DEFAULT_LENGTH//Maximum number of characters in each word
currentRow → **new Int**[maxLength +1], previousRow → **new Int**[maxLength +1],
transpositionRow →**new Int**[maxLength +1]
Int firstLength → first.Length, **Int** secondLength → second. Length//2Variable to store the length of string1 &2
If (firstLength == 0) **then Return** secondLength//If string1 was empty return the number of char. in string2
If (secondLength==0) **then Return** firstLength//If string2 was empty return the string1 length
If (firstLength > secondLength) **then**//Swap between string to make the second string with larger length and swap length
Swap (first, second), firstLength → secondLength
End If
If (secondLength - firstLength > max) **Return** max + 1// If the different is larger than threshold the return threshold+1
If (firstLength > _currentRow.Length) **then**
currentRow = **new Int** [firstLength + 1], previousRow = **new Int** [firstLength + 1],
transpositionRow = **new Int**[firstLength + 1]
End If
For i = 0 **to** firstLength **step** 1 **do**//As an initial value store the counter value then use this array to store the value of movements for each step(character)
previousRow[i] → i
End For
Char lastSecondCh → '\0'//The last used char in the second string
For i = 1 **to** secondLength **step** 1 **do**
Char secondCh → second[i - 1], currentRow[0] → i//Compute only diagonal stripe of width 2*(max+1)
Int from → Max(i - max - 1, 1), **Int** to → Min(i + max + 1, firstLength)//The start & end positions for checking process
Char lastFirstCh → '\0'//The last used char from first string
For j = from **to** to **step** 1 **do**
Char firstCh = first[j - 1]//Compute minimal cost of state change to current state from previous states of deletion, insertion and swapping
Int cost = 0
If (!(firstCh == secondCh)) **then** cost = 1
Int value = Min(Min(currentRow[j -1] + 1, previousRow[j]+1), previousRow[j -1]+ cost)
//If there was transposition, take in account its cost only if the transposed characters are adjacent
If (firstCh == lastSecondCh && secondCh ==

```
            lastFirstCh) then
    value = Min(value, _transpositionRow[j - 2] + cost),
    currentRow[j] = value, lastFirstCh = firstCh
    End if
End For
    lastSecondCh = secondCh, Int[] tempRow =
    transpositionRow, transpositionRow = previousRow
    previousRow = currentRow, currentRow = tempRow
  End For
  Return previousRow[firstLength]
End Class
```

C. DAL Measure

It is obtained by integrating Damerau–Levenshtein distance measure with the longest common subsequence measure. The longest common subsequence algorithm is used to handle the advantage of Damerau–Levenshtein efficacy and speed. It handles the cases of similar results for several words in the file to a given word, and hence, to decide which string is more similar to a given one. This measure checks the similar character sequence and takes the word with larger values of the sequence. Algorithm (3) presents the implementation steps for DAL.

Algorithm (3): DAL Algorithm

Objectives: Measuring the similarity between two given strings.
Input: Variable number of input words ($string_1$), Text File.
Output: Integer value, List of words containing the same number of input words, which is the most similar words from files.

```
Step1:
    String [] s1 → string1.Split(' ')//Read the given string and
    split it to words array using the space delimiter
    Double len → 0,Double total_len → 0, Double temp
    → -1,Int g→0//define the variables
    DamerauLevensteinMetric da=new DamerauLevenstein
    Metric()//define the object da as class of Damerau
    LevensteinMetric
Step2: StreamReader sr →new StreamReader(ss), line =
sr.ReadToEnd()//Read the file content
    String[] words = line.Split(' ')//Split the file content in to
    words using the space delimiter
    For i = 0 to s1.Length-1 step 1 do
    For j = 0 to words.Length-1 step 1 do If((s1[i].
    Length>=1)&(s1[i].Length<=5))&((s1[i].Length<=words[j].
    Length+1)&
    (s1[i].Length>=words[j].Length-1)) then//For words that
    have length 0-5 the threshold of error is 1char
    temp → da.GetDistance(s1[i], words[j], 100)
    If (len == 0) then len → temp, g → j
    If (temp > len) then len → temp, g → j
    Else If ((temp==len) & (j!=g) & (len! 0)) then//For words
    that have length 0-5 the threshold of error is 1 char.
            Double one → LongestCommonSubsequence(s1[i],
            words[g])
            Double two → LongestCommonSubsequence (s1[i],
            words[j])
            If (one > two) then g = j
    End If
Else If(((s1[i].Length>=6) & (s1[i].Length<=18)) & ((s1[i].
        Length<=words[j].Length+2) &
        (s1 [i].Length>=words[j].Length - 2))) then//For words
        that more than 5 char. the threshold of error is 2 char.
            temp → da.GetDistance(s1[i], words[j], 100)
            If (len == 0) then len=temp, g = j
            If (temp > len) then len = temp, g = j
            Else If ((temp == len) & (j!= g) & (len != 0)) then
            //For words that have length 0-5 the threshold of
            error is 1 char.
            Double one → LongestCommonSubsequence (s1[i],
            words[g])
            Double two → LongestCommonSubsequence (s1[i],
            words[j])
            If (one > two) then g = j
    End If
End If
    temp →0
    End For
    total_len = total_len + len//For collect distance of all
    words in the given string
    list1.Items.Add(words[g]), len → -1, temp → -1
    End for
Step3:
    Int Result_Distance= total_len/s1.Length, list1.show
End;
```

```
    Function1: Int LongestCommonSubsequence (String str1,
                String str2)
      String sequence → ""
      If ((str1.Length == 0) | (str2.Length == 0)) then Return
      0
      Int [,] num = new int[str1.Length, str2.Length]//Array
      used for count the number of identical char. in the given
      strings
      Int maxlen → 0, Int lastSubsBegin → 0, String
      sequencestring → ""
      For i = 0 to str1.Length-1 step 1 do
        For j = 0 to str2.Length step 1 do
          If (str1[i] != str2[j]) then num[i, j] = 0
          else If ((i == 0) || (j == 0)) then num[i, j] = 1//
          Every time check characters from it arrived to the
          end of char start from 1 for counter
          else num[i, j] → 1 + num[i - 1, j - 1]
          End If
    If (num[i, j] > maxlen)
      maxlen → num[i, j]
      Int thisSubsBegin → i - num[i, j] + 1
    If (lastSubsBegin == thisSubsBegin)
      sequencestring → sequencestring + str1[i]
    End If
    else//This block resets the string builder if a different LCS
          is found
    lastSubsBegin → thisSubsBegin, sequencestring → ""//Clear it
    sequencestring → sequencestring + str1. Subsequence
    (lastSubsBegin, (i + 1) - lastSubsBegin)
```

```
    End If
   End If
  End For
 End For
 sequence → sequencestring
Return maxlen
Class DamerauLevensteinMetric//The Same Class Steps as in
                                Algorithm(2)
```

After identifying the best algorithm, DADN, we modified it to deal with numbers rather than strings where this modification will produce a new method entitled dice coefficient, N-gram, and Damerau–Levenshtein using enumeration method (DADNEN). The test results of this algorithm indicated that the modified algorithm has a positive impact on the results for words with length ranging between 1 and 13, but has no effect on the words with the length which is equal or larger than 14. Hence, some conditions were used in the modified algorithms to control the performance of this algorithm with a wide range of word lengths (i.e., making the system work flexibly with all word lengths as much as possible). Algorithm (4) illustrates the implemented steps of the modified optimized DADNEN (ODADNEN) algorithm.

Algorithm (4): ODADNN Algorithm

Objectives: Measuring the similarity between two given strings.
Input: Variable number of input words ($string_1$), Text File.
Output: Integer value, List of words contains the same number of input words, which is the most similar words from files.

```
Step1: Define The Variables
  Byte[] bytes = Get Bytes(string1)//Read the given string
        and split it to words array using the space delimiter
  Int word_length → 0//Start and end and length for each
                      word in the input strings
  Int start → 0, Int end→0, Double len → -1//Number of
                movements required for each two strings
  Double total_len → 0//The total number of movements
for                                  all the given strings
  DamerauLevensteinMetricen da = new DamerauLevenste
  inMetricen()
                  //Define the object da as class of Damerau
                    Levenstein Metric
Step2: Read text files as blocks of bytes.//For each Text file
    read its content as blocks of bytes with size about 4 MB for
    each block till reaching the end of file
Step3: Count Length for each word.//Determine the start (s)
    and the end (e) of each word (array of bytes) for each word
    in the given string (bytes)
Step4:
  For Each Word in bytes
    For j = 0 to bytes2.Length-1 step 1 do
      While (end2 < bytes2.Length & (bytes2[end2] != 32))
        end2++
  End while
  wordfile_length[no] → end2 - start2 - 1
  If (wordfile_length[no] <= 18)
  (C, b)→ array of bytes [wordfile_length[no] + 1]
  Buffer.BlockCopy(bytes2, start2, b, (18 * no)
  wordfile_length[no] + 1)//To determine the start of each row
  Buffer.BlockCopy(bytes2, start2, c, 0, wordfile_length[no] + 1
  If ((word_length<=5) & (word_length<=wordfile_
  length[no]+1) & (word_length>= wordfile_length[no]-1))
  then//for words that have length 0-5 the threshold of error
  is 1 char.
  temp → da.GetDistance(a, c, 100)
  If (len == -1) then len →temp, g →no
  If (temp < len) then len → temp, g → no
  Else If ((temp == len) & (no != g) & (len != 0)) then
  Double one → DiceCoefficient(a, c), Double two →
  DiceCoefficient(a, c)
  If (one > two) then g = no
  End If
Else If (((word_length >= 6) & (word_length <= 18)) &
    ((word_length <= wordfile_length[no] + 2) & (word_length
    >= wordfile_length[no] - 2))) then
  //for words that have length larger 5 the threshold of error
is 2 char.
  If (s1[i].Length < 14) then//For decide if there is a need to
  use the enum methods according to the words length.
    Byte[] bytes1 = GetBytes(s1[i]), byte[] bytes2 =
    GetBytes(words[j])
    temp = da.GetDistanceen(bytes1, bytes2, 100)
    If (len == -1) then len = temp, g = j
    If (temp < len) then len = temp,g = j
    else if ((temp == len) & (j != g) & (len != 0)) then
        double one = DiceCoefficient(s1[i], words[g])
        double two = DiceCoefficient(s1[i], words[j])
        If (one > two) then g = j
  end if
else              //For words with length equal or larger than 14
    temp = da.GetDistance(s1[i], words[j], 100)
    If (len == -1) then len = temp, g = j
    If (temp < len) then len = temp,g = j
  else if ((temp == len) & (j != g) & (len != 0)) then
        double one = DiceCoefficient(s1[i], words[g])
        double two = DiceCoefficient(s1[i], words[no])
        If)one > two) then g = j
     end If
   end If
end If
  temp → -1, start2 → end2 + 1, j →start2, end2 → start2, no++
Next j
total_len → total_len + len, Int s → 0
For h = 0 to wordfile_length[g] step 1 do
  s → s + Convert.ToChar(b[g, h])
  Next h
  list1.Items.Add(s), len → -1, temp → -1, start → end + 1,
  i → start, end→ start
Step5:
  Int Result_Distance= total_len/s1.Length
End;
```

Function1: Double DiceCoefficient(string stOne, string stTwo)//The Same Function Steps (used to compare between

http://dx.doi.org/10.14500/aro.10180

two strings using Dice-Coefficient and N-gram) as in Algorithm(1)

Class DamerauLevensteinMetric//The Same Class Steps as in Algorithm(2) with one different, which convert all Strings to an array of bytes and deal with it on that basis

III. Results and Discussion

In this paper, all algorithms were implemented using C sharp 2015 programming language and applied on CPU 2.60 GHz with 16 GB RAM. For measuring the distance between two strings, many algorithms were tested to determine the most efficient one according to the elapsed time for each one. To test the system performance a text file that has size 171 KB which containing 15593 non-repeated words with lengths ranging from 1 to 16 characters; it was extracted from Oxford University Text Archive. This archive was designed to represent a wide cross-section of current British English (Burnard, 1976). In this paper, some of the non-repeated words were extracted from this dataset to test the system performance by typing ten words with different lengths for each user query.

The conducted test includes words have lengths ranging from 1 to 16, but for saving the space of this article only two lists of results are presented. Table IV lists the elapsed time for each method tested to the string distance measuring process; these methods were tested on 10 words with the same length in each time ranging from 1, 2, and 3. Table V lists the elapsed time for each method tested to the string distance measuring process; these methods were tested on 10 words with same length=16. Furthermore, for comparison purpose, the list given in Table VI shows the improved elapsed processing time ratio between the similar types of methods to find the best one for each type; it was computed using the following equation:

$$\text{Speed ratio}=100*(T_1-T_2)/T_1 \qquad (1)$$

Where T_1 is the elapsed time for first method and T_2 for the second one.

Then, the measures showed best similarity results are combined to increase the accuracy by overcoming the cases of similar comparison results for many words. These combined measures were used for measuring the string distance between pairs of strings. The considered measures are:

- DN: It was obtained by integrating the N-gram method with the dice coefficient method to increase the results accuracy by making use of the sequence of letters in the given words.
- DADN: It was obtained by integrating the previous mentioned DN method with Damerau–Levenshtein distance method to increase the result accuracy; this integration is aimed to take the advantage of Damerau–Levenshtein efficiency and speed. Then, handling the situation of equal single character movement results with a DN method to decide which string is more similar to a given one.
- DAL: It is obtained by integrating Damerau–Levenshtein distance with the longest common subsequence. The longest common subsequence is used to handle the advantage of Damerau–Levenshtein efficiency and speed. It handles

Table IV
The 8 of the String Metrics Method Tested using 10 Words with Different Lengths (1, 2 and 3 Characters) and Multiple Changes

Method name	Word length	1		2				3				
	Input status	Complete words	Complete words	Delete one char.	Exchange two char's	Error typing in one char.	Insert one char.	Complete words	Delete one char.	Exchange two char's	Error typing in one char.	Insert one char.
Jaro–Winkler distance*	Time (µs)	8017.9	8004.5	6004.3	7003.8	9023.7	6003.9	9991.7	7004.2	7005.8	8018.7	9006
	Distance	0	0	0.015	0.033	0.015	0.0178	0	0.0089	0.0175	0.0178	0.0067
Longest common substring**	Time (µs)	7003.8	8003.7	8006.1	6003.5	13009.2	8004.9	11007	12027.5	10973.9	12007	11005.1
	Similarity	10	20	19	19	19	20	30	29	29	29	29
Levenshtein distance***	Time (µs)	7023.5	11007.8	11026.8	12009	10007.1	10006.7	14009.9	12027.5	14010.4	13995	13009.2
	Movements	0	0	1	1	1	1	0	1	2	1	1
Damerau–Levenshtein distance***	Time (µs)	9005.2	11007	10007.5	18012.8	11007.8	14009.9	16011.3	23016.4	14993.3	17013	16013
	Movements	0	0	1	1	1	1	0	1	1	1	1
N-Gram****	Time (µs)	5003.2	11007.4	9988.5	7002.6	6003.4	5007.1	10005.5	10005.5	9006.4	10025	7996.6
	Similarity	0	10	9	9	9	10	20	20	19	19	19
Dice coefficient*****	Time (µs)	4985	8004.9	7004.6	7022.7	9002	8005.3	9006	16011.7	10006.8	7003.8	9023
	Distance	1	1	0.9667	0.95	0.95	0.9667	1	0.98	0.9333	0.9667	0.95
Overlap coefficient*****	Time (µs)	6003.5	7005.3	9006	7005.8	8005.3	10024.5	11006.6	13007.6	10025.3	13010	10008.3
	Distance	Division by zero	1	Division by zero	0.95	1	0.967	1	1	0.967	0.967	0.967
Matching coefficient******	Time (µs)	5001.6	9008	8005.3	12008.1	9006.8	8024.3	10006.7	13004.9	9006	9023	9006
	Distance	0.5	0.5	0.483	0.475	0.483	0.483	0.5	0.49	0.479	0.483	0.479

*Match=0, Not match=1, **Match=No. of all input char. For all words, No Match=0, ***Match=0, No Match=No. of all input char. for all words, ****Match=No of identical pairs=Σ(each word length−1), No match=0, *****Match=1, No Match=0, ******Match=0.5, No Match=0

the cases of similar results for several words in the file to a given word, and hence, to decide which string is more similar to a given one. This measure checks the similar character sequence and takes the word with larger values of the sequence.

The suggested measures were tested on 10 words with the same length in each time; they range from 1 to 16, as shown in Figs. 1-5, for finding the most appropriate algorithm for using in the next steps. The results showed that applying the DADN algorithm is the fastest one with maintaining the similarity results accuracy; the best algorithm can be selected by calculating the accumulative values for all execution times which obtained in the tests; that is, DDN=12032518.4 (μs), DADN=9673223 (μs), and DAL=9915123 (μs). The accumulative results showed that DADN algorithm has the smallest execution time. After identifying DADN as the best algorithm, we have modified it to deal with numbers rather than strings which we called it DADNEN for speeding up the process. The test results of this algorithm indicated that the modified algorithm has the positive impact on the results for words with length ranging between 1 and 13 but has no effect on the words with length more that. Hence, some conditions were used in the modified algorithms to control the performance of this algorithm, ODADNEN, with a wide range of word lengths (i.e., making the system works flexible with all word lengths as much as possible). The elapsed time for the tested results for (DADNEN, ODADNEN) algorithms, which select the most similar word for each word from the given word, are shown in Table VII and Table VIII.

Table V
The 8 of the Distance String Metrics Methods Tested using 10 Words 16 Characters and Multiple Changes

Method name	Word length	16				
	Input status	Complete words	Delete one char.	Exchange two char's	Error typing in one char.	Insert one char.
Jaro–Winkler distance*	Time (μs)	76053.3	73032.2	76071	73051.1	71050.5
	Distance	0	0.0013	0.0013	0.0013	0.0132
Longest common substring**	Time (μs)	129091	143120.3	137078.1	139098.5	116082.6
	Similarity	160	153	152	152	158
Levenshtein distance***	Time (μs)	140079.9	146105.4	134087.1	147121.2	127108.1
	Movements	0	1	2	1	1
Damerau–Levenshtein distance***	Time (μs)	160113.8	172122.7	171121.2	169119	142080.9
	Movements	0	1	1	1	1
N-gram****	Time (μs)	41032.7	42030.7	40026.5	39033.3	37026.7
	Similarity	150	140	147	142	139
Dice coefficient*****	Time (μs)	40046.6	41046.9	41027.2	42012.1	48033.4
	Distance	1	0.92	0.938	0.92	0.9235
Overlap coefficient*****	Time (μs)	41045.3	41033.1	40045	42028.7	46031.6
	Distance	1	0.943	0.988	0.953	0.941
Matching coefficient******	Time (μs)	43048.7	56033.9	39013.9	40027.7	44049.4
	Distance	0.5	0.471	0.494	0.476	0.471

*Match=0, Not match=1, **Match=No. of all input char. For all words, No Match=0, ***Match=0, No Match=No. of all input char. for all words, ****Match=No of identical pairs=Σ(each word length−1), No match=0, *****Match=1, No Match=0, ******Match=0.5, No Match=0

Table VI
The Improvement Ratio of the Elapsed Processing Time Measured between the Previously Tested Methods using 10 Words with Different Lengths (1, 2, 3, 16 Characters) and Multiple Changes

The speed ratio between methods		Levenshtein and Damerau–Levenshtein (%)	Dice and overlap (%)	Dice and matching (%)
W.L.	Input status			
1	Complete words	28.22	20.44	0.34
2	Complete words	−0.01	−12.49	12.54
	Delete one char.	−9.25	28.58	14.29
	Exchange two char's	50	−0.25	70.99
	Error typing in one char.	10	−11.08	0.06
	Insert one char.	40.01	25.23	0.24
3	Complete words	14.29	22.22	11.12
	Delete one char.	91.37	−18.77	−18.78
	Exchange two char's	7.02	0.19	−10.01
	Error typing in one char.	21.57	85.77	28.84
	Insert one char.	23.09	10.92	−0.19
16	Complete words	14.31	89.92	7.5
	Delete one char.	17.81	77.93	36.52
	Exchange two char's	27.62	85.42	−4.91
	Error typing in one char.	14.96	73.89	−4.73
	Insert one char.	11.78	47.92	−8.3

http://dx.doi.org/10.14500/aro.10180

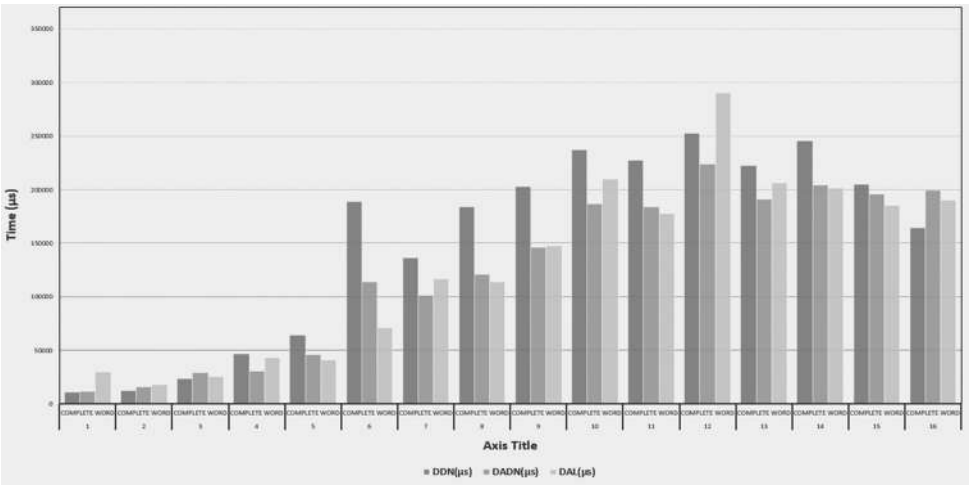

Fig. 1. The new algorithms tested using 10 complete words with different lengths ranging from 1 to 6 characters

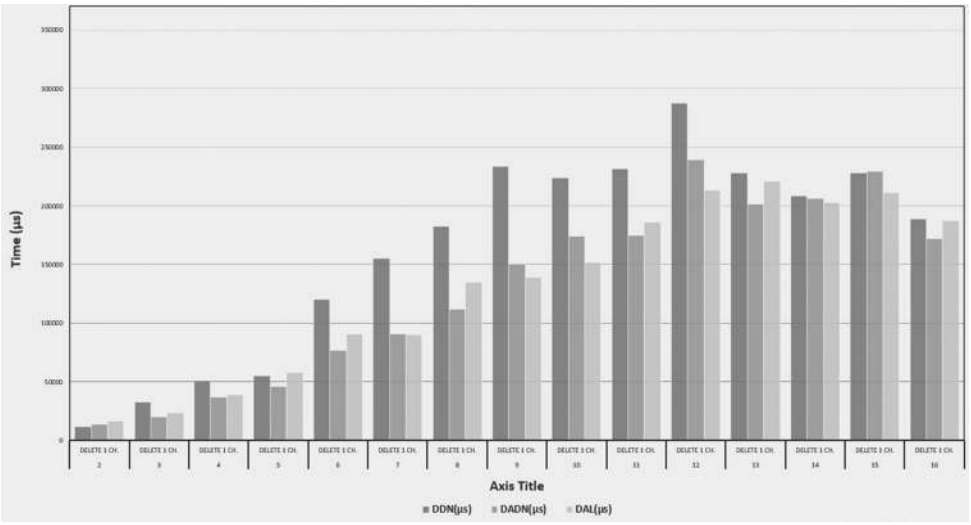

Fig. 2. The new algorithms tested using 10 words with different lengths ranging from 1 to 6 characters with deleting one character

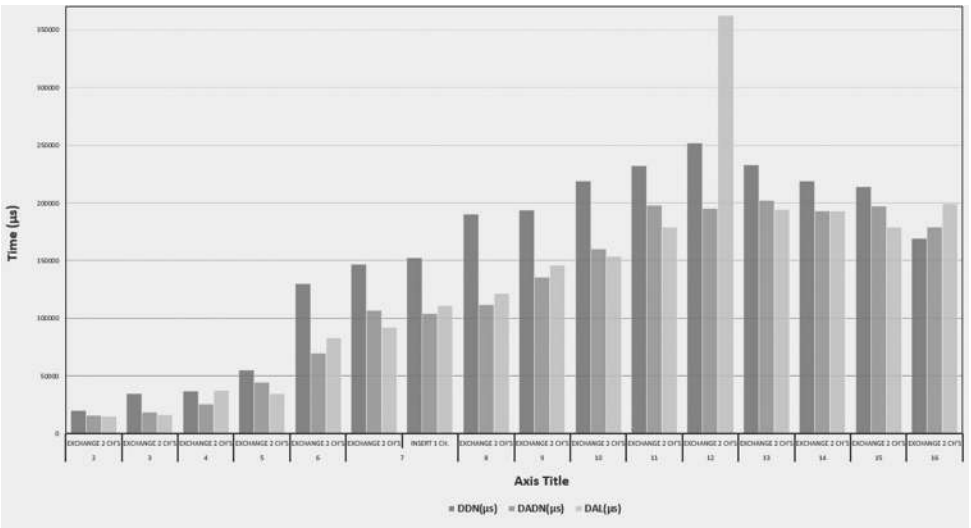

Fig. 3. The new algorithms tested using 10 words with different lengths ranging from 1 to 6 characters with exchange two characters

The test results showed that the proposed implementation of similarity measures reduces the processing time when compared with the commonly implemented methods while maintaining the results accuracy. Furthermore, it can be noticed that the baseline of the execution time is increased dramatically with the increase of words length (i.e., number of characters

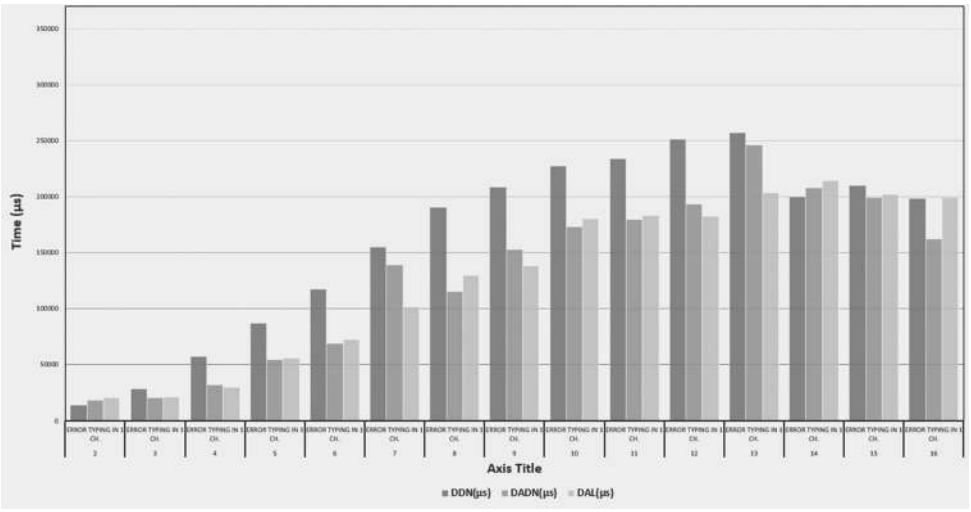

Fig. 4. The new algorithms tested using 10 words with different lengths ranging from 1 to 6 characters with one incorrect character

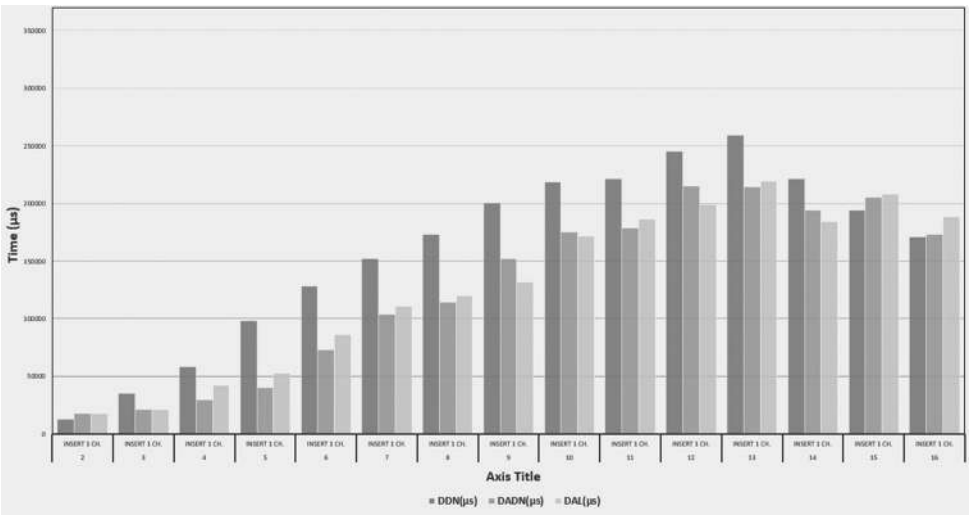

Fig. 5. The new algorithms tested using 10 words with different lengths ranging from 1 to 6 characters with insert one character

in each word) this due to the increase of matching operations that required in each execution. The presented results in Tables VII and VIII indicate that the elapsed time was slightly improved for words have lengths ranging between [1...5 and 14...16]. While the time improvements are relatively large with lengths between [6...13]; it depends on the processing time ratio of DNDA algorithm and DNDAEN algorithm. Hence, to achieve better performance results, the ODNDAEN algorithm is provided; it is used to process words according to some conditions depending on using the suggested enumeration methods. For clarification, the results of processing time improvement were explained using the processing time ratio for the DNDAEN and ODNDAEN algorithms.

IV. Conclusion

A new set of measures was introduced in this article for dealing with strings; it is based on combining some string similarity measures beside to using the string enumeration methodology. It reduces the elapsed time of each string matching operation; this remark can be simply noticed in the listed test results. A set of three combined similarity measures was suggested, and their performance was tested; these combined sets consist of some well-known similarity measures. The test results indicated significant performance improvements are attained when using these combined measures to overcome the lack of accuracy and to save spend time in the matching of misspelled words using the length threshold of words matching.

Furthermore, in this paper, a simple enumeration method was used together with the suggested combined measures to get a new scheme that offers more nearly stable and fast text similarity assessment; this scheme can be used for a wide range of word length. Because these three combined algorithms cause an enhancement in the processing results accuracy by dealing with many different cases that produce similar results (i.e. the same number of movements number of the given compared words). This number was used for measuring the distance between the given words. Hence, to identify the closest word between the given words with similar distances the modified Dice and N-gram algorithm were used.

ARO p-ISSN: 2410-9355, e-ISSN: 2307-549X

http://dx.doi.org/10.14500/aro.10180

Table VII
The Modified DADNEN Tested Using 10 Words with Different Lengths Ranging from 1 to 9 Characters with Multiple Changes

Method name		DADNEN (μs)	Speed ration between DADNEN (μs) and DANA (%)	DADNENs (μs)	Speed ration between DADENs (μs) and DANA (%)	Method name		DADNEN (μs)	Speed ration between DADNEN (μs) and DANA (%)	DADNENs (μs)	Speed ration between ODADNEN (μs) and DANA (%)
W.L.	Input status					W.L	Input Status				
1	Complete words	29038	141.82	12008.9	0.01	6	Complete words	83548.2	−26.77	115081	0.88
2	Complete words	37670.6	135.28	16011	−0.01		Delete one char.	62727.1	−18.6	91064.2	18.19
	Delete one char.	34023.8	140.69	14011.5	−0.89		Exchange two char's	62773.3	−10.39	122087	74.29
	Exchange two char's	41034.3	156.4	11994.7	−25.06		Error typing in one char.	65606.8	−4.99	100073	44.93
	Error typing in one char.	57040.2	216.67	13010.8	−27.77		Insert one char.	66307.9	−9.24	98068.4	34.24
	Insert one char.	43012	138.77	12023.5	−33.26	7	Complete words	130107	28.73	153107	51.48
3	Complete words	49279.6	69.92	18012.8	−37.9		Delete one char.	100552	10.4	139096	52.72
	Delete one char.	44041.2	114.04	17021.2	−17.28		Exchange two char's	102964	−3.84	135096	26.18
	Exchange two char's	42586.5	123.94	17011.6	−10.55		Error typing in one char.	131092	−5.77	149107	7.19
	Error typing in one char.	40029.3	96.78	22030.6	8.3		Insert one char.	120084	15.39	134096	28.85
	Insert one char.	43038.5	104.81	20013.8	−4.77	8	Complete words	124598	2.91	135098	11.58
4	Complete words	46519.1	49.96	36027.5	16.14		Delete one char.	126108	12.7	133094	18.95
	Delete one char.	56056.9	51.4	30021.7	−18.92		Exchange two char's	174124	55.71	146104	30.66
	Exchange two char's	49052.7	88.66	25037.1	−3.71		Error typing in one char.	136784	19	136080	18.39
	Error typing in one char.	55219.2	72.45	30040.3	−6.19		Insert one char.	145103	27.06	138096	20.92
	Insert one char.	46771.4	55.79	27020.3	−10.01	9	Complete words	204146	39.59	164070	12.19
5	Complete words	85060.1	84.79	43032.1	−6.52		Delete one char.	168126	11.66	134081	−10.96
	Delete one char.	55053.8	19.6	45030.8	−2.18		Exchange two char's	175971	29.54	159095	17.12
	Exchange two char's	78039.7	73.3	46038.2	2.24		Error typing in one char.	141642	−7.41	163096	6.63
	Error typing in one char.	55654.6	3	47049.9	−12.94		Insert one char	138238	−9.28	128090	−15.94
	Insert one char.	59425.3	48.55	48020.6	20.04		.				

DADNEN: Dice coefficient, N-gram, and Damerau–Levenshtein using enumeration, ODADNEN: Optimized dice coefficient, N-grame and Damerau–Levenshtein using enumeration, DANA: Dice Ccoefficient, N-grame and Damerau–Levenshtein Measure

Table VIII
The Modified DADNEN Tested Using 10 Words with Different Lengths Ranging from 10 to 16 Characters with Multiple Changes

Method name		DADNEN (μs)	Speed ration between DADNEN (μs) and DANA (%)	DADNENs (μs)	Speed ration between DADENs (μs) and DANA (%)	Method name		DADNEN (μs)	Speed ration between DADNEN (μs) and DANA (%)	DADNENs (μs)	Speed ration between DADENs (μs) and DANA (%)
W.L.	Input status					W.L.	Input Status				
10	Complete words	180127	−3.64	180111	−3.65	14	Complete words	213873	4.77	204127	−8.74
	Delete one char.	177144	1.92	140081	−19.42		Delete one char.	223007	8.18	188132	7.78
	Exchange two char's	199124	24.5	188133	17.63		Exchange two char's	241172	24.87	208148	−0.49
	Error typing in one char.	157921	−8.87	167136	−3.56		Error typing in one char.	227161	9.14	207148	−2.59
	Insert one char.	172124	−1.67	174124	−0.52		Insert one char.	206145	6.2	189115	−11.22
11	Complete words	198179	7.84	160131	−12.88	15	Complete words	200512	2.23	174142	−14.2
	Delete one char.	191103	9.29	161113	−7.87		Delete one char.	206454	−9.91	196620	12.22
	Exchange two char's	177125	−10.44	157128	−20.55		Exchange two char's	199274	1.09	221225	−3.05

(*Contd...*)

Table VIII
(Continued)

Method name		DADNEN (µs)	Speed ration between DADNEN (µs) and DANA (%)	DADNENs (µs)	Speed ration between DADENEs (µs) and DANA (%)	Method name		DADNEN (µs)	Speed ration between DADNEN (µs) and DANA (%)	DADNENs (µs)	Speed ration between DADENEs (µs) and DANA (%)
W.L.	Input status					W.L.	Input Status				
12	Error typing in one char.	170121	−5.33	186147	3.6	16	Error typing in one char.	230162	15.55	193136	−16.11
	Insert one char.	186132	4.2	181111	1.39		Insert one char.	212151	3.41	172122	-18.1
	Complete words	184130	−17.72	191120	−14.6		Complete words	209149	5.03	163115	−1.17
	Delete one char.	218155	−8.92	180127	−24.8		Delete one char.	194139	12.8	170122	2.81
	Exchange two char's	242169	23.97	200140	2.46		Exchange two char's	199141	11.18	184148	9.87
	Error typing in one char.	233164	20.6	209148	8.18		Error typing in one char.	188134	16.04	178120	4.45
	Insert one char.	222781	3.55	198143	−7.91		Insert one char.	188860	8.9	181143	−8.74
13	Complete words	225161	17.8	208152	8.9						
	Delete one char.	192155	−4.47	202140	0.5						
	Exchange two char's	216155	6.94	213150	5.45						
	Error typing in one char.	203981	−17.14	197139	−19.92						
	Insert one char.	234167	9.34	183128	−14.5						

DADNEN: Dice coefficient, N-gram and Damerau–Levenshtein using enumeration, DANA: Dice Coefficient, N-grame and Damerau–Levenshtein Measure

References

Alberto, B., Paolo, R., Eneko, A. and Gorka, L., 2010. Plagiarism detection across distant language Pairs. In: *Proceedings of the 23rd International Conference on Computational Linguistics*. pp.37-45.

Bunke, H. and Bühler, U., 1992. Invariant shape recognition using string matching. In: *Proceedings of 2nd International Conference on Automation*. Robotics and Computer Vision, Singapore.

Burnard, L., 1976. *The University of Oxford Text Archive University of Oxford*. Available from: http://www.ota.ox.ac.uk/catalogue/index.html.

Cortelazzo, G., Deretta, G., Mian, G.A. and Zamperoni, P., 1996. Normalized weighted Levensthein distance and triangle inequality in the context of similarity discrimination of bilevel images. Pattern Recognition Letters, 17(5), pp.431-436.

Cortelazzo, G., Mian, G.A., Vezzi, G. and Zamperoni, P., 1994. Trademark shapes description by string-matching techniques. Pattern Recognition, 27(8), pp.1005-1018.

Damerau, F.J., 1964. A technique for computer detection and correction of spelling errors. Communications of the ACM, 7(3), pp.171-176.

Dice, L.R., 1945. Measures of the amount of ecologic association between species. Ecology, 26(3), pp.297-302.

Fenz, D., Lange, D., Rheinländer, A., Naumann, F. and Leser, U., 2012. Efficient similarity search in very large string sets. In: *International Conference on Scientific and Statistical Database Management*. Springer Berlin, Heidelberg, pp262-279.

Gomaa, W.H. and Fahmy, A.A., 2013. A survey of text similarity approaches. International Journal of Computer Applications, 68(13), 13-18.

Hall, P.A. and Dowling, G.R., 1980. Approximate string matching. ACM Computing Surveys (CSUR), 12(4), pp.381-402.

Kashiap, R.L. and Oommen, B.J., 1984. String correction using probabilistic models. Pattern Recognition Letters, 2, pp.147-154.

Leusch, G., Ueffing, N. and Ney, H., 2003. A novel string-to-string distance measure with applications to machine translation evaluation. In: *Proceedings of MT Summit IX*, pp.240-247.

Martins, B., 2011. A supervised machine learning approach for duplicate detection over gazetteer records. In: *Proceedings of the 4th International Conference on Geospatial Semantics*. Springer, Berlin Heidelberg, pp.34-51.

Marzal, A. and Vidal, E., 1993. Computation of normalized edit distance and applications. IEEE Transactions on Pattern Analysis and Machine Intelligence, 15(9), pp.926-932.

Mohri, M., 2003. Edit-distance of weighted automata: General definitions and algorithms. International Journal of Foundations of Computer Science, 14(6), pp.957-982.

Oommen, B.J., 1987. Recognition of noisy subsequences using constrained edit distances. IEEE Transactions on Pattern Analysis and Machine Intelligence,5, pp.676-685.

Pande, B.P., Pawan, T. and Dhami, H.S., 2013. Generation, implementation and appraisal of an N-gram based stemming algorithm. ArXivpreprint arXiv 1312-4824. Available from: https://arxiv.org/ftp/arxiv/papers/1312/1312.4824.pdf.

Patel, D., 2016. Study of distance measurement techniques in context to prediction model of web caching and web prefetching. International Journal on Soft Computing, Artificial Intelligence and Applications (IJSCAI), 5(1), 1-8.

Peng, H.L. and Chen, S.Y., 1997. Trademark shape recognition using closed contours. Pattern Recognition Letters, 18(8), pp.791-803.

Pradhan, N., Gyanchandan, M. and Wadhvani, R., 2015. A review on text similarity technique used in IR and its application. International Journal of Computer Applications, 120(9), pp.29-34.

Rieck, K. and Wressnegger, C., 2016. Harry: A tool for measuring string similarity. Journal of Machine Learning Research, 17(9), pp.1-5.

Sehgal, V., Getoor, L. and Viechnicki, P.D., 2006. Entity resolution in geospatial data integration. In: *Proceedings of the 14th Annual ACM International Symposium on Advances in Geographic Information Systems.* ACM, New York, NY, pp.83-90.

Sellers, P.H., 1980. The theory and computation of evolutionary distances: Pattern recognition. Journal of Algorithms, 1(4), pp.359-373.

Wang, J., Li, G. and Feng, J., 2014. Extending string similarity join to tolerant fuzzy token matching. ACM Transaction Database Systems, 39(1), pp.1-45.

Winkler, W.E., 1999. The state of record linkage and current research problems. In: *Statistical Research Division, US Census Bureau*. Available from: http://www.census.gov/srd/www/byname.html.

Integrated Use of Geoelectrical Resistivity and Geochemical Analysis to Assess the Environmental Impact on Soil and Groundwater at Erbil Dumpsite, West of Erbil City - Iraqi Kurdistan Region

Sirwa Qader S. Gardi

Department of Geology, College of Science, University of Salahaddin,
Erbil, Kurdistan Region - F.R. Iraq

***Abstract* - Water is one of the most important commodities which people and other creatures have exploited more than any other resources for their survival. Many parts of Erbil City and surroundings rely on groundwater reserves for drinking and other purposes. The study area lies within Erbil plain, some 10 km west of Erbil City. The study is based on the electrical resistivity method as a tool for assessing the environmental impact on soil and groundwater. Soil and water samples were collected close to Erbil dumpsite to assess the baseline data. 28 vertical electrical sounding points were taken by Schlumberger array along three geoelectrical sections. These sections revealed five zones of alternating clastic sediments with lateral changes which represent the Bai Hassan Formation. The average depth from the surface to the top of the aquifer is about 80 m. The geoelectrical sections revealed that the septic tank discharge valleys have been polluting the soil in two zones in the vicinity of the household septic discharge site. On the other hand, no adverse impact on groundwater quality is anticipated in the present project. The geophysical method utilized in this study is fast, efficient, and cost-effective in delineating the extent of the probable contamination zone(s).**

***Index Terms*—Resistivity, Geochemical, Groundwater, Soil, Dumpsite, Erbil.**

I. Introduction

During the past few years, the concern about the protection of the environment has largely increased due to the contaminants mainly with the anthropogenic origin and has affected and continue to threaten human resources, especially air quality, surface soil, and groundwater. The major problem facing the construction of new communities or development is the source of water. Kurdistan region, like many parts of the world, experiences problems in terms of shortage and degradation. Many factors affect water pollution such as industrial, agriculture, and the wastes and affluence released by human activity. With the dwindling price of oil and the most likelihood of future reliance on water for agriculture and industrial activities (agriculture, industry, and domestic), surface and groundwater sustainability and integrity are of paramount importance in Kurdistan region. In the cities of Kurdistan, the rate of abstraction in some areas exceeds recharge from rain and snow. Therefore, its protection is part of our responsibility of both governorate and public.

Iraqi Kurdistan Region has experienced an economic development, intense urbanization, and change in consumption patterns that have resulted in an increase of solid waste generation. As a result of population growth and construction expansion, there is a large increase in demand for water, building material, and cleared land, and consequently, in the amount of industrial and domestic waste production.

Groundwater resources have been under rapidly increasing stress in large parts of the world due to pollution. Pollution is primarily the result of irrigated agriculture, industrialization, and urbanization, which generates diverse wastes, with the attendant impact on the ecosystem and groundwater. With a rapid increase in population and growth of industrialization, groundwater quality is being increasingly threatened by the disposal of urban and industrial solid waste (Raju, *et al*., 2011; Singh, *et al*., 2015a).

Groundwater is a major source of water supply for domestic, agricultural, recreational, and industrial purposes in Erbil. Consequently, the adequacy of groundwater resources, both in quality and quantity, is essential for socioeconomic sustainability in the area. Groundwater resources are very important for public water supply. Many of the environmental problems are directly or indirectly related to the location of groundwater and its protection from contamination sources of various kinds.

The environment at which waste is disposed poses a major problem on groundwater. Solid wastes are produced every day in urban societies as a result of human activities and in

ARO-The Scientific Journal of Koya University
Volume V, No 2(2017), Article ID: ARO.10192, 13 pages
DOI: 10.14500/aro.10192
Received 14 January 2017; Accepted 02 October 2017
Regular research paper: Published 25 October 2017
Corresponding author's e-mail: sirwa.gardi@su.edu.krd

an attempt to dispose off these materials; man has carelessly polluted the environment (Badmus, *et al*., 2014). Pollution from solid wastes always begins with precipitates carrying the leachates into land surface and ends with the water reaching surface water or groundwater. During the vertical percolation process (with rainwater), the water leaches both organic and inorganic constituents from refuse. The leachates become part of the groundwater flow system immediately reaching the water table. The effects are generally the same, but their level may be changed according to the region (Gulmez, 1999).

Among all the surface geophysical techniques for shallow subsurface prospecting, electrical resistivity method is the most widely applied method for this purpose. Geoelectrical measurements are an important and integral component of geophysical investigations connected with environmental problems. Electrical resistivity survey methods have been widely used to solve engineering, archeology, environmental, and geological problems in the past decades (Adli, *et al*., 2010).

In groundwater studies, several geophysical methods have been deployed since late 1915, of which the electrical method has shown a wider approach and better applicability in groundwater science (Arshad, *et al*., 2007). Among those, electrical methods have been found very suitable for such studies, due to the conductive nature of most contaminants (Jegede, *et al*., 2012).

The study was assisted with the use of the geophysics, namely, the electrical resistivity method, as a tool to examine this impact, employed to characterize the contaminant through changing resistivity behavior pattern.

Vertical electrical sounding (VES) survey and hydrochemical analysis of the water and soil samples from the surrounding wells in the study area were adopted. These were used to determine the contamination spread both in lateral and vertical directions.

The aim of the study is to provide an understanding of the ground conditions (geological and hydrogeological information) pertaining to Erbil dumpsite. This study is hoped to enable a scientific approach to assess the environmental impacts on soil and groundwater based on the resistivity and geochemical methods of the subsurface layers.

II. Study area and description

The study area site lies within Erbil plain, about 10 km west of Erbil City, covering about 7 km^2 with Latitude 36° 11’ 40.60”N and Longitude 43° 53’ 05.10”E (Fig. 1), and located on a hill conjoined by two drainage valleys. The elevation of this site is about 435m above sea level.

The Erbil dumpsite operation life is since year 2001 (Municipal ministry) and currently receives all types of solid waste. Daily disposal is about 1000 ton of solid waste of varied types.

The location is generally used for any type of general household waste. The waste dumped at this site includes domestic waste, for example, kitchen waste, food leftovers, paper, newspaper, metal and glass cans, packaging, plastic, glass, cartoon, wood, metals, ceramics, leather, cloths, and batteries (Fig. 2). These wastes can spontaneously ignite and produce noxious smoke smell and which varies according to waste composition with greater risk to the operating management staff. Construction and demolition wastes, which consist of sand, bricks, and concrete block, are also dumped. Dumping activities started from the top of the site by merely toppling the waste over the edge.

Some components of the waste are very hazardous or toxic such as liquid solvents seen along one of the valleys, north of the Erbil dumpsite ridge. Furthermore, it was observed that black water from household septic tanks was also discharged nearby the site.

With an increasing population in Erbil City, as the capital of the Iraqi Kurdistan Region, and changing production and consumption patterns in the past few years, the levels of degrading waste are increasing at alarming rates.

Existing waste disposal sites are rapidly filling up and with the ever-increasing costs for disposal of waste; it is becoming very difficult and expensive to dispose of food waste which is the main waste in the Erbil dumpsite. Therefore, any sector that generates food waste is facing a potentially huge disposal problem, particularly those establishments catering on a large scale, such as hospitals, schools, universities, Ministry of Defense sites, prisons, hotels, restaurants, and even shopping centers and parks, in addition to household food waste. The wastes in the Erbil dumpsite are decomposing continually, and a sludge of decomposed soup known as leachate will develop.

III. Geology and hydrogeology of the study area

The study area lies within the Chemchamal-Butma subzone of the foothill zone, which is the central unit of the Unstable Shelf. Butma-Chemchemal subzone, however, has very conspicuous long and deep synclines with thick Pliocene molasses dominated by a conglomerate, and the strata are neccessarily horizontal (Jassim and Goff, 2006). Erbil plain is considered to be among these plains as a broad syncline between two main anticlinal structures, Pirmam from the east and Khurmala-Avana from the west (Hassan, 1998). The inner parts of the synclines contain quaternary deposits, referred to here as the polygenetic synclinal fill. The geological formations in the study area are described from the older to younger rock units as follows: Mukdadiya Formation (Pliocene): It comprises of fining upward cycles of gravely sandstone, sandstone, and red mudstone (Jassim and Goff, 2006) and Bai Hassan Formation (Pliocene): It consists of molasses sediments represented by alternation of clay stones and conglomerates with some sandstones and siltstones, variations from one of the main constituents to the other, both laterally and vertically is very common (Hassan, 1998). The major part of the study area is covered by this formation (Fig. 3). No accurate information is present about the thickness of this formation and quaternary deposits (Pleistocene- Holocene): Quaternary sedimentary veneer of polygenetic origin covers large areas in the synclines of the foothill zone. These synclines often have

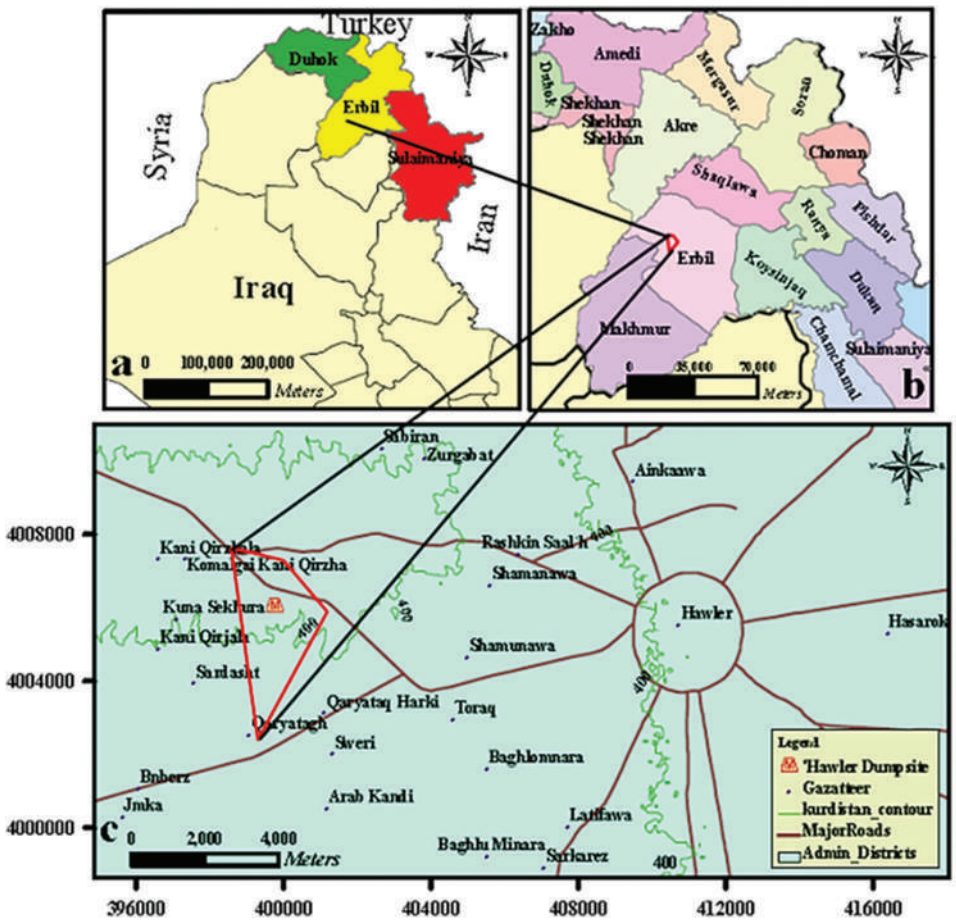

Fig. 1 (a) Iraq, location of Erbil province is indicated, (b) Kurdistan Region of Iraq, and (c) Erbil City, location of the study area is indicated (red line)

Fig. 2 Variety types of solid waste in the Erbil dumpsite

a central river system that cuts across or flows parallel to their axes, and the sediments filling the synclines consist mainly of a mixture of gravel and clay (Jassim and Goff, 2006).

Erbil hydrogeological basin is bounded by Greater Zab from north and Lesser Zab to the south. Erbil basin is a wide depression located between southern limb of Pirmam anticline and Dibaga hill zone (Zurgah Zraw Zurg) which gives a semicircular shape to Erbil basin (Majeed and Ahmad, 2002). The Pliocene formations, and especially the Bai Hassan, is considered as a major aquifer in the Erbil basin, and it is a continental deposit of gravel, conglomerate, sand, and clay. Depth to groundwater varies in short distances due to variable topography. In general, the Erbil Basin is divided into three sub-basins, which include the Northern (Kapran) sub-basin, the Central sub-basin, and the Southern (Bashtapa) sub-basin (Habib, *et al*., 1990). The study area is located in the central sub-basin. This sub-basin has an area of 1400 km^2. The formations in this sub-basin are the Mukdadiya and Bi Hassan Bakhtiary Formations and alluvium. The Bi Hassan formation consists of gravel, sand, clay, and conglomerate strata. However, in some of the deep wells in the Mukdadiya, formation consists of thin beds of gravel, sand, or conglomerate. The materials of alluvium aquifers are the same as Bi Hassan Bakhtiari Formation, with the exception that they contain silt in between the other layers instead of multiple clay layers (Dizayee, 2014). According to Hassan (1998), the groundwater table depth ranges between 30 and 50 m in Erbil City, and according to Al-Ansari, *et al*. (1981), the water table is usually 50 m deep. Hassan (1998), during his study, noticed that the groundwater moves from east to west side of the Erbil city, so it flows in the same direction as regional groundwater flows.

http://dx.doi.org/10.14500/aro.10192

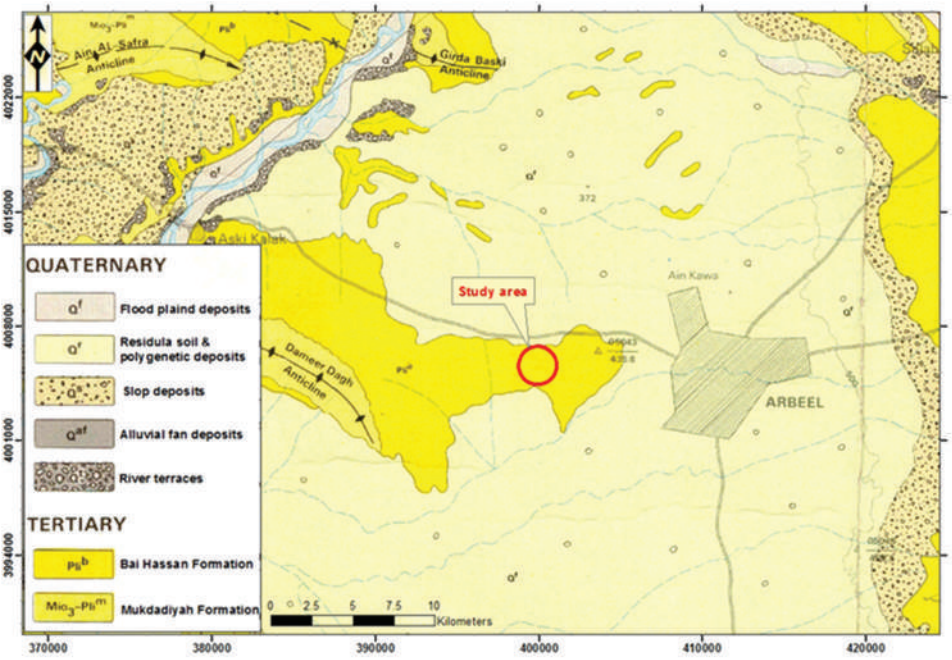

Fig. 3 Geological map showing the study area (After Sissakian, 1997)

IV. Methods of Investigation

A. Geophysical Technique

Resistivity measurements with electrical resistivity method are one of the simplest methods to be used in geophysics. Electrical method is used to determine the subsurface resistivity distribution by making suitable measurements on the surface. VES is used in this study to measure variation in resistivity with depth. VES uses direct current (DC) injected into the ground surface to investigate the subsurface electrical resistivity (Vladimir, *et al*., 2006). DC resistivity methods use artificial sources of current to produce an electrical potential field in the ground. A current is introduced into the ground through point electrodes (A and B) and the potential field is measured using two other electrodes (the potential electrodes M and N) (Fig. 4). As the potential between M and N, the current introduced through A and B, and the electrode configuration is known, the resistivity of the ground can be determined; this is referred to as the "apparent resistivity" (Knodel, *et al*., 2007).

The resistivity survey was completed with twenty-eight VES points along three traverses A-A^{-}, B-B^{-}, and C-C^{-} (Fig. 5). An ABEM Terrameter SAS 300B was utilized to acquire the VES data. The Schlumberger array was used with a maximum current electrode spacing (AB) ranging from 600 to 800 m (AB/2 ranging from 300 to 400 m). Schlumberger field array is usually used because it has proven effective for groundwater exploration (Edwards, 1977; Zohdy, *et al*., 1984). The Schlumberger configuration is symmetric and collinear and uses four electrodes (Evanston, 1979). The spacing between the potential electrodes is fixed and is less than the separation between the current electrodes which is progressively increased during the survey (Oghenekohwo,

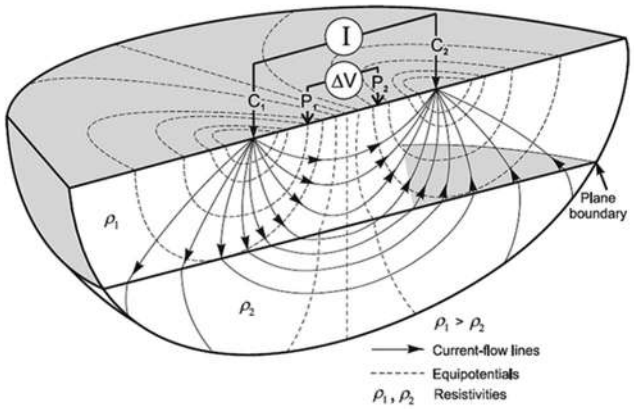

Fig. 4 Principle of resistivity measurement with four-electrode array (Knodel, *et al*., 2007). Where C1 = A, C2 = B, P1 = M, and P2 = N

2008). In a traditional Schlumberger or Wenner electrical sounding, the transmitting A and B electrodes are successively moved away from each other at each new reading to increase the depth of investigation (Bernard, 2003). The measured resistance values were converted into apparent resistivity (ρa) by multiplying with a geometric factor (K), such that

$$\rho a = \frac{\pi\left[\left(AB/2\right)^2 - \left(MN/2\right)^2\right]}{MN} \quad (1)$$

$$\rho a = K.R \quad (2)$$

The length of each traverse is 700 m, 800 m, and 900 m, respectively. The direction of the first and second traverses is parallel which are directed from NW to SE and the last traverse is directed from NE to SW. Location fixing and topographical heightening of the sample points and wells were achieved by means of twelve channel global

positioning system (GPS) set - the "GARMIN GPS 12." The resistivitimeter measures the apparent resistance directly. These measurements are then converted to apparent resistivity values by scaling them by a geometrical factor that depends on the type of array as well as the spacing between the electrodes. The last VES point was taken near the Tashyapi well to calibrate the instrument. The sounding spacing was about 100 m, and four of these VES points have been conducted near to existing wells for correlation purposes and obtaining the lithological and hydrogeological information (Fig. 4). The key to the success of any geophysical survey is the calibration of the geophysical data with hydrogeological and geological ground true information (Lashkaripour and Nakhaei, 2005). The spreading of electrodes is parallel to the general structure direction around the study area (NW-SE), though the beds in the study area are distributed subhorizontally because they are distributed in the broad polygenetic deposits.

B. Geochemical Methods

Soil and water samples were collected nearby the Erbil dumpsite to assess the baseline data.

Soil sample analysis

Soil samples were collected from different locations at about 25 cm depth within the activity area including three samples (Fig. 6). The pH of soil samples was measured by pH meter equipment and electrical conductivity (EC) by EC equipment in the Chemistry Department laboratory in Science College-Salahaddin University. The soil class is clay loam in first two samples and silty clay loam in sample three. The pH of soil is strongly alkaline based on the classification of Al-Agidi (1989) (Table I).

Fig. 5 Map showing the vertical electrical sounding points and calibration wells at the study area

Water sample analysis

Furthermore, water samples were collected from three water wells at different locations above and behind the Erbil dumpsite (Fig. 6). Major cations and anions were analyzed to determine the level of their contamination. The result obtained was compared with the International standard for drinking water after "WHO" to determine the level of contamination (If any). The pH measurements show that all water samples are of basic type. The chemical composition of the water wells compared with the WHO (2003) is given in (Table II). All water analyzed samples are suitable for drinking and irrigation.

Analyzed in the laboratory of Directorate of Water Quality Control Department in Erbil.

V. Geophysical Data Processing

There are many computer programs to compute and process the resistivity field data. Inspite of various uses of different programs, the final decision or assessment of inversion results is dependent on the user (geophysicist). Several computer programs are available for the inversion, allowing data processing, as well as editing of data sets and sounding array parameters or shifting of overlapping segment to produce continuous sounding curves. The inversion method is equivalent to matching automatically the observed and theoretical curves (Lowrie, 1997). The interpretation as determined by the program is mathematically correct but may not necessarily correspond to reality (Compbell and Horton, 2000). The interpretation of each VES curve was carried out by the use of automated interpretation computer program IPI2WIN (2001) (Fig. 7).

The IPI2WIN program is designed for VES and/or induced polarization data curves or 1D interpreting along a single profile, obtained with any of a variety of the most

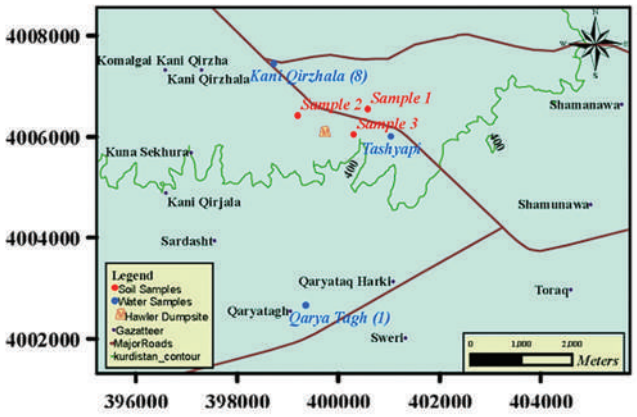

Fig. 6 Map showing water and soil samples locations

Table I Soil Sample Analysis

Sample No.	Class (Mirsal, 2008)	Texture (grain size) (Al-agidi, 1989)	Color (Munsell Book of Color, 1975)	Moisture content%	pH	EC (mS/cm)
1	Clay loam	Moderately to medium	Very dark brown	16.96	8.7	8.25
2	Clay loam	Moderately to medium	Dark-yellowish brown	13.25	8.7	13
3	Silty clay loam	Moderately to medium	Dark-yellowish brown	15.61	8.6	9.95

http://dx.doi.org/10.14500/aro.10192

TABLE II WATER SAMPLE ANALYSIS (MG/L)

Parameters	Tashyapi	Kani Qirzhala	QaryaTagh	WHO (2003)
Turbidity (NTU)	0.6	0.4	0.4	5
pH	7.6	7.4	7.1	8
EC (mmho/cm)	1062	703	516	1530
T.D.S.	680	450	330	1000
Hardness (as mg ($caco_3$)/l)	340	232	286	500
Ca	44	47	49	200
Mg	39	43	38	150
Na	16	9	12	200
K	0.51	0.65	0.59	3
HCO_3	20	31	37	200
SO_4	47	41	44	250
Cl	29	21	11	250
NO_3	5	8	8	50

popular arrays used in the electrical prospecting. It is presumed that a user is an experienced interpreter willing to solve the geological problem posed as well as to fit the sounding curves (Geoscan-M Ltd., 2001). In this program, the half distance between current electrodes spacing (AB/2), potential electrode spacing (MN), and apparent resistivity measurements is given to obtain resistivity curves.

VI. GEOPHYSICAL INTERPRETATION

The field results of the study are presented in both qualitative (curve shapes) and quantitative interpretations. Vertical sounding field curves can interpret qualitatively using simple curve shapes, semi-quantitatively with graphical

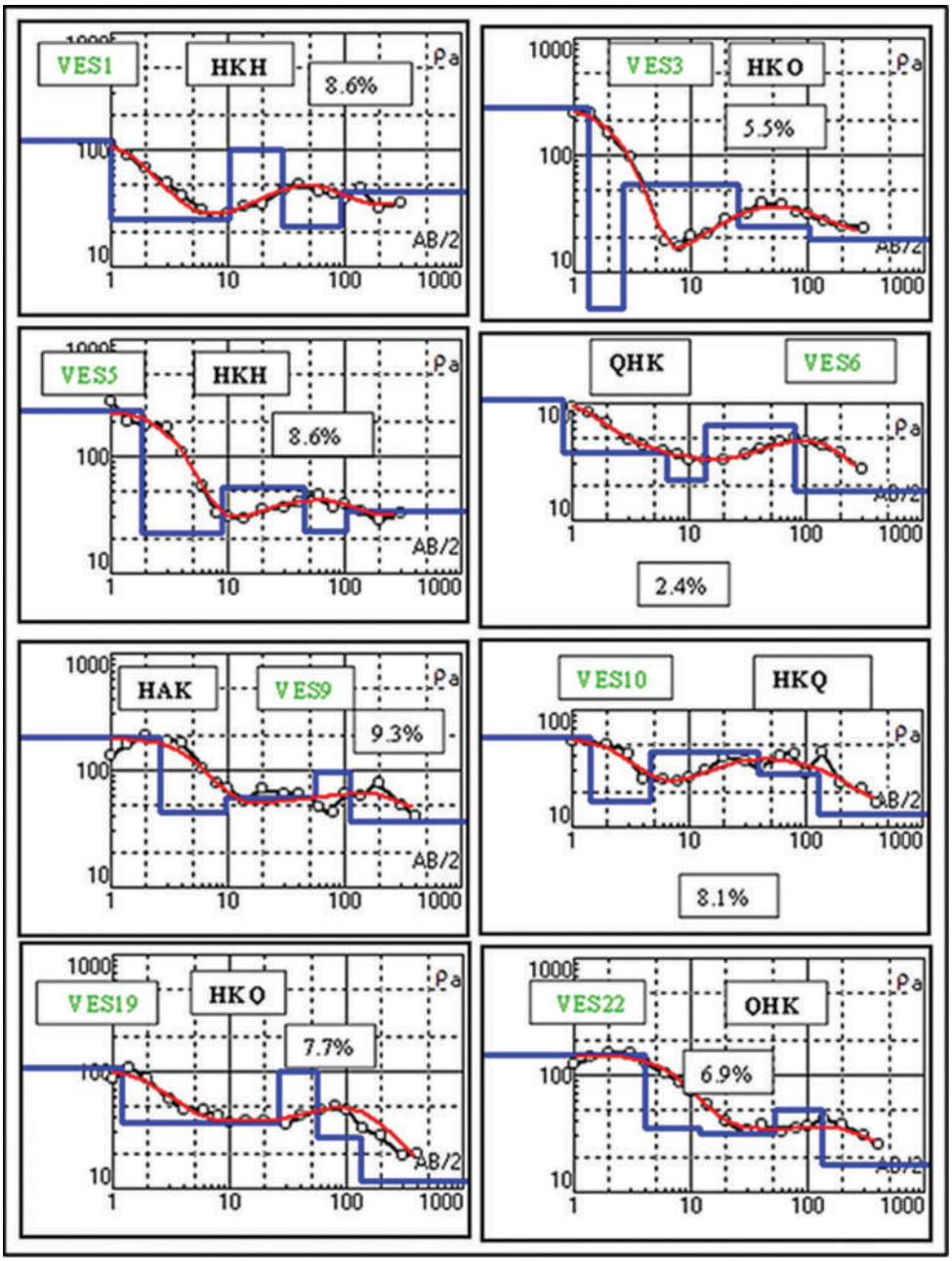

Fig. 7 Some examples of field curves along traverses A-A⁻, B-B⁻, and C-C⁻ interpreted by IPI2WIN (2001). X- axis: Resistivity (Ω.m), Y- axis: Spacing (AB/2) (m). Where VES9: VES point, HKQ: Curve type and 8.1% error percentages

model curves, or quantitatively with computer modeling (Reynolds, 2011). In the qualitative interpretation, the shape of the field curve is observed to get an idea qualitatively about the number of layers and the resistivity of layers. The results of this method of interpretation involved isoapparent electrical resistivity maps and geoelectrical pseudosections. In the quantitative method geoelectrical parameter, that is, true resistivity and layer thickness are obtained. The main objective of the quantitative interpretation of VES curve is to obtain the geoelectrical parameters and geoelectric section. A geoelectric layer is called by its fundamental characters, resistivity "ρ" and thickness "h." It is hoped that the results of this study could also be used to determine the groundwater potentials of the study area.

A. Qualitative Interpretation

The first stage of any interpretation of apparent resistivity sounding curves is to note the curve shape. A first appraisal of an area hydrogeologically can often be obtained by merely looking at the shapes of the field curves (type curves) and the ranges of apparent resistivity values. The shapes of curves are dependent on the thickness, resistivity, and outer electrode spacing of layers. Due to the distinctive characteristics feature in the field of the apparent resistivity curves, the VES stations show various types of field curves. These types of curves were defined in terms of the number of geoelectrical layers and their respective resistivity relationships.

Twenty-eight VES points were taken. We can group these VES points into ten groups, which all VES points are composed of five layers (Fig. 7). They reflect that the study area is composed of various types of sediments (heterogeneous). Among these types of curves, most of them are layer resistivities decreasing with depth. Such layers prove the presence of a low resistivity layer at the bottom of the section. By collecting the prior information from the water wells near the study area and geological information which have been conducted around and nearby the study area, we can conclude that the study area is composed of clastic materials.

B. Quantitative Interpretation

The mathematical analysis for quantitative interpretation of resistivity results is most highly developed for the vertical sounding technique (Telford, *et al.*, 1990). The quantitative treatment of the VES provided geoelectrical information characterized by the values of true resistivity and thickness. These geoelectrical parameters define the geoelectrical model. The latter will provide resistivity models whose layer boundaries are boundaries of geoelectrical layers but not necessarily of lithological layers (Knodel, *et al.*, 2007). The inversion of the field data was done using the IPI2WIN (2001) program (Table III). The results of inverse modeling are very close to the manual interpretation. The IPI2WIN data were used for interpretation and making geoelectrical sections. The geoelectrical model was determined as a function of the calibration with the data from wells and the resistivity contrast between high and low values. Overall, the results confirm that topographical variations of the study area can have a significant impact on measured resistivity data values and show that the significance of the distortions will vary according to the details of the topography and survey type. The resulted data (true resistivity and thickness) can be interpreted quantitatively through the geoelectrical sections.

VII. Geoelectrical sections

Geoelectrical sections can be constructed by linking a number of VES points which are located along one straight line. They will show the vertical and lateral distribution of resistivities of subsurface layers. Each layer in geoelectrical sections is characterized by its thickness and ranges of true resistivity and will give an idea of the kind of rock present in the subsurface, and hence, a model of the subsurface can be prepared (Oghenekohwo, 2008).

The resulting geoelectric models are used to produce three geoelectrical sections: Traverses A-A¯, B-B¯, and C-C¯. Each section has its characteristics of true resistivity and depth, and its lithology can be interpreted in detail in each geoelectrical section.

A. Geoelectrical Section Along Traverse A-A¯

This section shows the presence of five subsurface geoelectrical zones (Fig. 8). A first (Z1) continuous thin surface nearly horizontal zone is represented by topsoil with resistivity ranging from 47 to 421 Ω.m. These variations in

Table III The True Resistivity, Thickness, and Curve Types of Each Layer Which was Interpreted by IPI2WIN (2001) Program

VES No.	True resistivity (Ω.m)					Thickness (m)			
	ρ1	ρ2	ρ3	ρ4	ρ5	h1	h2	h3	h4
VES1	119.0	25.6	99.2	21.7	43.7	0.99	9.36	18.7	65.7
VES 2	47.1	3.82	322.0	26.1	17.6	1.06	1.59	6.07	66.4
VES 3	253.0	3.16	56.0	24.3	18.8	1.35	1.29	23	76.7
VES 4	421.0	35.7	50.3	23.8	17.7	1.22	18.4	41.1	40.8
VES 5	247.0	21.8	55.1	22.8	33.6	1.84	6.98	36.0	57.5
VES 6	108.0	37.7	21.7	64.6	17.8	0.83	5.56	7.52	66.2
VES 7	252.0	48.0	28.5	49.2	22.2	0.26	2.23	17.6	62.9
VES 8	274.0	38.7	25.5	69.5	16.3	1.3	9.86	21.2	50.7
VES 9	190.0	43.7	58.2	95.5	36.1	2.63	7.07	47.2	54.5
VES 10	58	16.8	43.5	28.5	12.8	1.43	3.32	34.3	87.6
VES 11	51.25	26.55	46.41	26.99	14.94	1.24	4.31	41.51	95.06
VES 12	98.0	27.90	37.70	22.50	11.70	1.77	3.52	55.4	66.0
VES 13	111.0	25.30	78.60	28.70	12.90	1.58	12.8	39.40	73.80
VES 14	139.0	28.4	81.1	17.0	10.20	2.45	8.78	46.1	58.5
VES 15	131.0	37.80	20.40	31.90	61.0	1.32	6.44	22.9	100.0
VES 16	106.0	10.70	59.70	11.10	26.70	1.71	3.43	19.90	101.0
VES 17	77.5	165	58.7	28.4	21.0	1.02	0.94	58.1	69.0
VES 18	112.0	27.5	161.0	69.0	15.30	6.19	33.4	36.60	54.90
VES 19	106.0	36.10	98.50	26.90	11.40	1.2	25.4	29.90	76.60
VES 20	117.0	49.90	28.80	22.20	33.40	2.87	20.2	30.0	77.0
VES 21	192.0	1.96	46.20	29.50	10.20	4.43	4.38	33.90	88.30
VES 22	146.0	35.80	31.60	49.90	17.20	4.08	8.05	40.50	80.70
VES 23	58.8	99.20	34.20	28.20	34.40	0.83	8.88	49.0	72.30
VES 24	41.9	79.5	21.10	25.20	46.80	0.90	20.40	22.0	88.0
VES 25	27.80	42.60	67.90	30.0	37.20	2.22	8.45	24.90	96.20
VES 26	48.6	93.10	20.30	15.10	35.90	1.92	9.54	29.60	89.8
VES 27	88.70	40.40	22.80	33.60	13.50	0.78	11.8	24.30	94.40
VES 28	192.0	42.10	17.60	35.0	16.40	2.55	12.40	22.40	94.70

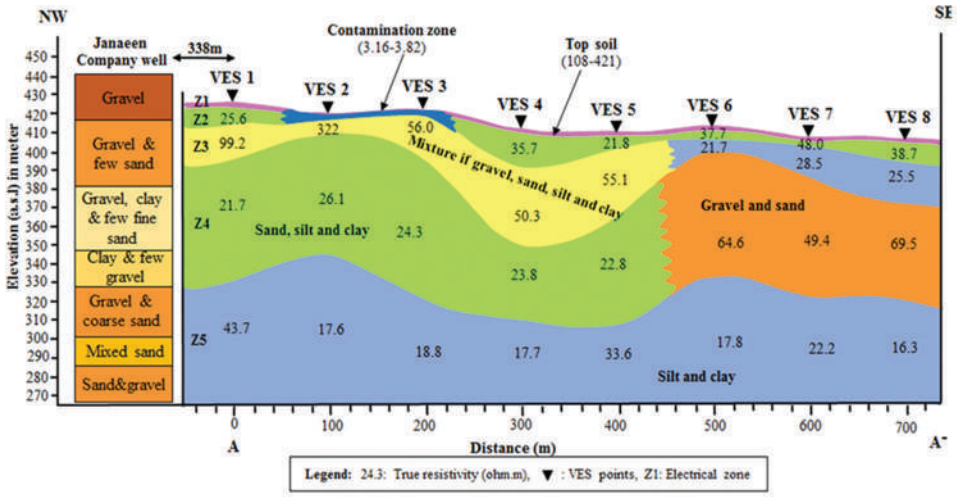

Fig. 8 Geoelectrical section along traverse A-A¯

resistivity value occur due to various types of sediments, fine and medium, to coarse grained material of sand and gravel with high ratio of relatively coarse gravel. The thickness varies from 0.25 to 1.85 m. The second geoelectrical zone (Z2) has resistivity ranging from 3.0 to 48.0 Ω.m and thickness ranging from 1.0 to 18.0 m. The resistivity is diagnostic of fine-grained sediments such as sand, silt, and clay. This geoelectrical section is in a contaminated area and shows a low resistivity ranging from 3.0 to 4.0 Ω.m under VES points VES2 and VES3 compared to those of the uncontaminated layer outside the disposal site and thickness of 1.0-1.5 m. It may be contaminated with the septic tanks discharge. Furthermore, the curve type is of HKQ type which shows the low resistivity value in this layer. The resistivity of the third zone (Z3) has values from 50.0 to 322.0 Ω.m and thickness ranging from 6.0 to 41.0.5 m. This horizon is composed of mixture gravel, sand, silt, and clay. The resistivity value under VES point VES2 is too high (322 Ω.m), due to the increase of the ratio of gravel toward the NW compared to other continuous VES points which are composed of mixture of gravel, sand, silt, and clay with lateral change to silt and clay (21.0-28.5 Ω.m) and thickness ranging from 7.0 to 21.0 m under VES points 6, 7, and 8. The fourth geoelectrical zone (Z4) of this geoelectrical section has resistivity ranging from 21.0 to 26.0 Ω.m and thickness from 40.0 to 76.0 m. This layer consists of sand, silt, and clay with lateral changes to a mixture of gravel, sand, silt, and clay (49.0-70 Ω.m) and thickness ranging from 50.0 to 66.0 m toward the Southeast direction of the study area. The fifth geoelectrical zone (Z5) has resistivity value ranging from 16.0 to 43.0 Ω.m. The thickness of this layer is not defined since it is the last layer. This layer consists of fine sediments such as silt and clay saturated with groundwater.

B. Geoelectrical Section Along Traverse B-B¯

This section shows the presence of five subsurface geoelectrical zones, which nearly has the same lithology, with difference of the layer thicknesses (Fig. 9): A first (Z1) is a continuous thin surface nearly horizontal zone is represented by topsoil with resistivity ranging from 51.0 to 191.0 Ω.m. These variations in resistivity value occur due to various types of sediments, fine and medium, to coarse-grained sand and gravel with variable size. The thickness varies from 0.5 to 2.5 m. The second geoelectrical zone (Z2) has resistivity ranging from 11.0 to 40.0 Ω.m and thickness ranging from 3.0 to 13.0 m. This horizon is not found under VES point 17. The resistivity is diagnostic of fine-grained sediments such as sand, silt, and clay. Furthermore, the curve type of this traverse shows the low resistivity value of HKQ type. The resistivity of the third zone (Z3) ranges from 37.0 to 81.8 Ω.m and thickness ranges from 20.0 to 58.0 m and becomes thinner at about 20.0-23.0 m under VES points 15 and 16. This horizon is composed of a mixture of gravel, sand, silt, and clay with high ratio of gravel under VES points 13 and 14. This horizon contains lens representing silt and clay (20.4 Ω.m) of about 23 m under VES point 15. The fourth geoelectrical zone (Z4) in this geoelectrical section has resistivity ranging from 11.0 to 32.0 Ω.m and thickness from 54.5 to 101.0 m. This horizon consists of sand, silt, and clay while the VES point 9 has high resistivity value (95.5 Ω.m) with about 69.0 m which may be interpreted due to increasing the ratio of gravel and sand toward the Northwest direction of the study area. The fifth geoelectrical zone (Z5) which represents an aquifer of groundwater has resistivity value ranging from 10.0 to 36.0 Ω.m (the curve types of this traverse are of HKQ and KQQ type) lateral lithological variations to coarser material with resistivity (61.0 Ω.m) under VES point 15 (as shown in curve type QHA). The thickness of this horizon is not defined since it is the last horizon. This horizon consists of fine sediment such as silt and clay with lateral lithological variations to coarser material such as a mixture of gravel, sand, silt, and clay.

C. Geoelectrical Section Along Traverse C-C¯

Furthermore, this section shows the presence of five subsurface geoelectrical zones. Thickness and lithology of the layers are as follows (Fig. 10): A first (Z1) uncontinuous thin surface nearly horizontal zone occurs at along traverse

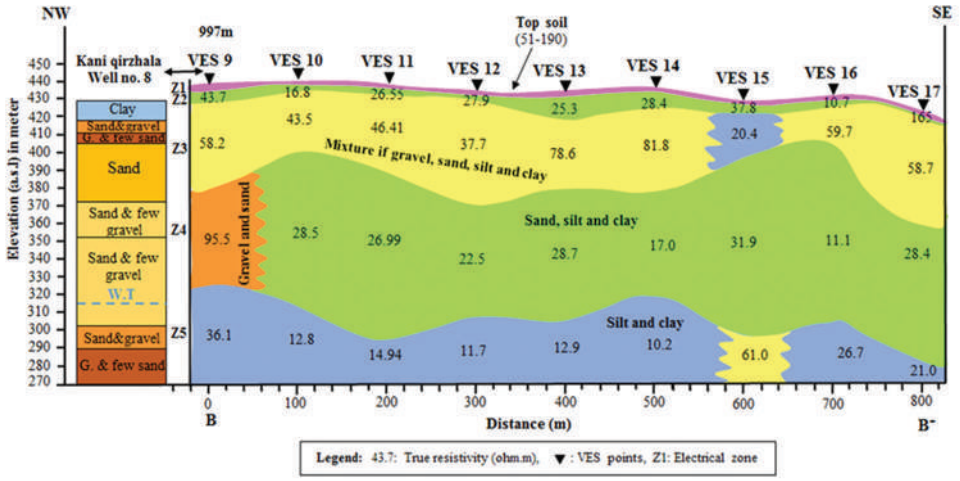

Fig. 9 Geoelectrical section along traverse B-B¯

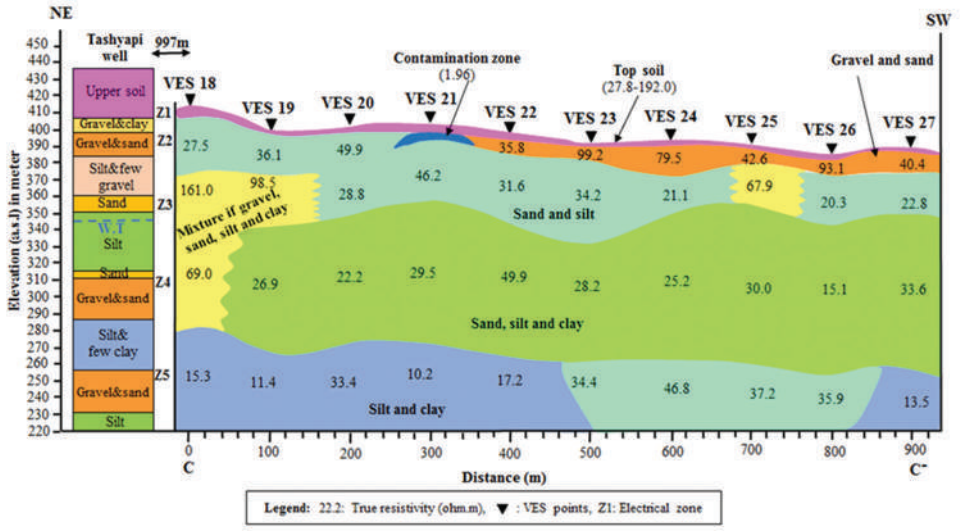

Fig. 10 Geoelectrical section along traverse C-C¯

represented by topsoil with resistivity ranging from 28.0 to 192.0 Ω.m. These variations in resistivity value occur due to various types of materials, fine- and medium-grained material of sand and gravel. The thickness varies from 0.8 to 6.0 m. The second geoelectrical zone (Z2) has a resistivity ranging from 27.5 to 99.2 Ω.m and a thickness ranging from 8.0 to 33.0 m. This horizon is composed of a mixture of gravel, sand, silt, and clay. In this section, a lens was shown within this horizon having a resistivity of about 2.0 Ω.m with a thickness about 4.5 m beneath VES point 21 (as shown in curve types HKQ). This lens may be representing the contaminated area because it is susceptible to pollution by septic tank discharges. The third geoelectrical zone (Z3) in this section has a resistivity ranging from 20.0 to 46.0 Ω.m and a thickness ranging from 22.0 to 49.0 m. This horizon is composed of sand and silt with lateral changes to a mixture of gravel, sand, silt, and clay with resistivities ranging from 67.0 to 161.0 Ω.m and a thickness ranging from 25.0 to 36.0 m under VES points 18, 19, and 25. Al-Naqib (1959) according to a geological study on the Bai Hassan formation mentioned that it is composed of an alternation of conglomerate, clay, and sand as large lenses and lateral rapid changes. Furthermore, the fourth geoelectrical zone (Z4) is present, and the same lithology (aquifer) was observed with relatively higher resistivity than other two geoelectrical sections, ranging from 15.0 to 50.0 Ω.m except under VES point 18 [69.0 Ω.m] due to changes in the lithology to mixture of gravel, sand, silt, and clay. This horizon consists of sand, silt, and clay which represent an aquifer of good quality groundwater. The thickness of this aquifer ranges from 55.0 to 96.0 m. The fifth geoelectrical zone (Z5) has resistivity value ranging from 10.0 to 33.0 Ω.m which is composed of fine sediments such as silt and clay with lateral variation to sand and silt (34.0-47.0 Ω.m). The thickness of this horizon is not defined since it is the last horizon.

VIII. Hydrogeological assessment

The results of the three geoelectrical sections in the study area show successions with variable lithology and thickness.

http://dx.doi.org/10.14500/aro.10192

This lithology reflects the Bai Hassan formation as given by Buday (1980) as he mentioned that the formation consists of molasses sediments represented by the alternation of clays and conglomerate with some sandstones and siltstones. The horizon that is composed of silt and clay and sand and silt is representing an aquifer in the study area in both tarverses A-A¯ and B-B¯, whereas in traverse C-C¯, the sand, silt, and clay horizon represent an aquifer. According to Stevanovic and Iurkiewicz (2009), it consists almost entirely of terrigenous clastics from silt size to boulder conglomerates (eroded and transported from the Zagros Mountains). The successive repetition of the fine-, medium-, and coarse-grained textures and the variation in permeability from one site to another within the same aquifer horizon are typical characteristics of this aquifer. Ghaib (2003) and Ghaib and Aziz (2002) during their studies on parts of Erbil City concluded that the resistivity of the saturated rock unit (mixture of clay, silt, sand, and gravel) ranges from 15 to 45 Ω.m. It is in a good agreement with the resistivity of the aquifer unit in the geoelectrical sections ranging from 10 to 69 Ω.m. The depth to the top of the aquifer from the surface is approximately ranging from 35.0 to 129.0m (Table IV). From the ground surface as the deep water, table has been detected ranging from 55 to 94 m by Ghaib and Aziz (2002) in parts of Erbil city. There is a deeper water table which was drilled; it may be due to the drought condition which has been facing our region since that time.

IX. Environmental assessment of resistivity study (detection of contamination zone)

From the results of geoelectrical resistivity, the contaminated area was indicated by its low resistivity value if compared with surrounding area. The contamination zone is detected in the geoelectrical section along traverse A-A¯ under VES points 2 and 3 in the contaminated area by septic tanks. The thickness of this zone is about 1.0-1.5 m (Figs. 11-13) which shows the impact of septic tanks to the near subsurface layers. In this study, we choose the spacing that shows the effect of the contamination which is related to the environment. It can flow by infiltration from the surface to the downward due to the high porosity and permeability of the lithology. If this process is continued, it may be in contact with groundwater surface and finally contaminate the groundwater. The depth that is subjected to contamination from the surface is about (1.0-18.0 m). The contamination zone at the geoelectrical section along traverse C-C¯ was detected also by its vicinity to the septic tank discharging valley (Fig. 14). The thickness of this zone is about 4.0 m under VES point 21. The water is from the Bakhtiari aquifer, and recent deposits are generally also of good quality, with the exception of the waters from shallow wells, located near cities and villages, which are often contaminated, mainly as a result of the free seepage of sewage water (Stevanovic and Iurkiewicz, 2009). The contamination zone is not detected at the geoelectrical section along traverse B-B¯ because it is far away from the dumpsite and septic tank impacts.

Table IV Represent the Depth, Resistivity, and Elevation of the Top Surface of Aquifer

VES NO.	Elevation a.s.l (m)	Depth to the top of aquifer (m)	Elevation of top surface of aquifer a.s.l (m)	Resistivity of aquifer (Ω.m)
VES1	426	94.7	421.3	43.7
VES 2	420	75.1	344.9	17.6
VES 3	423	102.0	321.0	18.8
VES4	413	102.0	311.0	17.7
VES5	411	102.0	309.0	33.6
VES6	414	80.1	333.9	17.8
VES7	407	83.0	324.0	22.2
VES8	407	83.1	323.9	16.3
VES9	438	111.0	327.0	36.1
VES10	440	127.0	313.0	12.8
VES11	438	127.6	310.4	14.9
VES12	434	127.0	307.0	11.7
VES13	434	128.0	306.0	12.9
VES14	437	116.0	321.0	10.2
VES15	429	131.0	298.0	61.0
VES16	432	126.0	306.0	26.7
VES17	423	129.0	294.0	21.0
VES18	414	76.2	337.8	69.0
VES19	400	56.5	343.5	26.9
VES20	402	53.1	348.9	22.2
VES21	403	42.7	360.3	29.5
VES22	398	52.6	345.4	49.9
VES23	392	58.7	333.3	28.2
VES24	393	43.3	349.7	25.2
VES25	391	35.6	355.4	30.0
VES26	385	41.1	343.9	15.1
VES27	388	36.9	351.1	33.6

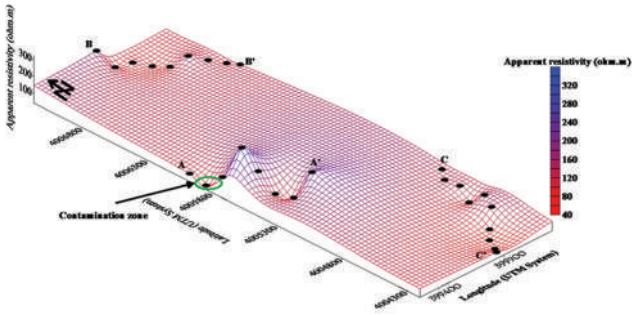

Fig. 11 Three-dimensional illustration of apparent resistivity values for half distance current electrode (1.4 m) (the origin of the block diagram coincides at each of the electrical sounding points [VES1-VES27])

X. Results and discussion

Areas near waste disposal sites have greater possibility of groundwater and soil contamination because of the potential pollution source of leachate and septic tanks discharge area originating from the nearby site. Such contamination of groundwater resource poses a substantial risk to local resource user and to the natural environment.

Erbil dumpsite, agricultural, and industrial activities (Fig. 15) have been identified as the main pollution sources to groundwater and soil in the study area. The main flows of heavy metals to the environment are from industrial and municipal wastes, both of which contained a variety of toxic

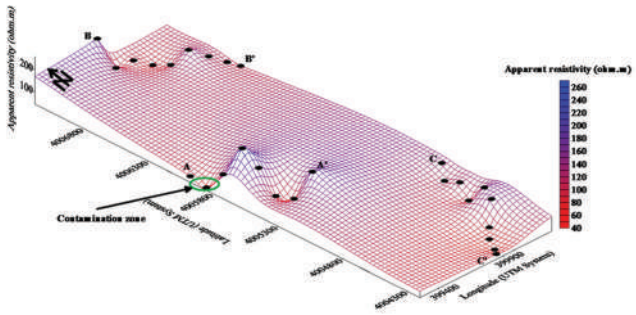

Fig. 12 Three-dimensional illustration of apparent resistivity values for half distance current electrode (2 m) (the origin of the block diagram coincides at each of the electrical sounding points [VES1-VES27])

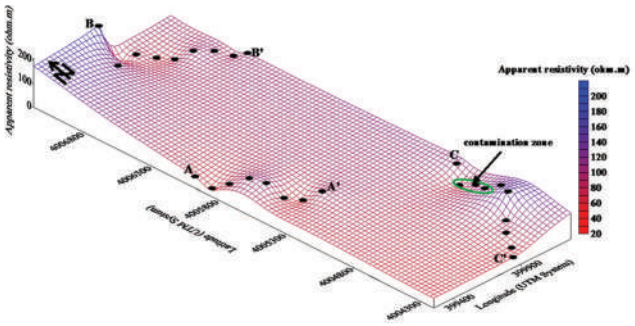

Fig. 14 Three-dimensional illustration of apparent resistivity values for half distance current electrode (4 m) (the origin of the block diagram coincides at each of the electrical sounding points [VES1-VES27])

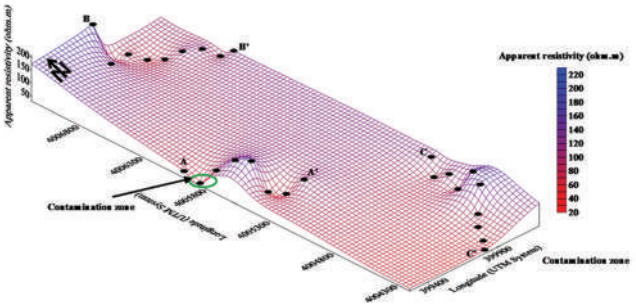

Fig. 13 Three-dimensional illustration of apparent resistivity values for half distance current electrode (3 m) (the origin of the block diagram coincides at each of the electrical sounding points [VES1-VES27])

Fig. 15 Industrial wastes in the study area (agricultural plots)

heavy metals (Chuangcham, *et al*., 2008). This problem is important, especially when industrial wastes are involved because many of these substances are resistant to biological or chemical degradation, and thus, are expected to persist in their original form for many years, perhaps even for centuries (Fatta, *et al*., 1999).

Groundwater from the quaternary aquifer is suitable for the use as a source of drinking water and for industrial uses. However, development of the contaminated sources in the study area is threatening the quality of the groundwater.

Contamination of groundwater can take place if the waste disposal site containing above substances gets leached and percolates into the groundwater table. Hence, no adverse impact on groundwater quality is anticipated in the present project. Even in the very long term (on a timescale of several 100 years), when these sources are continued, the potential impacts on groundwater quality are predicted to be slight.

The geophysical investigation revealed that the resistivity value of the study area near the dumpsite is relatively low about 3.0-4.0 Ω.m in VES points 2 and 3 compared to those of the uncontaminated areas outside the disposal site as we mentioned it. The electrical resistivity anomaly near the dumping site was related to septic tank discharges plumes which appear to have seeped at depth as far as 1.5 m below the surface.

The soil at the study area was found to be incapable of preventing the migration of contaminants, vertically and/or horizontally from the source point. Hence, this illustrates that the septic tank discharge valley has been polluting the soil as well as increasing its vulnerability not only to the soil and groundwater but also capable to have an effect on the fauna and flora.

The short pathway needed for these contaminants before reaching groundwater was enhanced by periodic water table fluctuations and infiltrating water during the rainy season. These metals accumulate near the soil surface and decrease with depth due to adsorption to soil particles. Adsorption occurs on surfaces of clay minerals, hydrous oxides or iron and aluminum, and organic matter (GWMAP, 1999). Furthermore, the nature of geology has important role to infiltrate the pollutants through it, as the geological composition of the study area is of clastic materials which have higher effect to infiltrate. This with time may reach to the groundwater and can contaminate it.

According to Shyler, *et al*. (2009), important soil characteristics that may affect the behavior of contaminants include soil mineralogy and clay content (soil texture); pH of the soil; amount of organic matter in the soil; moisture levels; temperature; and presence of other chemicals.

Septic waste discharged to coarse-textured soils proceeds vertically through the unsaturated zone and into groundwater (Fig. 16). Once in groundwater, a septic plume develops and moves with groundwater flow. Approximate times for septic effluent to pass through the unsaturated zone to groundwater range from a few hours to 50 days, depending on the volume of effluent and the distance to groundwater (Robertson, *et al*., 1991; Robertson, 1994 and Robertson and Cherry, 1995).

Nitrate is the primary chemical of concern in most septic plumes. Nitrate plumes slowly attenuate as a result of dilution from recharge water and dispersion within the aquifer. Nitrate concentrations can exceed drinking water criteria at distances of 100 m or more from the drain field (GWMAP, 1999).

Fig. 16 (a) Convoy of waste loading tankers heading toward the site, (b) sewage is discharged at one point, and (c) developing little stream as consequence to continued discharge

Factors that may affect an aquifer's susceptibility to nitrates and the concentration of nitrates in groundwater include land-use, climate, topography, groundwater flow, infiltration rates, subsurface biogeochemical conditions, bedrock types, and soil characteristics (Lindsey, *et al*., 1997; Nolan and Hitt, 2003).

XI. Conclusions and recommendations

Based on sample analysis and the interpretation of the resistivity data both qualitatively and quantitatively, seven types of curve types were obtained, and geoelectrical sections along three traverses conclude the following points:

1. The results of water sample analysis at three different locations show that they are within the acceptable limits according to the WHO (2003). All water analyzed samples are suitable for drinking and irrigation uses.
2. The results of soil sample analysis at three different locations at far distances away from the dumpsite show that they are clay loam types with pH of strongly alkaline with EC of 8.0- 13.0 m/cm.
3. In general, resistivity values indicate a decreasing trend with depth due to an increase in the fine sediments with some lateral changes.
4. The resulting geoelectric models are used to produce three geoelectric sections: Traverses A-A^{-}, B-B^{-}, and C-C^{-}. Each section has its characteristics of true resistivity, depth, and its lithology can be interpreted in detail, the following zones are outlined:
   - (Z1): A thin surface layer occurs in all traverses represented by topsoil with resistivity ranging from 28-421 Ω.m. These variations in resistivity value occur due to various types of materials, fine- and medium-grained material of sand and gravel. The thickness varies from 0.5 to 6.0 m.
   - (Z2): This zone has resistivity ranging from 3.0 to 40.0 Ω.m and composed of fine-grained sediments such as sand, silt, and clay with a thickness ranging from 1 to 18 m in traverses A-A^{-} and B-B^{-}, whereas in the traverse C-C^{-}, the resistivity ranges from 27.0 to 99 Ω.m and the thickness ranges between 8.0 and 33.0 m. This layer is composed of a mixture of gravel, sand, silt, and clay.
   - (Z3): This zone has a resistivity ranging from 20.0 to 322.0 Ω.m and a thickness ranging from 6.0 to 58.0 m. This horizon is composed of a mixture of gravel, sand, silt, and clay. Within this horizon, the lenses or lateral changes occur with the resistivity ranges from 20.0 to 40.0 Ω.m, and the thickness ranges between 7.0 and 49.0 m) This horizon is composed of sand, silt, and clay.
   - (Z4): This zone has resistivity ranging from 11.0 to 50.0 Ω.m and a thickness ranging from 41.0 to 101.0 m. It consists of sand, silt, and clay, which represents an aquifer for groundwater in traverse C-C^{-}.
   - (Z5): This zone has a resistivity value ranging from 10.0 to 44.0 Ω.m and composed of silt and clay, in traverse B-B^{-}, the lens occurs which is composed of a mixture of gravel, sand, silt, and clay and has resistivity (61.0 Ω.m). Furthermore, the traverse C- C^{-} is composed of silt and clay with lateral variation to sand and silt with resistivity ranges from 34.0 to 47.0 Ω.m. The thickness of this layer is not defined since it is the last layer.
5. The average depth from the surface to the top of the aquifer is about 80 m.
6. The septic tank discharges valley has been polluting the soil. While no adverse impact on groundwater quality is anticipated in the present project.
7. From the results of geoelectrical sections, the contaminated area occurred and revealed very low resistivity compared with surrounding area.
8. It iss recommended that the UNESCO program for solid waste management protocol should be enacted to ensure groundwater integrity in the urban parts of the region.

References

Adli, Z.H., Musa, M.H. and Arifin, M.N.K., 2010. Electrical resistivity of subsurface: Field and laboratory assessment. World Academy of Science, Engineering and Technology, 69, pp.805-808.

Al-Agidi, W.K., 1989. Pedology-soil survey and classification. *Ministry of Higher Education and Science Research, College of Agriculture, Soil Department.* Baghdad University, Mosul University Press, Arabic.

Al-Ansari, N.A., Hedeff, I.E. and Salim, Y.N., 1981. Water resources in Iraq. Journal of the Geological Society of Iraq, 14(1), pp.35-42.

Al-Naqib, K.M., 1959. Geology of the Southern Area of Kirkuk Liwa. Iraq, Iraqi Pet. Com. Ltd., pp.50

Arshad, M., Cheema, J.M. and Ahmed, S., 2007. Determination of lithology and groundwater quality using electrical resistivity survey. *International of Agriculture and Biology*, 9(1), pp.143-146.

Badmus, B.S., Ozebo, V.C., Idowu, O.A., Ganiyu, S.A., Olurin, O.T. and Atayese, A.O., 2014. Assessment of microbial contamination of groundwater near solid waste dumpsites in basement complex formation, using total plate count method. Nature and Science, 12(9), pp. 113-118.

Bernard, J., 2003. Short Notes on the Depth of Investigation of Electrical Methods. Available from: http://www.iris-instruments.com/Pdf_file/Resistivity_Imaging/methods_depth_investigation.pdf.

Buday, T., 1980. The regional geology of Iraq. *Stratigraphy and Paleogeography.* Vol. 1. Publications of GEOSURV, Baghdad, p445.

Chuangcham, U., Wirojanagud, W., Charusiri, P., Milne-Home, W. and Lertsirivorakul, R., 2008. Assessment of heavy metals from landfill leachate contaminated to soil: A case study of Kham Bon landfill, Khon Kaen province, NE Thailand. Journal of Applied Sciences, 8(8), pp.1383-1394.

Compbell, D.L. and Horton, R.J., 2000. *Graph and Tables Used to Describe Electrical Measurement of Samples of Unconsolidated Material.* USGS Petrophysical Laboratory-Denver, Open-File Report, Denver, p.16.

Dizayee, R., 2014. *Groundwater Degradation and Sustainability of the Erbil Basin, Erbil, Kurdistan Region, Iraq*. College of Science and Engineering, Texas Christian University, Fort Worth, Texas, p.84.

Edwards, L.S., 1977. A modified pseudo section for resistivity and IP. Geophysics, 42(5), pp.1020-1036.

Evanston., 1979. Earth Resistivity Manual. Evanston, Soil Test, INC. pp.52.

Fatta, D., Papadopoulos, A. and Loizidou, M., 1999. A study on the landfill leachate and its impact on the groundwater quality of the greater area. Environmental Geochemistry and Health, 21, pp.175-190.

Geoscan-M Ltd., 2001. *IPI2win Program, IPI- Res2, IPI- Res3 Users Guide. V. 2.1*. Moscow State University, Moscow, p.25.

Ghaib, F.A. and Aziz, B.K., 2002. A combination of electrical resistivity and gravity measurements for groundwater prospection in parts of Erbil city. Journal of Duhok University, 6(1), pp.105-111.

Ghaib, F.A., 2003. *Geophysical Survey for Groundwater in Some Selected Basins of Erbil Governorate. International Report*. FAO representation in Iraq, Erbil Sub-Office, p.69.

Gulmez, P., 1999. Predictive Tools in Environmental Impact Assessment of Solid Waste Projects. p.21.

GWMAP, Ground Water Monitoring and Assessment Program., 1999. *Effects of Septic Systems on Groundwater Quality.* Published by Minnesota Pollution Control Agency, Baxter, Minnesota, p.37.

Habib, H.R., Al-Saigh, N.H. and Hassan, Z.M., 1990. *Geochemistry of Under Groundwater in Erbil City, Iraq. Mosul University*, Mosul, Iraq, pp.173-188.

Hassan, E.O., 1998. *Urban Hydrogeology of Erbil City Region, Unpublished Ph.D. Thesis*, University of Baghdad, Iraq.

Jassim, S.Z. and Goff, J.C., 2006. *Geology of Iraq*. Published by Dolin, Prague and Moravian Museum, Brno, p.341.

Jegede, S.I., Ujuanbi, O., Abdullahi, N.K. and Iserhien-Emekeme, R.E., 2012, Mapping and monitoring of leachate plume migration at an open waste disposal site using non-invasive methods. Research Journal of Environment and Earth Science*,* 4(1), pp.26-33.

Knodel, K., Lange, G. and Voigt, H.J., 2007. Environmental geology, handbook of field methods and case studies. *Hannover Federal Institute for Geosciences and Natural Resources*. Springer Books, Heidelberg, p.1357.

Lashkaripour, G.R. and Nakhaei, M., 2005. Geoelectrical investigation for the assessment of groundwater conditions: A case study. Annals of Geophysics, 48(6), pp.937-944.

Lindsey, B.D., Loper, C.A. and Hainley, R.A., 1997. *Nitrate in Ground Water and Stream Base Flow in the Lower Susquehanna River Basin, Pennsylvania and Maryland, United States Geological Survey, Water-Resources Investigations Report 97-4146*. Lemoyne, Pennsylvania.

Lowrie, W., 1997. *Fundamentals of Geophysics.* Cambridge University Press, Cambridge. p.354.

Majeed, R.A. and Ahmad, M.A., 2002. *Brief References on Hydrogeological Characters of Erbil Basin*. Unpublished Report, Erbil-Iraq.

Mirsal, I.A., 2008. *Soil Pollution, Origin, Monitoring and Remediation*. 2nd ed. Springer, New York.

Munsell Book of Color, 1975. Munsell Color Co., Inc., Baltimore, Maryland, U.S.A.

Nolan, B.T. and Hitt, K.J., 2003. *Nutrients in Shallow Ground Waters Beneath Relatively Undeveloped Areas in the Conterminous United States, U.S. Geological Survey*. Water-Resources Report 02-4289, Denver, Colorado.

Oghenekohwo, F.O., 2008. A comparision of resistivity and electromagnetics as geophysical techniques. Postgraduate Diploma, 48, p.27.

Raju, N.J., Shukla, U.K. and Ram, P., 2011. Hydrogeochemistry for the assessment of groundwater quality in Varanasi: A fast-urbanizing center in Uttar Pradesh, India. Environmental Monitoring and Assessment, 173(1-4), 279-300.

Reynolds, J.M., 2011. *An Introduction to Applied and Environmental Geophysics*. Wiley-Blackwell, Chichester, UK, p.698.

Robertson, W.D. 1994. Chemical fate and transport in a domestic septic system: Site description and attenuation of dichlorobenzene. Environmental Toxicology and Chemistry, 13, pp.183-191.

Robertson, W.D. and Cherry, J.A., 1995. *In situ* denitrification of septic-system nitrate using reactive porous media barriers: Field trials. Ground Water, 33, pp.99-111.

Robertson, W.D., Cherry, J.A. and Sudicky, E.A., 1991. Ground-water contamination from two small septic systems on sand aquifers. Ground Water, 29, pp.82-92.

Shyler, H., McBride, M. and Harrison, E., 2009. *Sources and Impacts of Contaminants in Soils*. Cornell Waste Management Institute, Cornell University, Ithaca, NY, p.6.

Singh, S., Raju, N.J. and Nazneen, S., 2015a. Environmental risk of heavy metal pollution and contamination sources using multivariate analysis in the soils of Varanasi environs, India. Environmental Monitoring and Assessment, p.187. DOI: 10.1007/s10661-015-4577-4.

Sissakian, V.K., 1997. *Geological Map of Iraq, Scale 1:250000.* 1st ed. GEOSURV, Baghdad, Iraq.

Stevanovic, Z. and Iurkiewicz, A., 2009. Groundwater management in Northern Iraq. Hydrogeology Journal, 17, pp.367-378.

Telford, W.M., Geldart, L.P. and Sheriff, R.F., 1990. *Applied Geophysics.* 2nd ed. Cambridge University Press*,* Cambridge, p.770.

Vladimir, S., Rodríguez, O.D., Mousatov, A., Hernández, D.F., Martínez, H., Ryjov, A., 2006. Estimation of soil petrophysical parameters from resistivity data: Application to oil-contaminated site characterization. Geofísica Internacional, 45(3), pp.179-193

World Health Organization, WHO, 2003. *Guide Line for Drinking Water Quality*. 3rd ed., Vol. 1. WHO, Geneva, Switzerland, p.540.

Zohdy, A.A.R., Eaton, G.P. and Mabey, D.R., 1984. *Applications of Surface Geophysics to Groundwater Investigations: Department of Interior US Geological Survey, Third Printing.* US Government Printing Office, Washington, p.116.

http://dx.doi.org/10.14500/aro.10262

Factors Controlling the Development of Straight Valleys and Streams in the Kurdistan Region, North and Northeast of Iraq

Varoujan K. Sissakian[1,2], Ahmed T. Shihab[3] and Arsalan A. Othman[4]

[1]Department of Natural Resources Engineering and Management, School of Science and Engineering, University of Kurdistan Hewler, Erbil, Kurdistan Region - F.R. Iraq

[2]Private Consultant Geologist Ainkawa, Erbil 44001, Kurdistan Region - F.R. Iraq

[3]Iraq Geological Survey, Al-Andalus Square, Baghdad 10068, F.R. Iraq

[4]Iraq Geological Survey, Sulaymaniyah Office, Sulaymaniyah, Kurdistan Region - F.R. Iraq

***Abstract*–The Iraqi Kurdistan Region is a mountainous area with relief difference ranging from few hundred meters up to 3000 m, and locally more. Almost all of the mountains form anticlines that have NW–SE trend changing westwards of longitude to E–W. The carapace of the majority of the mountains is built up of Cretaceous rocks; however, some of them are of older rocks. Many of those anticlines are crossed by straight valleys and/or are crossed by streams and rivers which form again straight lines and almost coincide with regional lineaments, usually in N–S or NE–SW trend. The studied straight valleys are controlled, most probably by tectonic factors, therefore, exhibit special topographic forms, like straight lineaments crossing many successive anticlines, and also clear bending in some of the ridges in their crossing points to the valleys and/or streams. This paper aims to determine and discuss the factors that control the development of the straight valleys and/or lineaments. To achieve this aim, remote sensing and GIS techniques were followed, using Landsat, QuickBird images as well as geological maps of different scales, and different published articles.**

***Index Terms*–Iraq, Lineament, Straight valley, Zagros.**

I. Introduction

The northern and north-eastern parts of Iraq (Iraqi Kurdistan Region) form physiographically mountainous areas with very rugged topography, including many shallow plains; all of them are almost tectonically controlled (Sissakian and Fouad, 2012). The relief differences of the mountains are highly variable in different parts, increasing north- and northeast-wards and attaining up to 3000 m, and exceptionally more. This rugged topography with the presence of long and narrow anticlines (Sissakian and Fouad, 2012; Fouad, 2012; Othman and Gloaguen, 2014; 2013a; 2013b) and climatic effect has contributed in increasing the intensity of the erosion, the water being the main agent. Consequently, the anticlines are deeply dissected by tens of erosional forms, which are continuously developing and enlarged in size due to the continuous growth of the anticlines (Keller and Pinter, 2002; Huggett, 2007; Ramsey, *et al*., 2008).

The main aim of this study is to delineate and discuss the factors controlling the development of straight valleys that drain many developed wine glass forms in many anticlines within the study area.

The location of this study extends in the northern and northeastern parts of Iraq; it almost coincides with the southern limits of the Low Folded Zone in Iraq, which runs along the southern limits of Himreen–Makhoul–Sinjar Mountains (Fig. 1). The coverage area of the study area is about 83240 km^2. The studied area is located, physiographically in the extremely rugged, high amplitude mountainous and low mountainous provinces (Sissakian and Fouad, 2012), whereas tectonically, it is located in the Outer Platform of the Arabian Plate with small part of the Iranian Plate "Sanandaj–Sirjan Zone" (Fouad, 2012). The exposed rocks in the study area range from Ordovician up to Pliocene, but the Cretaceous rocks being the most widely exposed (Sissakian and Fouad, 2012).

A. Materials Used and Methodology

To achieve the main goal of this study, many materials were used represented by geological maps, at the scale of 1:100,000 and 1:250,000, topographical maps, at the scale of 1:100,000, Google Earth, DEM, and satellite images such as QuickBird data, with 0.6 m spatial resolution.

The geological and topographical maps with the satellite images of Landsat 8 Operational Land Imager (OLI) and QuickBird images were used to recognize those anticlines, which exhibit straight valleys and/or streams, in the studied

ARO-The Scientific Journal of Koya University
Volume V, No 2(2017), Article ID: ARO.10262, 17 pages
DOI: 10.14500/aro.10262
Received 06 September 2017; Accepted 25 October 2017
Regular research paper: Published 05 November 2017
Corresponding author's e-mail: ahmed.t.alrubaie@gmail.com

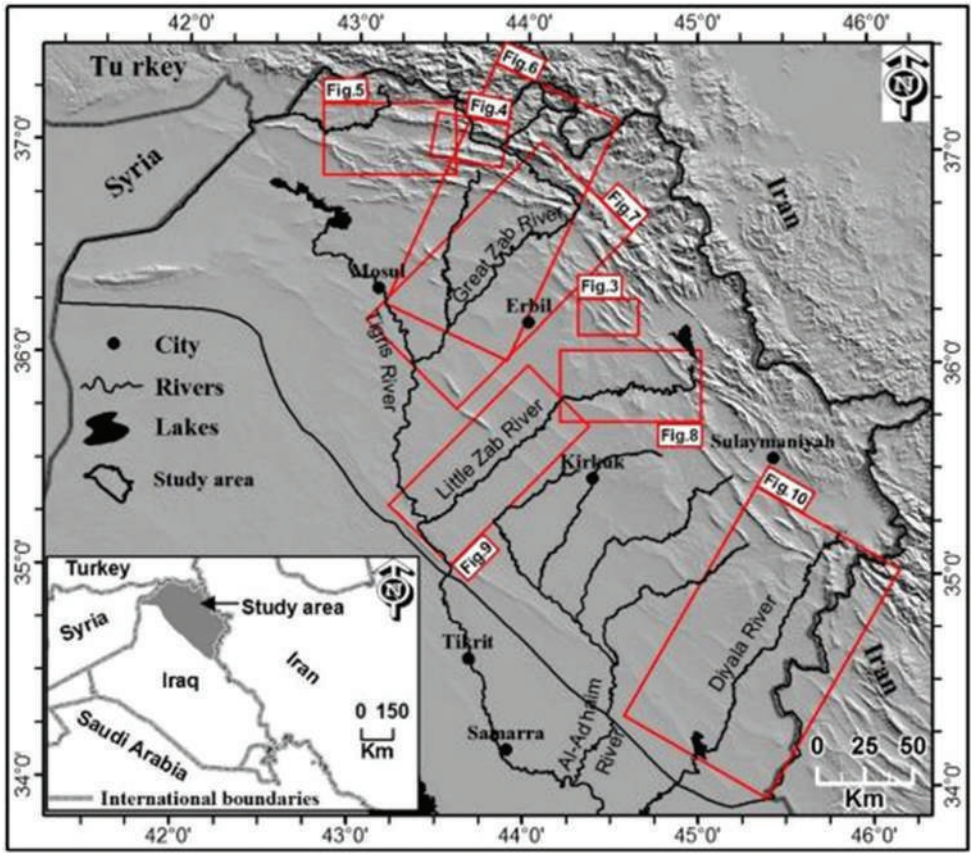

Fig. 1. Hillshade image generated from digital elevation model GMTED2010 (resolution 7.5 Arc) showing the location of the study area.

area. Geological maps and reports of the studied area are compiled by Sissakian (1995; 1993); Fouad (2007); Al-Mousawi, *et al*. (2008); and Sissakian and Fouad (2014a; 2014b; 2014c).

Fieldwork was carried out during 2006–2012 (Sissakian and Fouad, 2012) to acquire interesting data, such as type of the exposed rocks in and around the straight valleys and/or streams. Some structural data were also reviewed to elucidate the relationship between the straight valleys and the present structural features.

B. Previous Studies

The geomorphological and tectonic aspects of the studied area are dealt by many authors. However, none of them emphasized on the factors that control the development of the straight valleys and/or streams developed in some of the anticlines. Nevertheless, some dealt with the subject and they are mentioned bellow. Parts of the studied area were investigated by Al-Jaf and Kadhim (2010) and Al-Ma'amar, *et al*. (2011). They compiled the geomorphological map with a scale of 1:250,000 for Kirkuk, and Erbil and Mahabad Quadrangles, respectively (Sissakian 1993; Sissakian and Fouad, 2014a; 2014b). Both maps mentioned the presence of some wine glass forms but did not comment on the form of the draining straight valleys and/or streams. Yacoub, *et al*. (2012) and Sissakian, *et al*. (2014c) created the geomorphological map of the Low Folded Zone and the High Folded Zone in Iraq, respectively, and reported about the presence of many wine glass forms, and they also did not comment on the form of the draining straight valleys. In addition, Sissakian and Abdul-Jabbar (2010) studied the origin of many transversal gorges in the studied area, but they dealt only with those gorges that cross the whole anticline. Sissakian *et al*. (2014a) studied some transversal linear features in the study area but did not comment on the concerned straight valleys of the current study. Moreover, Sissakian *et al*. (2015) studied the Galley Ali Beg Gorge, which is within the current studied area, and dealt with many wine glass forms but again did not comment on the developed straight valleys and/or streams which are dealt with in the current study.

Tectonically, Jassim and Goff (2006) identified five major transversal blocks in Iraq, based on various sources, including satellite images, gravity and magnetic gradients, and to a lesser extent seismic data. These blocks are bounded by major transverse faults, which have a NE–SW or a N–S trend and are called "Transversal System." However, some of these transversal faults coincide with straight valleys in the current study area, such as the Greater Zab, Little Zab, Diyala Rivers, and Galley Ali Beg Gorge.

Shihab (2015) studied structural analysis in the High Folded Zone northeast of Iraq, and the results of his study manifested that the transversal faults could be grouped with another one, which is a type of strike-slip fault, and had played an important role to be developed with en echelon set or transpression zone. However, the structural model suggested by his study explains that the structural factors might have controlled and formed extensions to the valleys, being either straight or curved.

http://dx.doi.org/10.14500/aro.10262

II. Geological Setting and Study Area

The majority of the studied area is located in the extreme northeastern part of the Arabian Plate, except a very small part that is located in the Iranian (Eurasian) Plate, called Shalair Terrane (Sanandaj–Serjan Zone) (Fig. 2). The studied area is located within the Zagros Suture, Imbricate, and High Folded Zones, and most parts of the Low Folded Zone, from northeast toward southwest, respectively (Fig. 2).

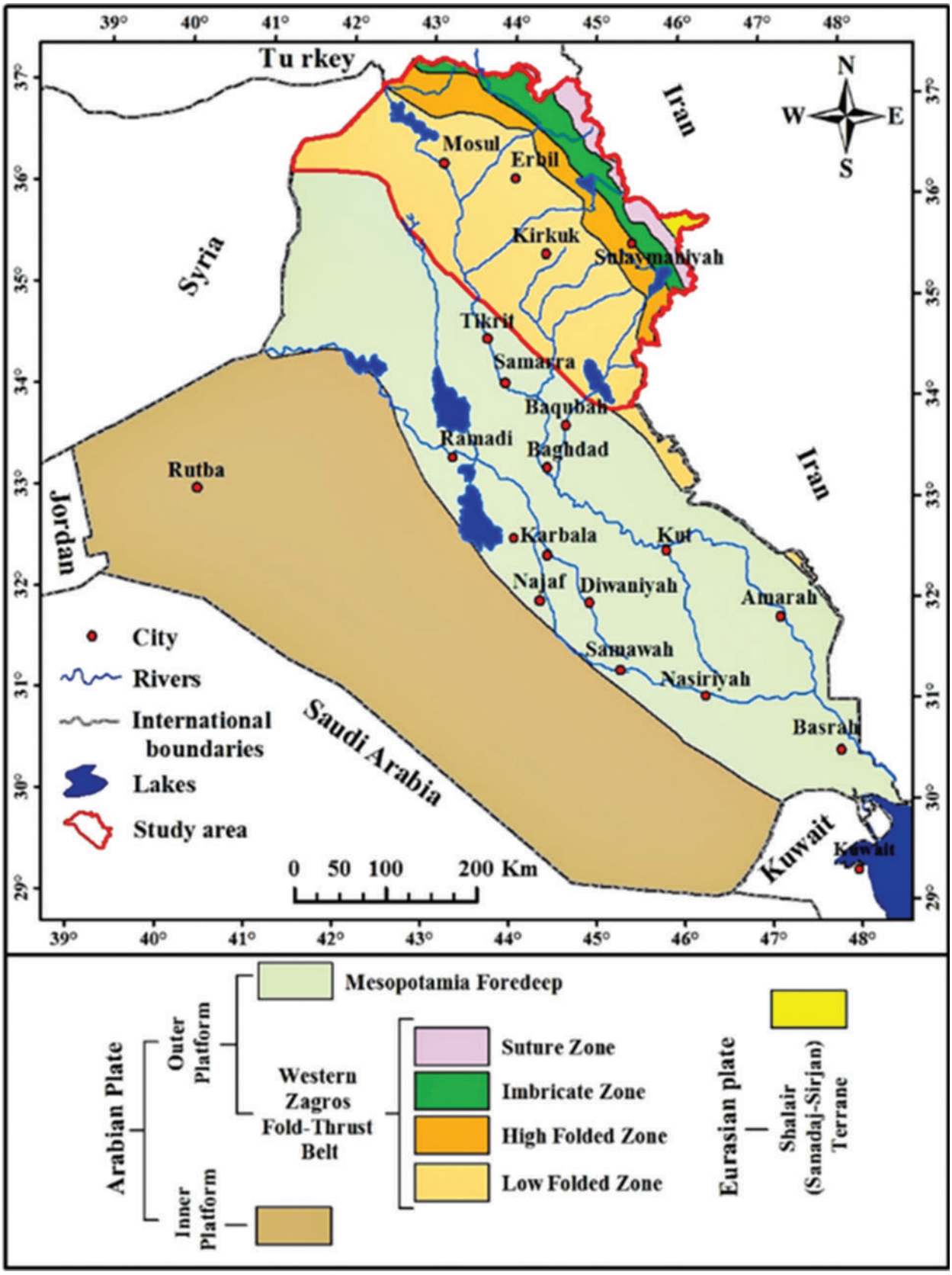

Fig. 2. Tectonic zones of Iraq (modified after Fouad, 2012) showing the limits of the study area.

The studied area is characterized by existing of N–SE anticlines, which change approximately west of the longitude 43°30′ E to E–W direction and the presence of transversal longitudinal structural elements with NE–SW trend (Fouad, 2012; Sissakian, *et al*., 2014a). Among those, longitudinal transversal forms are rivers, streams, valleys, playas, anticlines, and offsets, in parallel trend to the main compressional forces (Sissakian and Abdul-Jabbar, 2010; Sissakian, *et al*., 2014a) created by the collision of the Arabian and Iranian Plates (Fouad, 2012; Sissakian, 2013).

The carapaces of the majority of the anticlines are built up of Cretaceous rocks, characterized by massive and thick carbonate rocks of Qamchuqa and Bekhme formations; however, in the extreme northern parts of the studied area, older rocks form the carapaces of the anticlines. In contrary, in the extreme southern parts of the studied area, Eocene rocks of the Pila Spi formations form the carapace of all existing anticlines. The cores of the anticlines are usually built up of softer rocks of different ages, forming low lands as compared to the surrounding limbs, built up of hard rocks (Sissakian and Fouad, 2012; 2014a; 2014b; 2014c). Within those low lands, hundreds of wine glass forms are developed (Sissakian, *et al*., 2017). Some of those wine glass forms are drained by straight valleys with NE–SW and N–S trends, which extend occasionally to cross successive anticlines or both limbs of an anticline.

The most significant morphological units and forms in the studied area are the structural–Denudational units represented by anticlinal ridges and erosional cliffs (Sissakian, *et al*., 2014c) formed along banks of the outlets of the developed wine glass forms, and more especially, those forming straight valleys (Fig. 3), which are the main scope of this study. Moreover, flat iron forms are also well developed on thickly bedded carbonate rocks, some of them exhibit large bending off their main trend, indicating a deep-seated weakness zone that had contributed in the development of the outlet (Fig. 3).

III. Straight River Courses and Valleys

The studied area is characterized by a large number of straight valleys that are controlled structurally. The authors have presented many of them. Other structurally controlled valleys are many river courses, such as the Greater Zab, Little Zab, Diyala (Sirwan), and Adhaim rivers. All of these rivers have straight courses, and each one of them crosses many anticlines and/or ridges without shifting their courses. However, small meanderings and curvatures may occur mainly due to the effect of mass movement phenomena and/or growth of alluvial fans. Each of the mentioned rivers is described hereinafter with available presentation images.

Majority of the anticlines in the studied area exhibit wine glass forms of different sizes and shapes. Each of those wine glass forms has an outlet; however, occasionally, they may have many outlets (Sissakian, *et al*., 2017). Among those outlets, few are in the form of straight valleys and extend for few kilometers with many features and forms that are directly related to the straight valleys, indicating deep-seated weakness zones, which may represent faults.

Many examples of those straight valleys are selected from the studied area and presented in the current study, showing their details and explaining the related features and forms. This does not mean, however, that there are no more such valleys in the studied area. The following examples are selected to represent different valleys with different indications clarifying their development.

A. Degala Gorge Lineament

Degala Gorge is located NE of Erbil city; it is represented by a straight valley before and after the gorge (Fig. 3). The length of the valley is 3.89 km, whereas the length of the gorge is about 0.75 km. The gorge is developed within the carbonate rocks of the Pila Spi Formation, whereas the valley starts from Kolosh Formation (point P2, Fig. 3) and crosses Gercus, Pila Spi, Fatha, Injana, and Mukdadiya formations (point P1, Fig. 3) (Sissakian and Fouad, 2012; 2014b). The indications for the presence of a deep-seated weakness zone along which the Degala Gorge and the straight valley (Fig. 3) are developed and are presented by the following aspects:

1. Bending of the flat irons within the Pila Spi formation (point P3) and Shiranish formation (point P4).
2. Presence of three springs on both sides of Safeen anticline; opposite to each other (points S1, S2, and S3, Fig. 3A and B, respectively).
3. Bending of the axis of Safeen anticline between the points S1 and S3 (Fig. 3).
4. Plunging of the hanging syncline; north of Safeen anticline (point HS).
5. Disturbance of the beds, possibly due to a fault within the beds of the Pila Spi formation and development of large V-shaped feature (point P6, Fig. 3C).
6. Presence of a straight valley that dissects the southeastern plunge of Safeen anticline; parallel to Degala valley and gorge (point SG).

B. Greater Zab River Lineament (Upper Reach)

Greater Zab River is one of the main tributaries of the Tigris River. It enters the Iraqi territory from Turkey north of Erbil city. The concerned part of the river in this study forms a straight course in N–S direction, with a length of 11.54 km (Fig. 4, points P3–P2), and its extension southwards as a valley in S–N direction for 11.34 km (Fig. 4, points P1 – P2) that means the total length of the straight lineament is 22.88 km (P1–P3 in Fig. 4).

The southwards extension of the Greater Zab River is represented by a straight valley that crosses Gara anticline, northwards between points P2 and P3 (Fig. 4A), whereas the Greater Zab River has straight course crossing Mateen anticline between the points P1 and P2 (Fig. 4A) (Sissakian and Fouad, 2012; 2014b).

The Greater Zab River and the straight valley (will be called Dera L'lok valley) have opposite flowing direction to each other (Fig. 4A). They both have carved very hard and massively bedded carbonate rock of the Qamchuqa and Bekhme formations (Fig. 4B), although the beds of the

http://dx.doi.org/10.14500/aro.10262

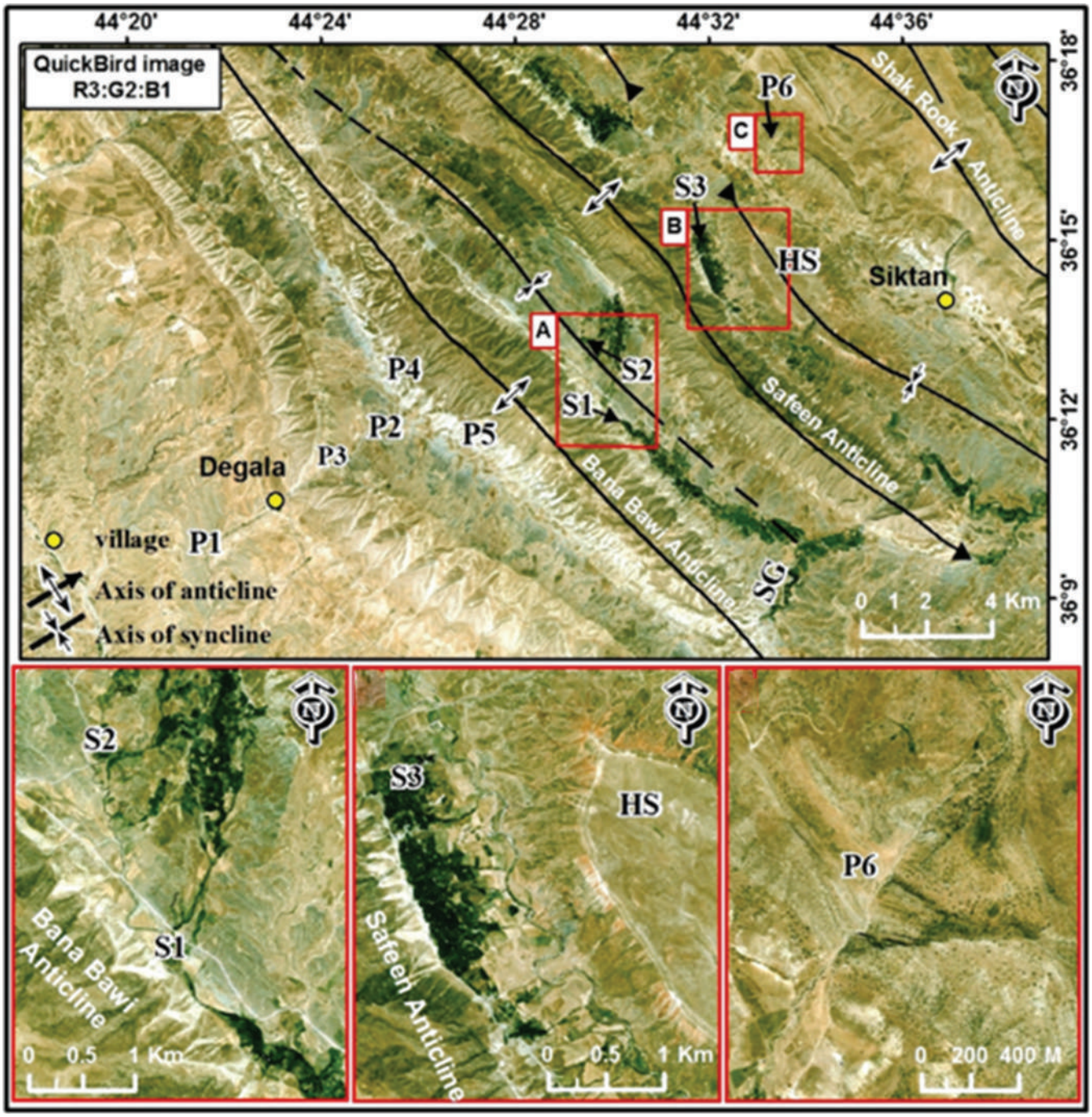

Fig. 3. QuickBird images (R3: G2: B1) of Degala Gorge and the indication of the straight valley. P1–P2 = straight valley, P4 = Bending of the flat irons of the Shiranish Formation (the white colored), S1, S2, and S3 = Springs, HS = Plunging of a hanging syncline, P6 = A fault trace, and SG = Sami Quly Gorge.

carbonates in the latter formation are not massive like those of the former.

The gradient of the Greater Zab River in its straight course (P3 – P2 in Fig. 4A) is 1.8%, whereas that of Dera L'lok valley (P1–P2 in Fig. 4A) is 2.26%. The former forms typical water gap when crossing Mateen anticline. Such water gaps are a good indication for the eastwards growth of the anticline (Keller and Pinter, 2002; Huggett, 2007; Ramsey, *et al*., 2008; Sissakian, *et al*., 2015).

Although many gentle curvatures occur within the straight courses of the Greater Zab River and Dera L'lok valley (Fig. 4C-E), still they both are considered to form a straight line lineament. The curvatures are related either to mass movements or growth of alluvial fans. Such curvatures in the courses of the streams and valleys are very common in the studied area (Sissakian, *et al*., 2015). The Greater Zab River exhibits many such curvatures. Two of them are related to mass movement features (Fig. 4C), whereas another one is related to alluvial fan development that has shifted the river course westwards, near Dera L'lok town (Fig. 4D). Dera L'lok valley also exhibits such curvatures; all are related to mass movement features (Fig. 4E).

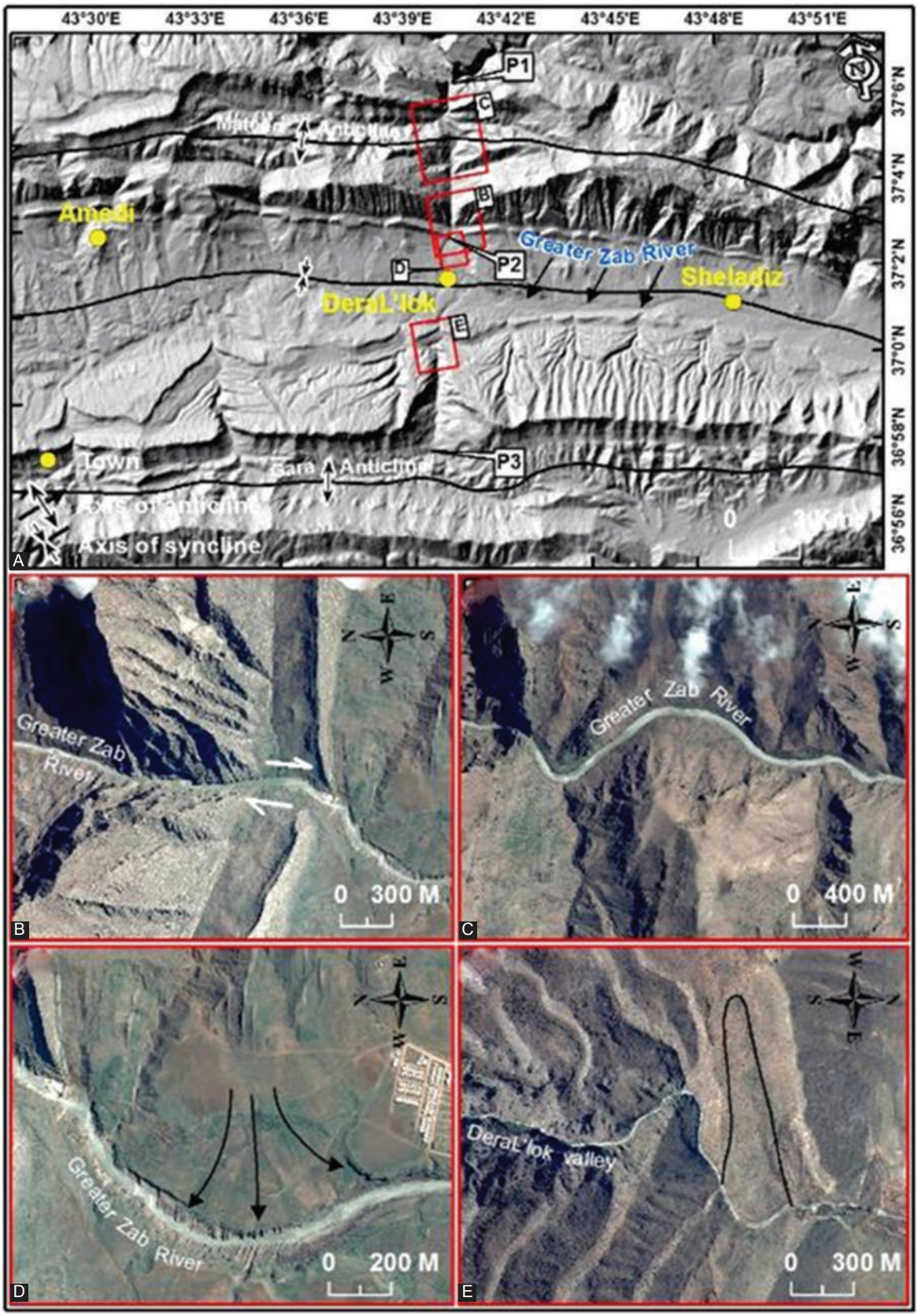

Fig. 4. (A) Hillshade image generated from digital elevation model SRTM (resolution 1 Arc) showing the straight courses of the Greater Zab River and Dera L'lok valley, (B) a dextral strike-slip fault across the southern limb of Mateen anticline, (C) two curvatures within the course of the Greater Zab River, (D) Alluvial fan near Dera L'lok town, (E) two curvatures within the course of Dera L'lok valley.

In this particular area of the Greater Zab–Dera L'lok Lineament, many other lineaments represented by straight valleys can be seen. A very obvious one is located just west of the described straight valley, east of Amadia town.

It is represented by a straight valley flowing downslope of the northern limb of Gara anticline, and its continuation northwards is represented by another straight valley flowing southwards on the southern limb of Mateen anticline. Moreover, there is a faint expression of the latter valley on the northern limb of Mateen anticline (Fig. 4A). Further northwards, the continuation of this faint expression coincides with the straight course of the Greater Zab River when entering the Iraqi territory (Fig. 1).

C. Khabour River–Mangesh Lineament

This lineament is represented by many sectors; all are forming straight valleys. It starts in the northern part from the area where the Khabour River leaves the Thrust Zone running southwards to near Mangesh town in the south (Fig. 5). The total length of the lineament is about 30 km divided into sectors; the most prominent one is the southern part with a length of about 3 km (Fig. 5). The straight valleys are indicated by the following aspects:

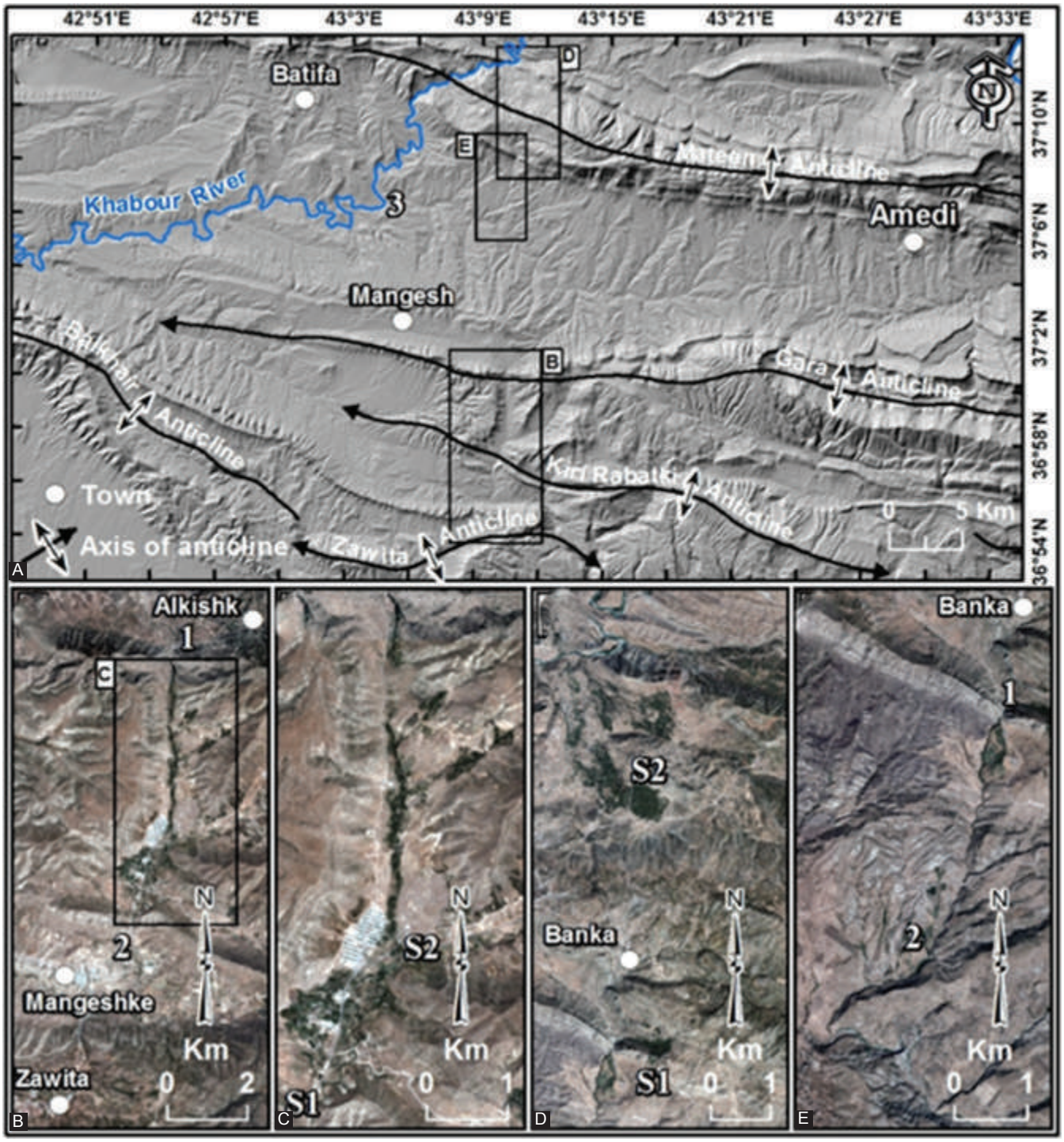

Fig. 5. Hillshade image generated from digital elevation model SRTM (resolution 1 Arc). (A) Khabour River–Mangesh Lineament, (B and C) crossing of Gara and Kiri Rabitki anticlines, note the straight valley and springs S1 and S2, (D) crossing of Mateen anticline, note the springs S1 and S2, and (E) note the straight valley between points 1 and 2, and merging in the Khabour River (point 3 in A).

1. The straight carved valley in Gara and Kiri Rabitki anticlines (Fig. 5B and E, points 1 and 2).
2. The developed springs across the western plunge of Gara and Kiri Rabitki anticlines (Fig. 5C; S1 and S2).
3. The developed gorges on both limbs of Mateen anticline and the presence of springs (Fig. 5D; S1 and S2).
4. The straight valley that starts from Mateen anticline at point 1 to point 2 (Fig. 5E), then turns westwards to merge in the Khabour River at point 3 (Fig. 5A).

D. Shamdinan–Sheladiz–Bakerman Lineament

This is one of the most prominent and unique lineaments in the studied area, and it extends for 134 km in NE–SW trend but changes its trend to N–S to be in coincidence with the regional strike of the beds (Fig. 6A, points 1, 2, and 3). This is attributed to the change of the trend of the anticlines in the studied area from NW–SE to E–W, as it is clearly visible in Fig. 6A west of Sheladiz town.

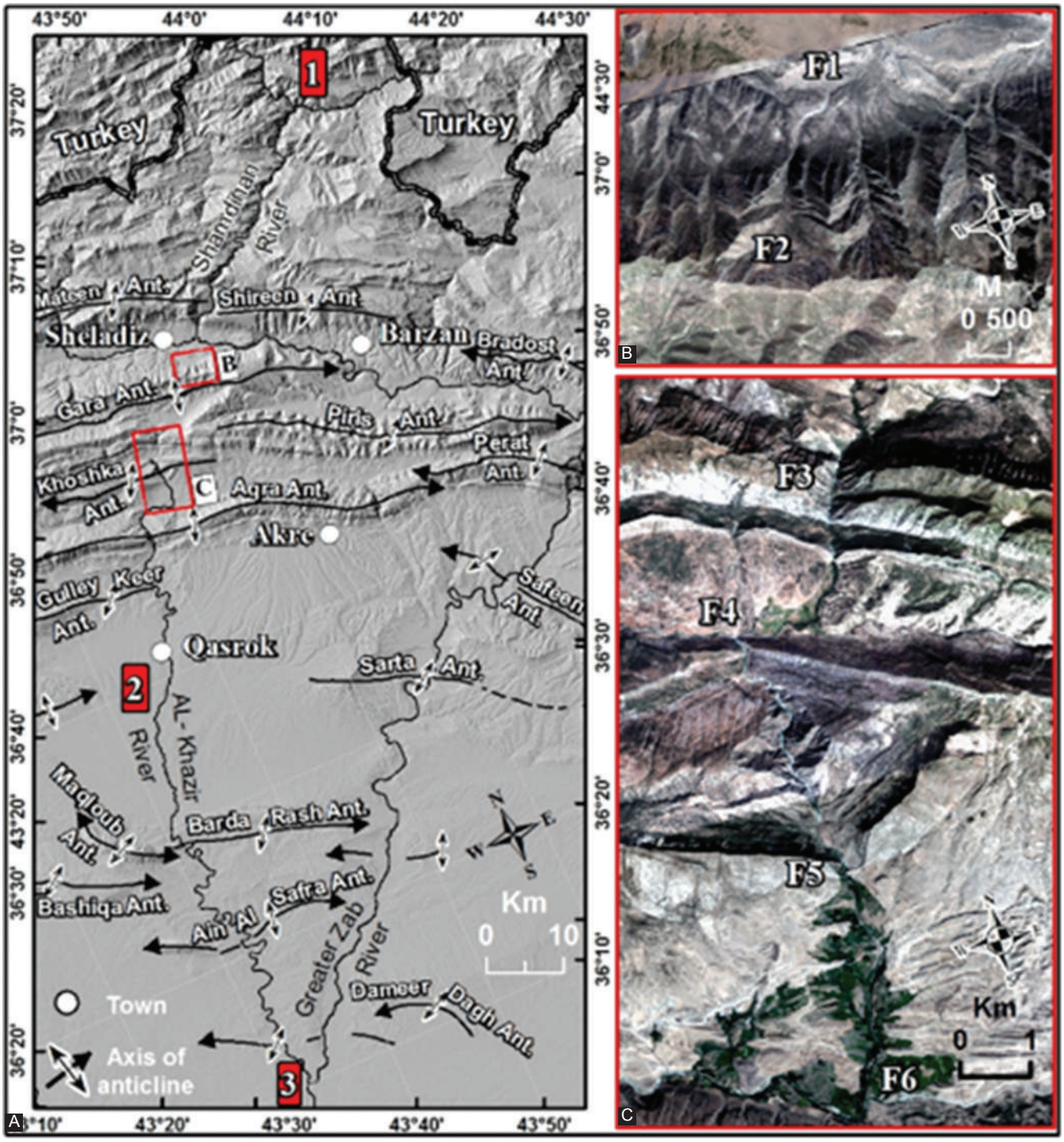

Fig. 6. (A) Is hillshade image generated from digital elevation model SRTM (resolution 1 Arc) showing Shamdinan–Sheladiz–Bakerman Lineament (1 – 2 – 3). Note the change in the direction of the lineament at point 2. (B and C) are enlarged parts of the main area.

 http://dx.doi.org/10.14500/aro.10262

The Shamdinan–Sheladiz–Bakerman Lineament consists of two parts. The northern part starts near the Iraqi–Turkish international borders, represented by Shamdinan stream, and continues southwestwards to Sheladiz town where it merges with the Greater Zab River. The extension of the lineament more southwestwards is represented by a dry valley along the north-easterner limb of Mateen anticline. The valley's trend is clearly different from the neighboring valleys along the limb of Mateen anticline (F1–F2 in caption B of Fig. 6). Moreover, the flat irons have also changed their trends and size, west of the concerned valley.

The southwards extension of Shamdinan–Sheladiz–Bakerman Lineament, after crossing the northeastern limb of Mateen anticline by a dry valley (point F2 caption B in Fig. 6), becomes very faint, although another stream runs parallel to it until it crosses the southwestern limb of Mateen anticline in the form of a small gorge (point F3, caption C in Fig. 6). After that crossing, the stream continues in N–S direction and crosses the eastern side of Khoshka anticline (F3 – F4, caption C in Fig. 6). The local change in the main trend of the stream is attributed to local change in the main trend of Khoshka anticline (Fig. 6A). After crossing Khoshka anticline, the stream continues in N–S trend for 6.3 Km, and then returns to its original trend of NE–SW (point F5, caption C in Fig. 6).

E. Greater Zab River Lineament (Lower Reach)

The Greater Zab River after crossing the mountainous area in Bekhme Gorge runs in flat to undulatory plains, crossing many anticlines (Fig. 7A). The length of the straight course is 110.2 km, whereas the thalweg length is 153 km with NE–SW flow direction. After crossing Bekhme Gorge, the Greater Zab River can be divided into three parts. The straight length of the first one is 12.7 km, whereas the thalweg length is 13.6 km, flowing in a straight line in NE–SW direction. The straight length of the second part is about 11 km, whereas the thalweg length is 23.25 km with ENE–WSW flow direction and includes three main meanders; the first one is caused by plunging of Safeen anticline. The others are due to mass movements' phenomena and/or alluvial fans (Sissakian, *et al*., 2015). The straight length of the third part is 116.9 km, whereas the thalweg length is 91 km with NE–SW flow direction and includes 4 main meanders; all are tectonically controlled (Fig. 7A-C).

F. Little Zab River Lineament

The Little Zab River after crossing the mountainous area in Haibat Sultan Range (Fig. 8) runs in flat and undulatory plains, crossing many anticlines. The total length of the straight course is about 164 km. After crossing Haibat Sultan Range, the Little Zab River can be divided into two parts. The length of the first one is about 67 km, flows in a straight line in E–W direction, and includes 9 main meanders (Fig. 8 A and B). Three of the meanders are formed due to plunging of Agh Jalar, Taq Taq, and Cham Chamal North anticlines (Fig. 8).

The length of the second part of the Lesser Zab River is about 97 km with NE–SW flow direction and includes many meanders; almost all of them are due to over maturation of the river and running in a flat plain with wide floodplain (Fig. 9). The river crosses two main ranges: Kirkuk structure, which includes three domes, and Qara Chough Range, which also includes three domes. In between the two ranges, a small anticline exists, called Bai Hassan anticline. The river crosses the three ranges in the sharp straight course, although small meanders do exist in the wide floodplain (Fig. 9b and c). However, in the southwestern part of the river course, before merging into the Tigris River, two meanders exist. They are caused due to the plunging of growing Dhahir and Shari'a subsurface anticlines, indicating neotectonic activity in that particular area.

G. Diyala (Sirwan) River

The Diyala River is another straight lineament trending NE–SW between Derbendi Khan and Himreen lakes (Fig. 10A), and its length is about 135 km; although, after Himreen lake, the river continues in a straight course, it is not included in this study due to numerous bifurcation of the river into distributaries causing hindering of the main course of the river. The straight course of the river can be divided into two main parts, the upper and lower (Fig. 10B and C, points D1–D2 and Fig. 10D and E, points D3–D4). The length of the upper part is 59 km, while the thalweg length is 81.9 km, whereas the length of the lower part is 67 km, while the thalweg length is 75.7 km.

At the lower end of the upper part, there is a clear change in the trend of the straight course of the Diyala River (Fig. 10 points D2 – D2′). The change in the main trend of the river is attributed to Chia Surkh anticline, and it can be seen clearly that the river has changed its course to cross the anticline almost perpendicularly. The same case can be seen within the middle of the lower part (Fig. 10 points D3–D3′), where the river crosses Pulkhana and Qumar anticlines perpendicularly.

The main difference between the two parts is that in the upper part of the Diyala River runs in area built up mainly of conglomerates of the Bai Hassan Formation (Sissakian and Fouad, 2012; Barwary and Slewa, 2014) and within two wide synclines (Fouad, 2012; Barwary and Slewa, 2014). The second part, however, runs in area built up of the Bai Hassan, Mukdadiya, and Injana formations (Sissakian and Fouad, 2012; Barwary and Slewa, 2014) and within five main anticlines with NW–SE trend. Some of the anticlines exhibit thrust faulting, where the northeastern limb is thrusted over the southwestern limb (Fouad, 2012; Barwary and Slewa, 2014). Significantly, these factors have influenced on the course of the river.

Within the two parts of the Diyala River, tens of major meanders are developed within the course of the river. In the upper part, a majority of the meanders are developed due to alluvial fans and mass movements, and such meanders are very common in the rivers and main streams in the northern part of Iraq (Sissakian, *et al*., 2014b). In the lower part, however, the main meanders are developed due to the

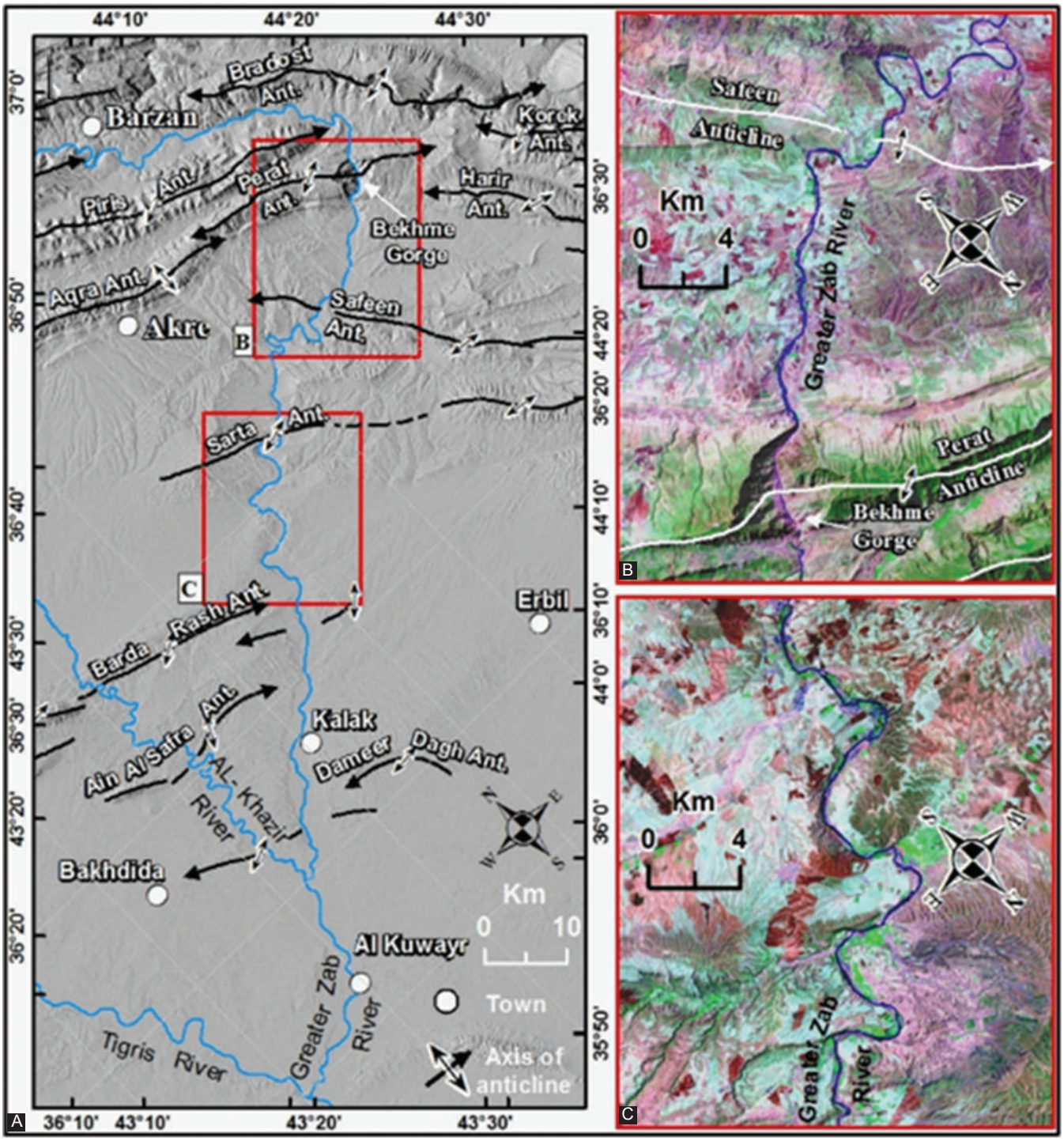

Fig. 7. (A) Digital elevation model SRTM (resolution 1 Arc) in hillshaded mode image showing the course of the Greater Zab River. B and C Landsat 8 (Operational Land Imager) (R7: G5: B3). (B) The first and second parts, (C) upper half of the third part. Note the existing meanders, which are either controlled structurally or developed due to the growth of alluvial fans.

presence of anticlines and alternation of hard and soft rocks in the exposed formations.

It is worth mentioning that in both parts, hundreds of small meanders are developed within the course of the Diyala River (Fig. 11 B-E). These meanders are developed when the floodplain is wide and the river starts exhibiting braided style and partly starts behaving as mature river.

IV. Discussion

The Iraqi territory is located in the extreme northeastern part of Arabian Plate, which is in collision with the Eurasian (Iranian) Plate since Cretaceous (Buday and Jassim, 1987; Jassim and Goff, 2006; Aqrawi, *et al*., 2010; Fouad, 2012). The continuous collision has formed the nowadays structural regime and morphology, consequently, forming the present

http://dx.doi.org/10.14500/aro.10262

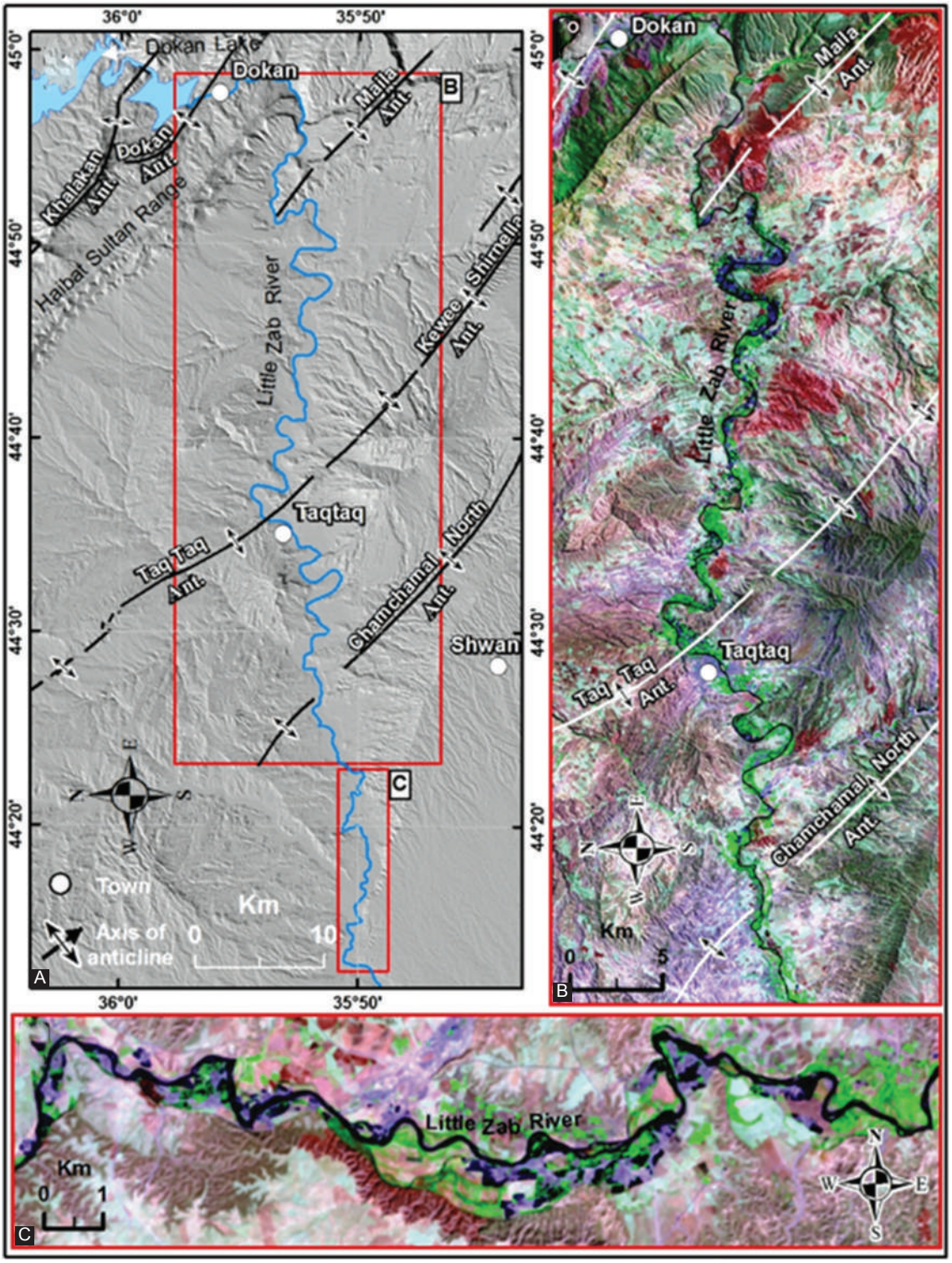

Fig. 8. (A) Digital elevation model SRTM (resolution 1 Arc) in hillshaded mode image showing the first part of the Little Zab River. Note the acute meanders in B and C. B and C are Landsat 8 (Operational Land Imager) (R7: G5: B3).

folds and faults. Among the main faults are the longitudinal and transversal faults that are recognized by Buday and Jassim (1987); Jassim and Goff (2006); and Aqrawi, *et al*. (2010); however, Fouad (2010) did not confirm them. Moreover, some of them have names (Fig. 12) and partly coincide with those lineaments mentioned in the current study.

The majority of the mentioned lineaments, in the current study, have NE–SW trend; others have N–S trend. The formers follow the Zagros regime, whereas the latter's follow the Torus regime. However, some of them have combined both regimes, depending on their locations where the folding system in Iraq changes from Zagros regime to Torus regime; consequently, the trends change from NE–SW to N–S,

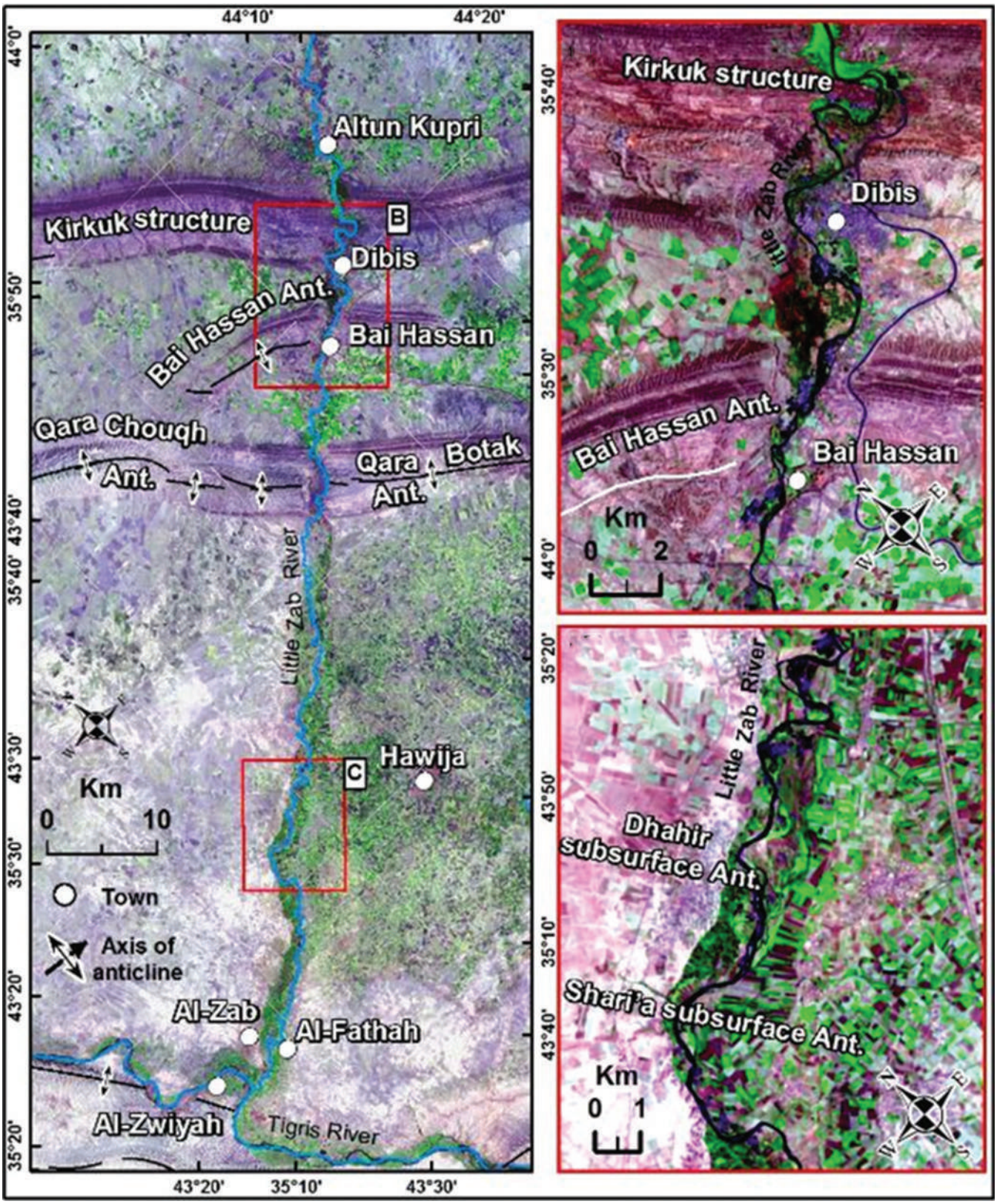

Fig. 9. Landsat 8 (Operational Land Imager) (R7: G5: B3) showing the second part of the Little Zab River. Note the structurally controlled meanders, especially those of Dhahir and Shari'a subsurface anticlines.

which are normal to the fold axes, from NW–SE and E–W, respectively.

Majority of the lineaments are believed to be expressions of deep-seated faults (Ditmar, *et al*., 1971; Buday, 1980; Buday and Jassim, 1987; Al-Kadhimi, *et al*., 1997; Jassim and Goff, 2006; Aqrawi, *et al*., 2010). Some of them have very clear indication, even on surface, such as Sirwan Fault (Figs. 10 and 11D). Others are represented on the surface

http://dx.doi.org/10.14500/aro.10262

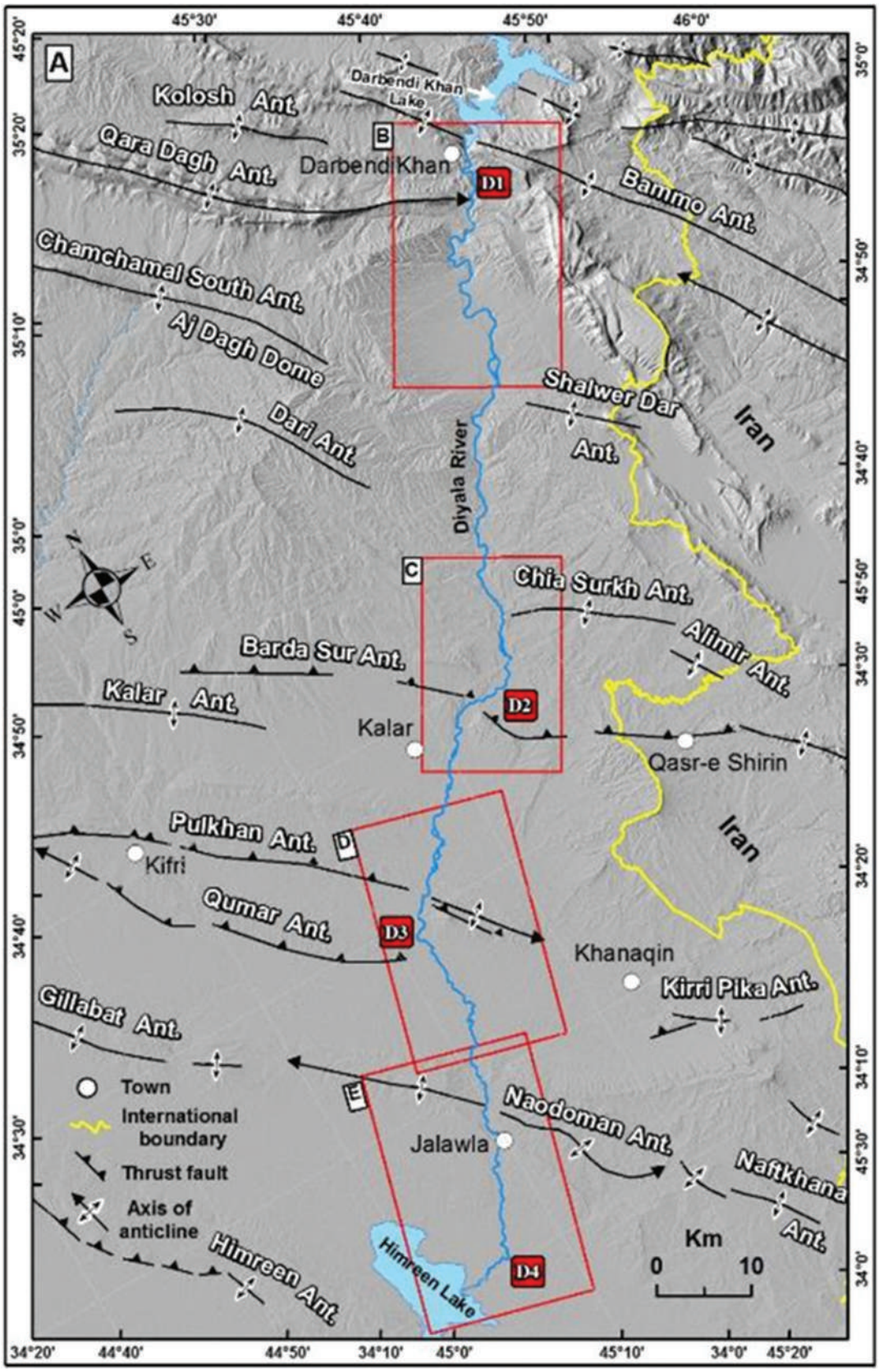

Fig. 10. Digital elevation model (DEM) provided by SRTM, the DEM is 1 Arc resolution in hill-shade model image showing the Diyala River with locations of four enlarged images in Fig. 11.

as lineaments of different lengths that are presented in the current study. Others have been proved by geophysical methods where clear anomalies confirm their presence (Jassim and Goff, 2006).

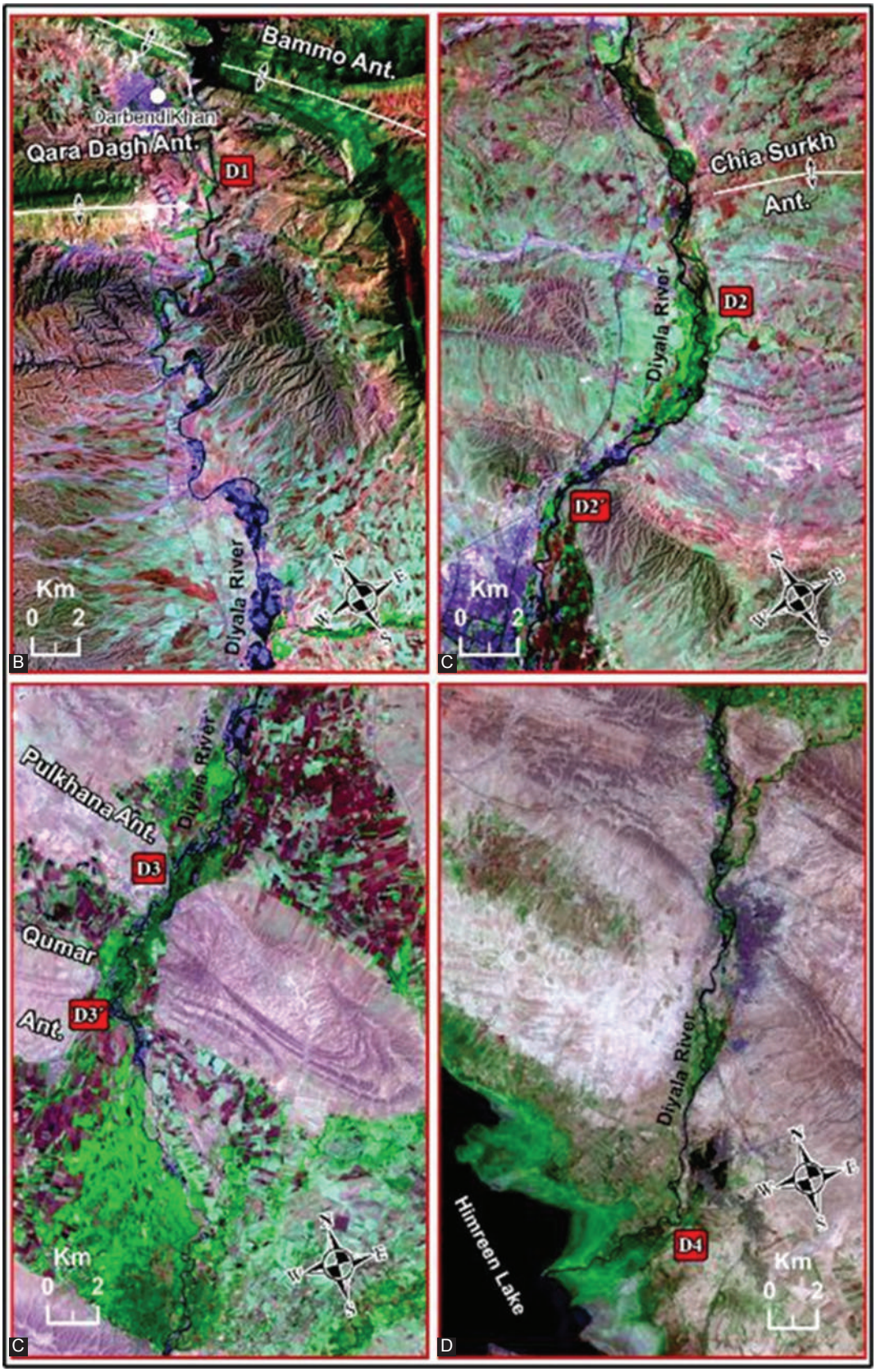

Fig. 11. (B-E) Landsat 8 (Operational Land Imager) (R7: G5: B3) Four enlarged parts of the Diyala River. Note the developed meanders, either due to structural effect or mass movements, and alluvial fans.

The straight courses of rivers and streams and even dry valleys are excellent expressions for those lineaments. However, those rivers, streams, and dry valleys after suffering different tectonic and morphological effects have developed

http://dx.doi.org/10.14500/aro.10262

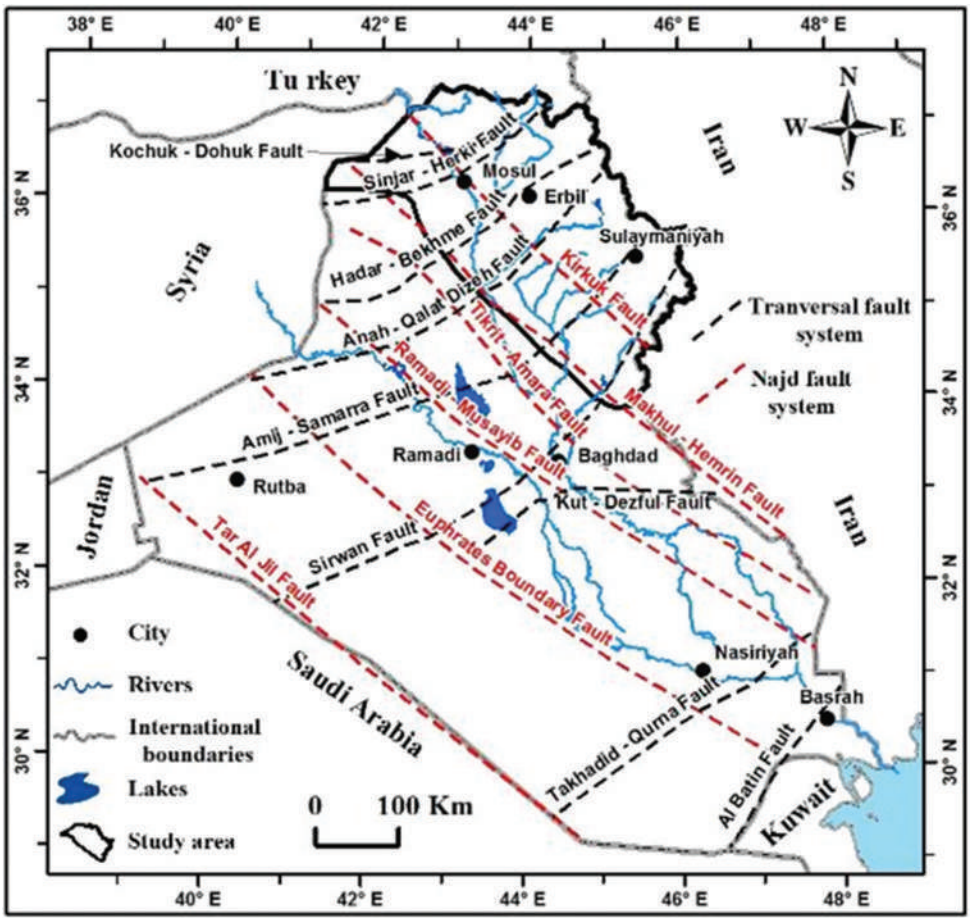

Fig. 12. Distribution of fault system in Iraq (modified after Jassim and Goff, 2006).

tens of meanderings along their courses; nevertheless, they still preserve their straight courses as a main trend. The different aspects that have developed meanders along the courses of the rivers, streams, and valleys are explained hereinafter.

- Subsurface growing anticlines: Subsurface growing anticlines are present crossing the lower part of the Little Zab River (Fig. 9C), as in Shari'a and Dhahir subsurface anticlines.
- Curved water gaps: Curved water gaps are developed following the plunges of existing anticlines (Fig. 9B) as in Kirkuk structure and Barda Sur anticline (Fig. 10). This phenomenon indicates that the rate of the incision of the river was more than the rate of the growth of the anticline; otherwise, the river would not have the ability to cross the anticline. Such cases are proved by Keller and Pinter (2002) and Ramsey, *et al*. (2008) and were observed by Sissakian and Abdul-Jabbar (2010) and Sissakian, *et al*. (2014b).
- Plunging anticlines: In many cases, rivers have developed acute meanders following the plunge of anticlines such as in Maila anticline (Fig. 8A) and Qara Dagh anticline (Fig. 10). A good example is Maila anticline near Dokan town, where the Little Zab River follows the plunge of the anticline forming acute meandering. This phenomenon indicates that the rate of the incision of the river was less than the rate of the growth of the anticline; otherwise, the river would cross the growing anticline. Such cases are proved by Keller and Pinter (2002) and Ramsey, *et al*. (2008) and recognized by Sissakian and Abdul-Jabbar (2010).
- Growing alluvial fans: This phenomenon is more abundant in dry valleys and small streams rather than rivers. This is attributed to the fact that the amount of the flowing water in the rivers has the ability to wash out the sediments of alluvial fans, and hence, less chance for developing meanders. Some rivers, however, have developed meanders due to growing alluvial fans in the studied area. A good example is the Greater Zab River (Fig. 4D), the Little Zab River (Fig. 8A-C), and the Diyala River (Figs. 10 and 11), where wide or acute meanders are developed depending on the size of the growing alluvial fan. Such forms were observed and studied by Sissakian *et al*. (2014a; 2014b) in the studied area too.
- Mass movements: Mudflows and landslides are common types in the studied area. Such movements have caused the development of meanders along rivers, streams, and dry valleys. A good example is along the Greater Zab River (Fig. 4E), where a large landslide has developed an acute meandering to the river. Such forms were observed and studied by Sissakian *et al*. (2014a; 2014b) in the studied area too.

Locally and very rarely, the rivers change their straight courses by certain angles and return to gain the same

trend. This phenomenon is recognized and attributed due to different aspects; these are as follows:

- Change in tectonic style: As it was aforementioned, the Iraqi territory is under the effect of two tectonic regimes: Zagros and Taurus. Therefore, when a certain lineament, especially when is a long one and extends within the two tectonic regimes' zones, then it changes its trend following the two main trends. A good example is Shamdinan–Sheladiz–Bakerman Lineament (Fig. 6), where the lineament changes its trend from NE–SW to N–S due to the change of the tectonic regime.
- Crossing anticlines: Some of the river courses change their trend for very short distance to be normal to anticlinal trend during their crossing to the anticline. A good example is the Little Zab River in crossing Cahm Chamal North anticline (Fig. 8B) and Diyala River in crossing Barda Sur anticline (Fig. 11C, at point D2), crossing Qumar anticline, after crossing Pulkhana anticline (Fig. 11D, at point D3) and crossing Naodoman anticline (Fig. 11E). This phenomenon is recognized when the river crosses an anticline in its middle part or far from plunge area. It indicates that the rate of the anticlinal growth is lower than the rate of the river's incision; otherwise, it was not possible for the river to cross the anticline in its middle part. Therefore, the perpendicular trend to cross the anticline is easier with shorter distance; consequently, the river has changed its trend slightly to be in perpendicular trend on the anticlinal trend, and then returns to its original course with the regional trend.
- Structurally controlled factors: In the studied area, the large-scale lineaments express different orientations, which are nearly restricted between N–S and E–W trends; however, the majority of these lineaments have NE–SW orientation and they have an acute angle between them. However, these oriented lineaments may represent shear lineaments and/or system of two sets of large-scale fractures. Structurally, the direction of the maximum stress axes ($\sigma 1$) should bisect this acute angle. However, the orientation of the main stress axes or the stress inversion results have been proved nearly with N–S to NE–SW direction in many studies in the north and northeastern parts of Iraq; among those studies are Abdulnaby, *et al*. (2014) and Shihab (2015). As well, the movement direction toward north and northeast and anticlockwise rotation of the Arabian Plate and collision with Eurasian Plate play a key role to generate this system of lineaments. In the studied area, a good example coincides with the concept of generated system of two set fractures. As can be seen the orientation of the two parts of the Shamdinan–Sheladiz–Bakerman Lineament (Fig. 6A), the convergence extension lineaments represented by two river courses of Al-Khazir River and Greater Zab River (Fig. 6A) and the Tigris River and the Greater Zab River (Fig. 7A), the two parts of the Little Zab River (Fig. 1) and Al-Adhaim River's main course with the concerned valleys (Fig. 1).

Other indications for the coincidence of the lineaments to deep-seated faults are geomorphological, structural, and hydrogeological indications. These are explained hereinafter.

- Geomorphological indications*:* In many anticlines, flat irons are well developed due to the type of the exposed rocks. A good example is Bana Bawi anticline with Degala Gorge lineament (Fig. 3). There, the flat irons change their trend and size near the lineament (Fig. 3A, points P3, P4, and P5) to be in a perpendicular direction to the lineament. This is a good indication that the deep-seated faults are initiated during the beginning of the folding and with the continuation of the folds growth; the folds have manifested their present-day forms including the shape, size, and trend of the developed flat irons. Otherwise, the flat irons would not change their trends on both sides of the lineaments. Another geomorphological aspect is the braided river style for some of the rivers on crossing the anticlines, not near to their plunge areas, such as the Little Zab River (Fig. 9) and the Diyala River (Fig. 11). Such aspects are considered as geomorphological evidence for location and orientation of neotectonic activity (Whitney and Hengesh, 2015).
- Structural indications: In many anticlines and synclines, it was recognized that the folds exhibit plunging along the lineaments. A good example is the Degala Gorge Lineament (Fig. 3). Many anticlines and synclines exhibit plunging along both sides of the lineaments, between Safeen and Shakrook anticlines (Fig. 3). Moreover, some fault traces are recognized near and along the lineaments (Fig. 3C, point P6). Bending of the axes near the lineaments is another indication for the presence of a weakness zone, represented by the lineament.
- Hydrogeological indications: Along the lineaments, many springs are developed indicating weakness zones that are represented by the lineaments indicating most probably deep-seated faults. A good example is along Degala Gorge Lineament, where many springs are developed along the lineament (Fig. 3), and Khabour River–Mangesh Lineament, where many springs are developed too along the lineament (Fig. 5C and D).

V. Conclusions

The studied area is a part of Zagros mountainous areas. Almost all of these mountains form anticlines. Most of the cores of the anticlines are built up of soft rocks, forming low lands as compared to the surrounding limbs, which are built up of hard rocks. The studied area is drained by straight valleys that cross successive anticlines or both limbs of an anticline. We used several examples of these valleys to delineate and discuss the factors controlling the development of the straight valleys that drain many anticlines within the studied area. This was achieved using different types of DEM, Landsat 8 OLI Landsat, and QuickBird satellite data. Some of these valleys are in the form of straight valleys and extend for few tens of kilometers with many features and forms that are directly related to the straight valley with N–S to NE–SW trends, which represent shear systems of strike-slip faults. The NE–SW straight valleys follow the Zagros regime, whereas the N–S follows the Torus regime. These straight valleys may indicate deep-seated faults zones. Some of these straight valleys have very clear indication(s), even on the surface, such as Sirwan Fault. Others are represented on the surface as straight valleys of different lengths. Some

others have been proved by geophysical methods, where clear anomalies confirm their presence. Along the straight valley courses, several meanders are present witnessing different tectonic and morphological effects. Nevertheless, they still preserve their straight courses as a main trend. These meanders are developed as results of subsurface growing anticlines, curved water gaps, plunging anticlines, growing alluvial fans, and mass movements. Locally, the valleys change their straight courses by particular angles and return to gain the same trend. The main reasons of that are either due to the change in tectonic style or during crossing anticlines, to be in right angle as much as possible, or structurally controlled factors.

References

Abdulnaby, W., Mahdi, H., Al-Shukri, H. and Numan, NS., 2014. Stress patterns in northern iraq and surrounding regions from formal stress inversion of earthquake focal mechanism solutions. Pure and Applied Geophysics, 171, pp.2137-2153.

Al-Jaf, A.A. and Kadhim, T.H., 2010. *The Geomorphological Map of Kirkuk Quadrangle, Sheet No. N1-38-2, Scale 1:250000. International Rep. No. 3297.* Iraq Geological Survey, Baghdad-Iraq.

Al-Kadhimi, J.A.M., Sissakian, V.K., Fattah, A.S. and Deikran, D.B., 1997. *Tectonic Map of Iraq, 2nd ed., Scale 1: 1000 000*. GEOSURV, Baghdad, Iraq.

Al-Ma'amar, A.F., Al-Saady, Y.I. and Al-Saati, R.M., 2011. *Series of Geomorphological Maps of Iraq, Scale 1: 250000, Erbil and Mahabad Quadrangles, Sheets No. NJ-38-14 and NJ-38-15. Iraq Geological Survey Library Internal Report No. 3358.* GEOSURV, Baghdad.

Al-Mousawi, H.A., Sissakian, V.K. and Fouad, S.F., 2008. *The Geology of Zakho Quadrangle, Scale 1:250000*. Iraq Geological Survey, Baghdad, Iraq.

Aqrawi, A.A.M., Goff, J.C., Horbury, A.D. and Sadooni, F.N., 2010. *The Petroleum Geology of Iraq*. Scientific Press Ltd., United Kingdom, p.424.

Barwary, A.M. and Slewa, N.A., 2014. *Geological Map of Khanaqin Quadrangle, Scale 1: 250000.* Geosurv Systems Ltd., Baghdad, Iraq.

Buday, T. and Jassim, S.Z., 1987. *The Geology of Iraq, Tectonism, Volcanism and Magmatism. Part II.* Iraq Geological Survey, Baghdad, Iraq.

Buday, T., 1980. *The Regional Geology of Iraq. Stratigraphy and Paleogeography. Vol.1*. Iraq Geological Survey, Baghdad, Iraq, p.445.

Ditmar, V.J., Begisher, F.A., Afansiey, J.T., Belousova, B.A., Petchernikov, V.V., Cheremnyh, E.M., Shamakov, E.I., Koverzner, V.Y. and Nazarov, N.P., 1971. *Geological Conditions and Hydrocarbon Prospect of the Republic of Iraq*. Northern and Central Parts, Baghdad, Iraq.

Fouad, S.F., 2007. *The Geology of Kani Rash Quadrangle, Scale 1:250000.* Iraq Geological Survey, Baghdad, Iraq.

Fouad, S.F., 2010. *Tectonic Map of Iraq. Scale 1:1,000,000, 3rd, ed*. GEOSURV: Baghdad, Iraq.

Fouad, S.F., 2012. *Tectonic Map of Iraq, Scale 1:1000 000, 3rd ed.* Iraq Geological Survey, Baghdad, Iraq.

Huggett, R., 2007. *Fundamentals of Geomorphology, Routledge Fundamentals of Physical Geography*. Taylor & Francis Ltd., United Kingdom.

Jassim, S.Z. and Goff, J.C., 2006. *Geology of Iraq*. Geological Society, London, p.341.

Keller, E. and Pinter, N., 2002. *Active Tectonics, Earthquakes, Uplift and Landscape.* Prentice Hall, New Jersey.

Othman, A.A. and Gloaguen, R., 2013a. Automatic extraction and size distribution of landslides in kurdistan region, N.E. Iraq. Remote Sensing, 5, pp.2389-2410.

Othman, A.A. and Gloaguen, R., 2013b. River courses affected by landslides and implications for hazard assessment: A high resolution remote sensing case study in NE Iraq-W Iran. Remote Sensing, 5, pp.1024-1044.

Othman, A.A. and Gloaguen, R., 2014. Improving lithological mapping by SVM classification of spectral and morphological features: The discovery of a new chromite body in the mawat ophiolite complex (Kurdistan, NE Iraq). Remote Sensing, 6, pp.6867-6896.

Ramsey, L.A., Walker R.T. and Jackson, J., 2008. Fold evolution and drainage development in the zagros mountains of fars province, SE Iran. Basin Research, 20, pp.23-48.

Shihab, A.T., 2015. *Structural Analysis Using Remote Sensing and GIS Techniques in the High Folded Zone Between Harir and Bradost Anticlines*. University of Baghdad, Northeast Iraq.

Sissakian, V.K. and Abdul-Jabbar, M.F., 2010. Morphometry and genesis of the main transversal gorges in North and Northeast Iraq. Iraqi Bulletin Geological Mining, 6, pp.95-120.

Sissakian, V.K. and Fouad, S.F., 2012. *Geological Map of Iraq, Scale 1: 1000 000, 4th ed*. Iraq Geological Survey, Baghdad-Iraq.

Sissakian, V.K. and Fouad, S.F., 2014a. *The Geology of Erbil and Mahabad Quadrangles, Scale 1:250 000, Sheets No. NJ-38-14 and NJ-38-15, 2nd ed.* Iraq Geological Survey, Baghdad, Iraq.

Sissakian, V.K. and Fouad, S.F., 2014b. *The Geology of Kirkuk Quadrangle, Scale 1:250 000, Sheet No. NI-38-2, 2nd ed.* Iraq Geological Survey, Baghdad, Iraq.

Sissakian, V.K. and Fouad, S.F., 2014c. *The Geology of Sulaimaniyah Quadrangles, Scale 1:250 000, Sheet No. NI-38-03, 2nd ed.* Iraq Geological Survey, Baghdad, Iraq.

Sissakian, V.K., 1993. *Geological Report on Kirkuk Quadrangle, Sheet No. NI-38-02, Scale 1:250 000.* Iraq Geological Survey, Baghdad, Iraq.

Sissakian, V.K., 1995. *Geological Report on Al-Mosul Quadrangle, Sheet No. NJ-38-03, Scale 1:250 000*. Iraq Geological Survey, Baghdad, Iraq.

Sissakian, V.K., 2013. Geological evolution of the Iraqi mesopotamia foredeep, inner platform and near surroundings of the Arabian plate. Journal of Asian Earth Sciences 72, pp.152-163.

Sissakian, V.K., Abdul Jab'bar, M.F., Al-Ansari, N. and Knutson, S., 2015. Development of galley ali beg gorge, rawnadouz area, North Iraq. Engineering, 7, pp.16-30.

Sissakian, V.K., Abdul-Jab'bar, M.F., Al-Ansari, N. and Knutson, S., 2014a. Meandering of tributaries of the tigris river due to mass movements, within Iraq. Engineering, 6, pp.712-730.

Sissakian, V.K., Al-Ansari, N. and Knutson, S., 2014b. Origin of some transversal linear features of NE - SW trend in Iraq and their geological characters. Natural Science, 6, pp.1-16.

Sissakian, V.K., Kadhum, T.H. and Abdul Jab'bar, M., 2014c. Geomorphology. In: Geology of the high folded zone. Iraqi Bulletin Geological Mining, 6, pp.7-56.

Sissakian, V.K., Othman, A.A. and Ahmed, T.S.H., 2017. *Factors Controlling the Development of Wine Glass Forms in the Mountains of the Kurdistan Region.* Submitted to GeoKyrdistan/3 Conference, Iraq.

Whitney, B.B. and Hengesh, J.V., 2015. Geomorphological evidence of neotectonic deformation in the carnarvon basin, Western Austrlia. Geomorphology, 228, pp.579-596.

Yacoub, S.Y., Othman, A.A. and Kadhum, T.H., 2012. Geomorphology. In: Geology of the low folded zone. Iraqi Bulletin Geological Mining, 5, pp.7-38.

Thermodynamic Excess Properties and Intermolecular Interaction Using Fourier Transform Infrared for the Dodecylbenzenesulfonic Acid-Acetone Binary Liquid Mixture

Ali A. Jazie

Department of Chemical Engineering, University of Al-Qadisiyah,
Al-Qadisiyah, Al-Diwaniyah, Iraq

***Abstract*–Density, viscosity, and surface tension for the dodecylbenzenesulfonic acid (DBSA)-acetone system at the temperatures (293.15°K, 298.15°K, and 301.15°K) have been investigated experimentally. Excess molar volume, viscosity deviation, surface tension deviation, and molar excess Gibbs free energy deviation are calculated at (293.15°K, 298.15°K, and 301.15°K). All the non-ideal properties calculated are fitted to Redlich-Kister equation. The Fourier transform infrared (FTIR) spectrum of the DBSA-acetone mixture has been characterized for studying the intermolecular interaction. The result of molar excess Gibbs free energy deviation and FTIR studies showed a weak hydrogen bonding for the mixture solution. The intra-molecular interaction is strong in the case of pure DBSA and acetone due to the self-association of DBSA molecule or decreasing the dipole-dipole of acetone molecule. The result of FTIR supported the result of thermodynamic excess, where the excess molar volumes were positive. The calculated values of excess molar volume are positive for all the temperatures ranging from 293.15 to 301.15°K. It was found that the values of viscosity deviation, surface tension deviation, and molar excess Gibbs free energy deviation are negative for all the temperatures studied.**

***Index Terms*—Acetone, Density, Dodecylbenzenesulfonic acid, Excess properties, Fourier Transform infrared spectral analysis, Hydrogen bonding, Intermolecular interaction, Surface tension, Viscosity.**

I. Introduction

Surfactants are widely used in the chemical industries, and the dodecylbenzenesulfonic acid (DBSA) is one of the very important anionic surfactant which can be used as a brønsted acid-catalyst in a wide range of chemical reactions. DBSA had the dual role of surfactant and acid catalyst (Shrikhande, 2007). In many studies, the role of DBSA has been investigated as an acid catalyst for the esterification (Jing, et al., 2008), dehydration (Chai, et al., 2007), Mannich type (Shiri and Zolfigol, 2009), and thia-Michael addition reactions in water (Manabe, et al., 2002). The hydrophobic property of DBSA has also been studied (Manabe, et al., 2001). As a dopant, DBSA has been tested in the synthesis of poly-aniline (Haba, et al., 1999; Machado, et al., 2006). Moreover, the large alkyl groups of DBSA can improve the melting and solution processability for the poly-aniline (Han, et al., 2002). The study of the thermodynamic properties and the intermolecular interactions for the binary mixture of DBSA-acetone system is very important in the modeling, design, and optimization of the chemical industrial processes. The behavior of the solution and the type of interaction has been explained through the present study, and the data provided may play a vital role in the industrial synthesis of many organic products, solvent extraction, and many other mass transfer phenomena. Acetone has been chosen as a solvent in the present work because of the high polar and self-associative nature of it. Many of the spectroscopic studies have focused on the acetone (Schindler, et al., 1982; Ancian, et al., 1983; Knözinger and Wittenbeck, 1984; Jalilian and Zahedi-Tabrizi, 2008; Shikata, et al., 2012; Kollipost, et al., 2014; Srivastava, et al., 2003). In a recent research, the shift in the frequency of C=O and CH_3 group has been interpreted (Arivazhagan, et al., 2015). A combination of bronsted acid+ hydroxymethyl group binary system was discussed in a recent paper (Liu, et al., 2017). To the best of our knowledge, no work has been focused on the DBSA-acetone mixture which is used industrially and deviate from the idieality of the pure liquid state leading to the errors in the equation of state calculation and the other thermodynamic calculations. The deviation from the ideality can affect the design calculation for the industrial units, which contains a binary liquid system of DBSA-acetone. The novelty of this paper depends on the analysis thermodynamic properties and interactions between the molecules of DBSA and acetone. The objective of the present work is to provide

ARO-The Scientific Journal of Koya University
Volume V, No 2(2017), Article ID: ARO.10229, 6 pages
DOI: 10.14500/aro.10229
Received 13 April 2017; Accepted 10 August 2017
Regular research paper: Published 28 November 2017
Corresponding author's e-mail: ali.Jazie@qu.edu.iq

 http://dx.doi.org/10.14500/aro.10229

an experimental data of density, viscosity, and surface tension for the pure compound and the thermodynamic excess volume, viscosity deviation, surface tension deviation, and excess Gibss free energy of activation for the binary mixture of DBSA-acetone system. Moreover, the intermolecular interaction has been investigated using the Fourier transform infrared (FTIR) spectroscopy method.

II. Materials and Procedure

A. Materials

DBSA (>0.99) was procured from Shanghai Hanhong Scientific Co.,Ltd., and acetone (>0.997 GC) of a high chromatographic purity was procured from Sigma-Aldrich. No further purification has been done for the reagents. All the chemical materials used were analytical reagents.

B. Measuring and Procedure

An electronic balance with a precision of $\pm 10^{-4}$ (OHAUS) has been used in the preparation of (0.1-0.9 mole percent) of DBSA-acetone binary mixtures. The experimental uncertainty of mole fractions were <±0.0003. Density of the pure and DBSA-acetone binary mixtures were measured using Anton-Paar dens meter (DSA111 5000) with uncertainty in density of $\pm 2 \times 10^{-3}$ kg m^{-3}. Anton-Paar viscometer has been used for measuring the dynamic viscosity (η) of the pure and binary liquid mixtures for DBSA-acetone with uncertainty of ±0.06 mPa.s. The pendant drop method (KRÜSS GmbH) was used for testing the surface tension of the pure and the binary liquid mixtures. Each test was conducted in triplicate. The FTIR spectra for the pure and binary liquid mixtures for DBSA-acetone are recorded using (Tensor 37, Bruker) in the range 400-4000 cm^{-1}, a resolution of 4 cm^{-1} and average of 16 scans were recorded.

III. Theory

The experimental density (ρ) data were used for calculating the excess molar volumes (VE) according to the following equation,

$$V^E = \frac{x_1M_1 + x_2M_2}{\rho_m} - \left(\frac{x_1M_1}{\rho_1} + \frac{x_2M_2}{\rho_2}\right) \quad (1)$$

Where, x, M, and ρ the mole fraction, molecular weight, and density, respectively. The subscript 1, 2, and m denoted DBSA, acetone, and the DBSA-acetone mixture, respectively.

The deviation in viscosity (Δη) was calculated from the experimental data of viscosity (η) as the following equation,

$$\Delta\eta = \eta_m - (x_1\eta_1 + x_2\eta_2) \quad (2)$$

Where, x, η the mole fraction, and viscosity, respectively. The subscript 1, 2, m denoted DBSA, acetone, and the DBSA-acetone mixture, respectively.

The surface tension deviation (Δσ) was calculated from the experimental data of surface tension (σ) as the following equation,

$$\Delta\sigma = \sigma_m - (x_1\sigma_1 + x_2\sigma_2) \quad (3)$$

Where, x, σ the mole fraction, and surface tension, respectively. The subscript 1, 2, m denoted DBSA, acetone, and the DBSA-acetone mixture, respectively.

Molar excess Gibbs free energy of activation (ΔG^{*E}) was calculated from the experimental molar volume (V) and viscosity (η) data as the following equation,

$$\Delta G^{*E} = RT[\ln(\eta_m V_m) - (x_1\ln(\eta_1 V_1) + x_2\ln(\eta_2 V_2))] \quad (4)$$

Where, x, η, R, T, V the mole fraction, viscosity, universal gas constant, absolute temperature, and molar volume, respectively. The subscript 1, 2, m denoted DBSA, acetone, and the DBSA-acetone mixture, respectively.

Excess molar volumes, deviations in the viscosity, surface tension, and molar excess Gibbs free energy for the mixtures of DBSA-acetone were fitted to Redlich-Kister (RK) equation as follow (Tahery, 2017):

$$RK^E = x_1x_2\sum_{i=0}^{2} A_i\left(x_1 - x_2\right)^i \quad (5)$$

Where, x_1, x_2, and A_i are the mole fraction of DBSA, mole fraction of acetone, and the binary coefficients, respectively. The coefficients of RK equation are calculated using least squares method and the standard deviation (SD) for the data are calculated using the following relation:

$$SD_{F^E} = \left(\frac{\sum_{i=1}^{M}\left(F^E_{exp} - F^E_{cal}\right)^2}{M - N}\right)^{1/2} \quad (6)$$

Where, M, N are the number of experimental data and the number of polynomial coefficients, respectively.

IV. Results and Discussion

A. Thermodynamic Properties

The data of density, viscosity, and surface tension for the pure DBSA and acetone were compared with the literature data and presented in Table I. For the binary mixtures of DBSA-acetone, at three temperatures (293.15°K, 298.15°K, and 301.15°K), the density, viscosity, surface tension, excess molar volume, viscosity deviation, surface tension deviation, and molar excess Gibbs free energy were presented in Table II. All the data showed a nonlinear increase or decrease in the property with mole fraction due to the non-ideal behavior of DBSA-acetone binary mixture. The intermolecular and intramolecular interactions between the components were concluded from the non-ideal behavior of the binary system (Gnanakumari, et al., 2007). The calculated values of the excess molar volumes for the DBSA-acetone binary system exhibited a positive values for all mole fractions and temperatures, as presented in the Table II and Fig. 1. Moreover, the values of excess molar volumes increase with increasing temperature. The maximum value of excess molar volume is positioned at 0.4 mole fraction of DBSA.

The same scenario was concluded for the viscosity deviation, but with negative values for all mole fractions and

TABLE I
EXPERIMENTAL AND LITERATURE VALUES OF DENSITY Ρ, DYNAMIC VISCOSITY H, AND SURFACE TENSION Σ FOR THE PURE DBSA AND ACETONE AT 298.15 K

Component	$10^{-3}\rho$, (kg.m^{-3})		η, (mPa.s)		σ, (mN. m^{-1})	
	Experimental	Literature	Experimental	Literature	Experimental	Literature
DBSA	1.05343	1.05354 (Kumar, et al., 2016) [24]	1056	1055.9 (Kumar, et al., 2016) [24]	39.91	39.89 (Kumar, et al., 2016) [24]
Acetone	0.74924	0.74879 (Qian, et al., 2011) [25]	0.33	0.329 (Qian, et al., 2011) [25]	24.21	24.19 (Dash and Mohanty) [26]

DBSA: Dodecylbenzenesulfonic acid

TABLE II
DENSITY (P), EXCESS MOLAR VOLUME (VE), DYNAMIC VISCOSITY (H), VISCOSITY DEVIATION (ΔH), SURFACE TENSION (Σ), SURFACE TENSION DEVIATION (ΔΣ), EXCESS MOLAR GIBBS FREE ENERGY OF ACTIVATION ΔG*E FOR THE BINARY MIXTURE OF DBSA-ACETONE AT TEMPERATURES (293.15-303.15) K AND P=1 ATM

X_1	$10^{-3}\rho$, (kg.m^{-3})	10^6 VE, (m^3.mol^{-1})	η, (mPa.s)	Δη	σ, (mN. m^{-1})	Δσ	ΔG^{*E}, J.mol^{-1}
293.15°K							
0.0	0.75352	0.000000	000.340	0.000	24.28	0.000	000.0
0.1	0.80465	4.784837	104.785	−1.112	25.53	−0.249	−648.2
0.2	0.86753	4.838747	209.987	−1.477	26.78	−0.568	−922.7
0.3	0.89942	6.873256	315.483	−1.548	27.89	−1.027	−989.2
0.4	0.93247	6.955084	421.097	−1.501	29.23	−1.256	−950.3
0.5	0.95703	7.205812	526.856	−1.309	30.34	−1.715	−865.3
0.6	0.97796	7.108916	632.721	−1.011	32.64	−0.984	−654.6
0.7	0.99687	6.540582	738.583	−0.716	34.48	−0.713	−597.8
0.8	1.01588	5.101230	844.343	−0.523	36.26	−0.502	−396.9
0.9	1.04048	1.304930	950.112	−0.321	38.19	−0.141	−198.7
1.0	1.05937	0.000000	1056.87	0.000	39.97	0.000	000.0
298.15°K							
0.0	0.74924	0.000000	000.330	0.000	24.21	0.000	000.0
0.1	0.80164	5.180777	104.985	−0.912	25.12	−0.659	−612.4
0.2	0.85996	5.972145	210.087	−1.377	26.43	−0.918	−878.3
0.3	0.89579	7.497479	315.498	−1.533	27.63	−1.287	−928.5
0.4	0.92602	8.190561	421.197	−1.401	29.23	−1.256	−897.8
0.5	0.95103	8.473149	526.956	−1.209	30.1	−1.955	−815.6
0.6	0.97326	8.190809	632.821	−0.911	32.41	−1.214	−610.4
0.7	0.99207	7.734298	738.683	−0.616	34.36	−0.833	−556.8
0.8	1.01388	5.630941	844.353	−0.513	36.02	−0.742	−365.8
0.9	1.04021	1.379681	950.122	−0.311	37.96	−0.371	−167.9
1.0	1.05343	0.000000	1056.00	0.000	39.91	0.000	000.0
303.15°K							
0.0	0.74435	0.000000	000.325	0.000	24.01	0.000	000.0
0.1	0.79164	6.517810	105.085	−0.812	25.01	−0.769	−576.4
0.2	0.84996	7.500318	210.287	−1.177	26.33	−1.018	−837.9
0.3	0.89279	8.017197	315.698	−1.333	27.53	−1.387	−878.7
0.4	0.92428	8.526806	421.397	−1.201	29.13	−1.356	−847.6
0.5	0.94903	8.899156	527.056	−1.109	30.01	−2.045	−765.8
0.6	0.97108	8.696178	632.921	−0.811	32.31	−1.314	−571.4
0.7	0.99001	8.250151	738.783	−0.516	34.26	−0.933	−517.2
0.8	1.01088	6.429437	844.453	−0.413	35.92	−0.842	−334.7
0.9	1.04001	1.435077	950.222	−0.211	37.86	−0.471	−136.8
1.0	1.05021	0.000000	1055.60	0.000	39.51	0.000	000.0

DBSA: Dodecylbenzenesulfonic acid

temperatures. The negative values of viscosity deviation are reduced with increasing temperature. The maximum value of viscosity deviation positions at nearly 0.3 mole fraction of DBSA, as presented in the Table II and Fig. 2. The deviation of surface tension data for the DBSA-acetone binary system, presented in the Table II and Fig. 3, are negative at all mole fractions and temperatures and the maximum value is located at about 0.6 mole fraction of DBSA. In addition, the negative values of surface tension are reduced with increasing temperature. As stated in the literature, the molar excess Gibbs free energy of activation had a vital role in the study of the molecular interaction (Bajić, et al., 2013a; 2013b). For the interpretation of inter- and intra-molecular interaction in the DBSA-acetone binary system, the molar excess Gibbs free energy of activation is calculated and the data are presented in Table II and Fig. 4. All the calculated values of molar excess Gibbs free energy values are negative for all the mole fractions and temperatures range and have a maximum negative value at a mole fraction of 0.3. The negative values of the molar excess Gibbs free energy increase with increasing temperature. The coefficients and results of the R-K equation for all functions are presented in Table III and for all the functions in the Figs. 1-4. Moreover, the values of SDs are given in Table III as calculated using the equation (6).

http://dx.doi.org/10.14500/aro.10229

TABLE III
CALCULATED RK COEFFICIENTS FOR EXCESS MOLAR VOLUME (V^E), VISCOSITY DEVIATION (ΔH), SURFACE TENSION DEVIATION ($\Delta\Sigma$), EXCESS MOLAR GIBBS FREE ENERGY OF ACTIVATION ΔG^{*E} FOR THE BINARY MIXTURE OF DBSA-ACETONE AT TEMPERATURES (293.15-303.15) K AND P=1 ATM

Function	Temperature (°K)	A_0	A_1	A_2	A_3	A_4	SD
V^E	293.15	0.332	19.06	52.318	−147.2	75.266	0.00315
	298.15	0.282	26.106	24.154	−103.23	52.285	0.00321
	301.15	0.4073	61.655	−121.3	95.805	−36.865	0.00322
$\Delta\eta$	293.15	−0.0251	−13.592	38.113	−38.953	14.452	0.03674
	298.15	0.0185	−12.805	35.188	−35.026	12.602	0.02956
	301.15	0.0017	−10.576	27.469	−25.139	8.2314	0.02187
$\Delta\sigma$	293.15	0.0151	−1.453	−15.592	36.552	−19.551	0.00020
	298.15	−0.0141	−6.7685	9.5825	−2.2591	−0.5536	0.00015
	301.15	−0.0282	7.9855	15.744	−12.801	5.0699	0.00010
ΔG^{*E}	293.15	−9.6839	−8170.4	22183	-22658	8667.2	7.5
	298.15	−10.113	−7692.2	20750	−20916	7882.6	7.4
	301.15	−9.4252	−7261.1	19425	−19248	7109.3	7.2

RK: Redlich-Kister

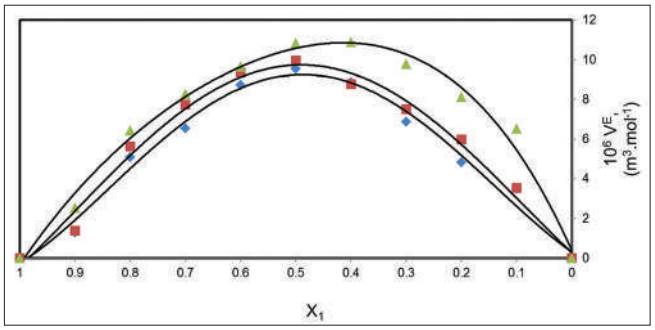

Fig. 1. Excess molar volume V^E as a function of X_1 for the binary system dodecylbenzenesulfonic acid-acetone for the temperature as following (◆293.15, ■298.15, ▲303.15)°K.

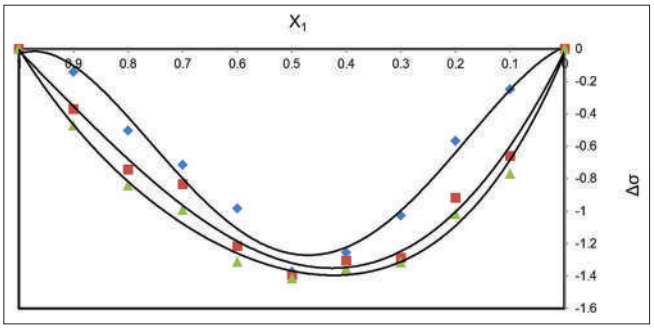

Fig. 3. Surface tension deviation $\Delta\sigma$ as a function of X_1 for the binary system dodecylbenzenesulfonic acid-acetone for the temperature as following (◆293.15, ■298.15, ▲303.15)°K.

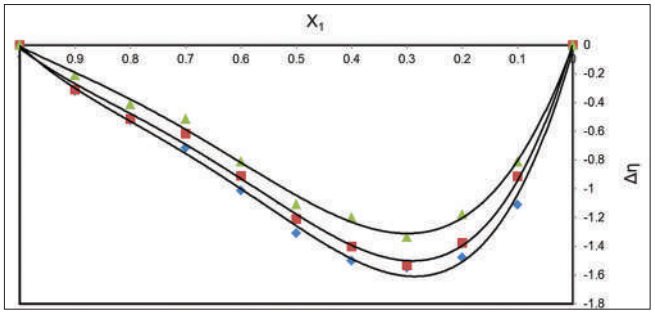

Fig. 2. Viscosity deviation $\Delta\eta$ as a function of X_1 for the binary system dodecylbenzenesulfonic acid-acetone for the temperature as following (◆293.15, ■298.15, ▲303.15)°K.

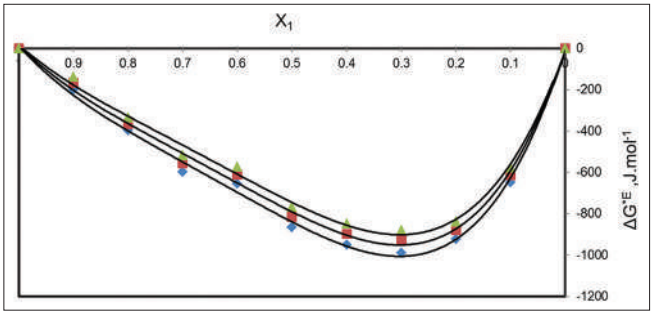

Fig. 4. Excess molar Gibbs free energy of activation ΔG^{*E} as a function of X_1 for the binary system dodecylbenzenesulfonic acid-acetone for the temperature as following (◆293.15, ■298.15, ▲303.15)°K.

B. FTIR and Intermolecular Interaction

For the investigation of functional group, molecular structure, inter- and intra-molecular interaction, FTIR play a crucial role (Wei, et al., 2013). The binary mixture of DBSA-acetone system showed a deviation from the ideality and was explained in the previous section that the nonideality and the deviation in the thermodynamic properties was explained due to the intermolecular interaction in hydrogen bonding. Two types of hydrogen bonding can be concluded from the broadening and sharpening of the hydrogen beaks, broadening referred to intermolecular bonding and sharpening referred to intramolecular bonding. The intensity of hydrogen beaks due to the intermolecular bonding was decreased with increasing the dilution until totally it disappears. The FTIR spectrum for the pure DBSA showed S=O stretch at 1345 cm^{-1}, broad O-H stretch at 2900 cm^{-1}, =C-H stretch (aromatic) in benzene ring at 3100 cm^{-1}, 3070 cm^{-1}, and 3050 cm^{-1}, C-H stretch (alkyl) at 2950 cm^{-1}, C-C stretch in ring (aromatic) at 1590 cm^{-1}, 1478 cm^{-1}, and 1400 cm^{-1} due to vibration in the benzene ring, C-H in-plane bending at 1100, 1050 cm^{-1} (weak band), C-H out-of-plane bending at 750 cm^{-1}, Overtones bands in the region 2000-1665 cm^{-1}, C=C stretch at 1644 cm^{-1}.

The FTIR spectrum for the pure Acetone showed C=O at 1715 cm^{-1}, CH_3 asymmetric stretch at 3014 cm^{-1}, CH_3

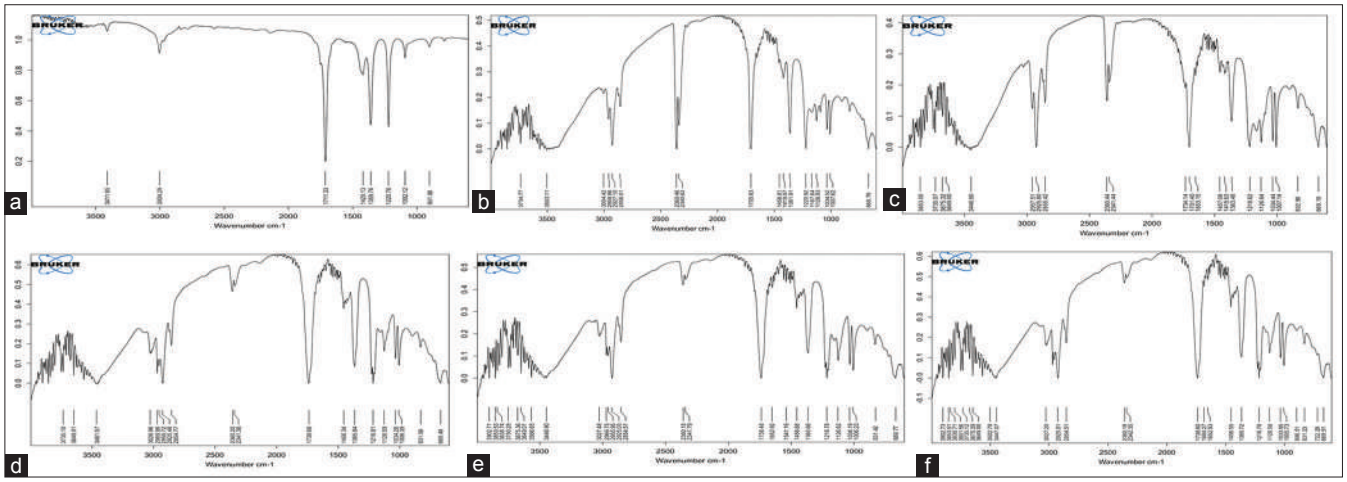

Fig. 5. Fourier transform infrared spectrum for the (a) pure acetone, dodecylbenzenesulfonic acid (DBSA)-acetone mixture of (b) $X_1 = 0.2$, (c) $X_1 = 0.4$, (d) $X_1 = 0.6$, (e) $X_1 = 0.8$, (f) pure DBSA at (298.15°K and P=1 atm)

symmetric stretch at 2971 cm^{-1}, C-C at 1218 cm^{-1}. Clear broad O-H beak at 2900 cm^{-1} in the pure DBSA is the marked sign of it. With increase the dilution of DBSA, it is clear from the Fig. 5 that the OH stretching vibration beak is shifted to a higher wavenumber in the mixtures due to the intermolecular interaction in hydrogen bonding. Moreover, for pure acetone it has been recognized a strong C=O stretch beak at 1715 cm^{-1}. After mixing with DBSA there is a slightly shifting in the C=O stretch beak to a higher wave number. The FTIR characterization for the binary mixture of DBSA-acetone showed a weakness in all the present hydrogen bond in the mixture means that the intermolecular interaction between (O-H) of DBSA and (C=O) of acetone are weak (Hasan, et al., 2011). In the pure case of DBSA and acetone, the intramolecular interaction due to the dispersion is stronger than in the case of their mixtures due to the self-association of DBSA or decreasing the dipole-dipole of the acetone molecules. The result of FTIR supported the result of thermodynamic excess where the excess molar volumes were positive.

V. Conclusion

The experimental values of density, viscosity, and surface tension for the pure case of DBSA and acetone liquids at the temperatures (293.15°K, 298.15°K, 301.15°K) and atmospheric pressure are presented in this paper. Excess molar volume, viscosity deviation, surface tension deviation, and molar excess Gibbs free energy deviation are calculated at the above-mentioned temperatures and correlated to the RK equation. FTIR spectrum of the DBSA-acetone mixture shows a weak intermolecular hydrogen bonding interaction between the molecules of DBSA and acetone. The result of molar excess Gibbs free energy deviation supports the above conclusion of FTIR where the excess molar volume is positive. The intramolecular interaction is strong in the case of pure DBSA and acetone due to the self-association of DBSA molecule or decreasing the dipole-dipole of acetone molecule. The calculated values of excess molar volume are positive for all the temperatures ranging from 293.15°K to 301.15°K. while, the values of viscosity deviation, surface tension deviation, and molar excess Gibbs free energy deviation are negative for all the temperatures studied.

References

Ancian, B., Tiffon, B. and Dubois, J.E., 1983. Molecular interactions and reorientational motion of neat acetone in the liquid state. 17 O NMR chemical shifts and linewidths at variable temperature. *Chemical Physics*, 74(2), pp.171-177.

Arivazhagan, G., Elangovan, A., Shanmugam, R., Vijayalakshmi, R. and Kannan, P.P., 2015. Spectroscopic studies, NBO analysis and dielectric studies on the behaviour of acetone molecules in non-polar solvent environment. *Chemical Physics Letters*, 627, pp.101-106.

Bajić, D.M., Ivaniš, G.R., Visak, Z.P., Živković, E.M., Šerbanović, S.P. and Kijevčanin, M.L., 2013a. Densities, viscosities, and refractive indices of the binary systems (PEG200+1, 2-propanediol,+1, 3-propanediol) and (PEG400+1, 2-propanediol,+1, 3-propanediol) at (288.15 to 333.15) K and atmospheric pressure: Measurements and modeling. *The Journal of Chemical Thermodynamics*, 57, pp.510-529.

Bajić, D.M., Jovanović, J., Živković, E.M., Visak, Z.P., Šerbanović, S.P. and Kijevčanin, M.L., 2013b. Experimental measurement and modelling of viscosity of the binary systems pyridine or nicotine with polyethylene glycols at T=(288.15–333.15) K. New UNIFAC–VISCO and ASOG–VISCO interaction parameters. *Fluid Phase Equilibria*, 338, pp.282-293.

Chai, Y., Dong, D., Ouyang, Y., Liang, Y., Wang,Y., Li, M. and Liu, Q., 2007. Thia-michael addition reactions in water using 3-[Bis(Alkylthio) methylene] pentane-2,4-diones as odorless and efficient thiol equivalents. *Letters Organic Chemistry*, 4, pp.281.

Dash, U.N. and Mohanty, B.K., 1997. Thermodynamic functions of solutions of homologous dicarboxylic acids in water+acetone mixtures from surface tension measurements. *Fluid Phase Equilibria*, 134(1-2), pp.267-276.

Gnanakumari, P., Venkatesu, P., Mohan, K.R., Rao, M.P. and Prasad, D.H.L., 2007. Excess volumes and excess enthalpies of N-methyl-2-pyrrolidone with branched alcohols. *Fluid Phase Equilibria*, 252(1), pp.137-142.

Haba, Y., Segal, E., Narkis, M., Titelman, G.I. and Siegmann, A., 1999. Polymerization of aniline in the presence of DBSA in an aqueous dispersion. *Synthetic Metals*, 106(1), pp.59-66.

Han, M.G., Cho, S.K., Oh, S.G. and Im, S.S., 2002. Preparation and characterization of polyaniline nanoparticles synthesized from DBSA micellar solution. *Synthetic Metals*, 126(1), pp.53-60.

Hasan, M., Hiray, A.P., Kadam, U.B., Shirude, D.F., Kurhe, K.J. and Sawant, A.B., 2011. Densities, viscosities, speeds of sound, FT-IR and 1H-NMR studies of binary mixtures of n-butyl acetate with ethanol, propan-1-ol, butan-1-ol and pentan-1-ol at 298.15, 303.15, 308.15 and 313.15 K. *Journal of Solution Chemistry*, 40(3), pp.415-429.

Jalilian, M.R. and Zahedi-Tabrizi, M., 2008. Spectra and structure of binary azeotropes V-acetone–cyclopentane. *Spectrochimica Acta Part A: Molecular and Biomolecular Spectroscopy*, 69(1), pp.278-281.

Jing, L., Li, X., Che Li, X., ChunHan, Y. and Chu, Y., 2008. The esterification in cyclohexane/DBSA/water microemulsion system. *Colloid Surface A: Physicochemical Engineering*, 326, pp.37.

Knözinger, E. and Wittenbeck, R., 1984. Far-infrared spectra of strongly polar molecules in solid solution: Acetone and nitromethane. *Journal of Molecular Spectroscopy*, 105(2), pp.314-323.

Kollipost, F., Domanskaya, A.V. and Suhm, M.A., 2014. Microscopic roots of alcohol-ketone demixing: Infrared spectroscopy of methanol-acetone clusters. *The Journal of Physical Chemistry A*, 119(11), pp.2225-2232.

Kumar, V., Yokozeki, T., Goto, T. and Takahashi, T., 2016. Synthesis and characterization of PANI-DBSA/DVB composite using roll-milled PANI-DBSA complex. *Polymer*, 86, pp.129-137.

Liu, Y., Jia, L., Guo, X. and Zhao, Z., 2017. Surface activities and thermodynamic properties of novel cationic surfactants with hydroxymethyl group. *Journal of Dispersion Science and Technology*, 38(2), pp.236-240.

Machado, D.S., Moraes, S.R. and Motheo, A.J., 2006. Aspects of the chemical synthesis of PAni-DBSA and its properties. *Molecular Crystals and Liquid Crystals*, 447(1), pp.215-533.

Manabe, K., Lumura, S., Sun, X. and Kobayashi, S., 2002. Dehydration reactions in water. Brønsted acid-surfactant-combined catalyst for ester, ether, thioether, and dithioacetal formation in water. *Jurnal American Chemical Society*, 124, pp.11971.

Manabe, K., Mori, Y. and Kobayashi, S., 2001. Three-component carbon-carbon bond-forming reactions catalyzed by a Brønsted acid-surfactant-combined catalyst in water. *Tetrahedron*, 57(13), pp.2537-2544.

Qian, L.I.U., Zhang, S., Shaochuan, S.H.E., Junxian, Y.U.N. and Kejian, Y.A.O., 2011. Density and viscosity of ternary systems (poloxamer 188+ethanol/acetone+water) at temperatures from 288.15 K to 308.15 K. *Chinese Journal of Chemical Engineering*, 19(3), pp.478-483.

Schindler, W., Sharko, P.T. and Jonas, J., 1982. Raman study of pressure effects on frequencies and isotropic line shapes in liquid acetone. *The Journal of Chemical Physics*, 76(7), pp.3493-3496.

Shikata, T., Sugimoto, N., Sakai, Y. and Watanabe, J., 2012. Dielectric behaviors of typical benzene monosubstitutes, bromobenzene and benzonitrile. *The Journal of Physical Chemistry B*, 116(41), pp.12605-12613.

Shiri, M. and Zolfigol, M.A., 2009. Surfactant-type catalysts in organic reactions. *Tetrahedron*, 65(3), pp.587-598.

Shrikhande, J.J. 2007. p-Dodecylbenzenesulfonic acid: A Brønsted acid-surfactant-combined catalyst. *Research Jurnal Chemical Environmental*, 11, pp.82.

Srivastava, S.K., Ojha, A.K., Koster, J., Shukla, M.K., Leszczynski, J., Asthana, B.P. and Kiefer, W., 2003. Isotopic dilution, self-association, and Raman non-coincidence in the binary system $(CH^3)^2C=O+(CD^3)^2C=O$ reinvestigated by polarized Raman measurement and ab initio calculations. *Journal of Molecular Structure*, 661, pp.11-21.

Tahery, R., 2017. Surface tension and density of mixtures of m-xylene+n-alkane at 293.15 K: Analysis under the extended langmuir and shereshefsky models. *The Journal of Chemical Thermodynamics*, 106, pp.95-103.

Wei, Q., Guo, X., Wang, Y. and Yang, H., 2013. Temperature-dependent FTIR study on three kinds of hydrogen-bonded benzoic acid dimers in their melt states. *Journal of Molecular Liquids*, 177, pp.225-228.

Two New Records of Orchid Species for the Flora of Iraq: *Anacamptis papilionacea* (L.) R.M. Bateman, Pridgeon & M.W. Chase and *Dactylorhiza romana* (Sebast.) Soó

Sami M.A.Youssef[1,2], Honar S. Mahdi[1], Zerevan A. Mergyé[1], Jihad I. Saleem[3], Ahmed M.H.M. Mahmood[1] and Errol Véla[2]

[1]Department of Recreation and Ecotourism, College of Agriculture, University of Duhok, Sumail-Duhok 1063 BD, Kurdistan Region – F.R. Iraq

[2]Botany and Modelling of Plant Architecture and Vegetation (AMAP), Université de Montpellier (CIRAD/CNRS/INRA/IRD, TA A51/PS2), 34398 Montpellier Cedex 5, France

[3]Department of Horticulture, Akre Technical College, Duhok Polytechnic University, Akre, Kurdistan Region – F.R. Iraq

***Abstract*–*The Orchidaceae* is one of the most cosmopolitan flowering families; however, the national floristic knowledge for Iraqi territories is restricted by the outdated and incomplete status of Flora of Iraq. We already recently add two new records of orchid species for Iraq, and the study objective was to pursue the dynamics on field studies and thus provides new contribution for the Flora of Iraq. Two new orchid species were recorded for the first time in Iraq: (i) *Anacamptis papilionacea* found on Silé waterfall locality (Dostaka mountain, Duhok governorate), and (ii) *Dactylorhiza romana* found in Hariké locality (Gara mountain, Duhok governorate). Field illustrations, infraspecific identification (*A. papilionacea* subsp. *schirwanica* and *D. romana* subsp. *georgica*), environment and geographical distribution, conservation status, and a brief discussion about the new records are provided. This study highlights the importance of floristic surveys and their continuity over time as a first step toward the modern floristic knowledge including open databases.**

***Index Terms*—Anacamptis papilionacea subsp. schirwanica, Biodiversity, Dactylorhiza romana subsp. georgica, Flora databases floristic, Kurdistan Region.**

I. Introduction

The *Orchidaceae* family has a wide ecological niche range with a center of diversity on tropical rain forest: Almost all orchids occurring in tropical and subtropical are perennial epiphytes (growing with trees and shrubs), whereas grassland and forest are the favorable habitats for terrestrial orchids in the temperate and Mediterranean regions (Arlott, 1978; Dressler, 1993; Ramírez, et al., 2007). As a consequence, *Orchidaceae* is one of the most cosmopolitan and diversified flowering families (about 800 genera with some 20-30,000 taxa) occurring in all territories except real desert and glaciers (Dressler, 1993; Cozzolino and Widmer, 2005; Christenhusz and Byng, 2016). The orchids flower has specific traits that can be recognized easily from other plant species (for example, spectacular specific petal "labellum" often similar to animal shapes, for example, bees, spiders, lizards, and monkey-like; anthers produce large pollen masses "pollinia"). These specific flowers play an important role in pollination by developing a particular life history strategy in response to evolutionary selective pollinator pressure (Adams and Lawson, 1993; Weston, et al., 2005). In terms of ethnobotany, in Eastern Mediterranean countries called "Levant," the dried underground tubercles of some *Orchis* species often used as a cooking powder by the local people in a hot beverage named "Saleb" or refreshment ice cream named "dondurma" (Kasparek and Grimm, 1999; Kreutz and Çolak, 2009; Löki, et al., 2015). However, it has been reported (Sezik, 2002; Kreutz, 2004; Löki, et al., 2015) that these tubercles collecting activity became threats to *Orchidaceae* family, especially subtribe Orchidinae (*Ophrys, Orchis, Himantoglossum,* and *Anacamptis*) in the Levant. In Kurdistan Region, the local people (such as in Amadyia and Barwarya Bala) collect Orchids' tubercles and then sell the powder to Turkish traders which they in turn sell it in traditional Turkish markets (Véla, et al., 2013; Youssef, et al., 2015).

Although the terrestrial Orchid family is well represented in the Kurdistan Region, as a part of the Flora of Iraq,

ARO-The Scientific Journal of Koya University
Volume V, No 2(2017), Article ID: ARO.10261, 6 pages
DOI: 10.14500/aro.10261
Received 02 June 2017; Accepted 09 November 2017
Regular research paper: Published 28 November 2017
Corresponding author's e-mail: sami.youssef@uod.ac

http://dx.doi.org/10.14500/aro.10261

due to its Mediterranean and/or Eurasiatic biogeographical affinities (Wood, 1985; Véla, et al., 2013; Youssef, et al., 2015), the diversity and taxonomical status of these Orchid taxa still far from being updated and achieved: For example, in the recent field guide work of European and Middle-East orchids (Baumann, et al., 2006), only the 13 regional endemism taxa are accurately cited for Kurdistan Region and/or all Northern Iraq but without any explicit geographical distribution mention for each country. At a starting point, in the previous documented works such as Flora of Iranica (Renz, 1978) and Flora of Iraq (Wood, 1985), 20 and 25 taxa are respectively recorded in the Northern Iraq territories. Whereas, according to Govaerts, et al., (2017) which is the recent world checklist, there are 28 orchids species mentioned for Iraq, but deleted or added taxa are not justified due to lacking of bibliographic data. Therefore, this partial floristic knowledge highlights the importance of the continuity of field surveys to update the Flora of Iraq. It demonstrates also the importance of the new floristic paradigm (Heywood, 2002; 2004) as opportunity to provide precise data such as photo-illustrations, ecological niche information, and accurate recording of geographical coordinates for each locality and checking the accepted name. In this context, we have initiated since 2013 a botanical research project mainly based on field surveying to spotlight on the Orchids' diversity and distribution in Kurdistan Region. In the first floristic survey on *Orchidaceae*, 10 orchids species had been found in Duhok province including one new record "*Ophrys cilicica*" for the Flora of Iraq (Véla, et al., 2013); in the second phase of this project in 2014-2015, another new record "*Orchis spitzelii* subsp. *latiflora*" has been added to the Flora of Iraq, and 8 new orchids taxa have been recorded for Duhok province for the first time which majority of records were new localities and/or rare taxa (Youssef, et al., 2015). Most of these Orchid species are found on the middle mountain zone with a climatic transition between Mediterranean and Irano-Anatolian, confirming the status of Kurdistan Region as a part of the global hotspots for biodiversity (Mittermeier, et al., 2004) but coldspot for floristic knowledge. Although many efforts have been spent in the past years, especially on orchids species, it still needs contributions to enrich the Flora of Iraq. Therefore, the present study aims to fill the gap of floristic field studies about the Flora of Iraq.

II. Materials and Methods

The botanical field surveys were conducted during spring 2016 in diverse locations of Duhok governorate, Kurdistan Region of Iraq. The main botanical field exploration area focused on a tetragon Duhok–Zaxo–Barzan–Kani Massi (former "Ain Nuni" according to the Flora of Iraq) situated on the northern part of Kurdistan Region of Iraq. The diversity landscape's features of this study area are characterized by a mixture of hills, cultivated plains, deep valleys, and mountain chains which are generally extending from West to East. The two fundamental areas deeply investigated are those in Hariké locality on Gara Mountain, Diralok province, and Silé waterfall locality on Dostaka Mountain, Akré province (Fig. 1).

The taxonomical identification of Orchid species was carried out by the help of illustration photos. Initially, the identification process followed Wood (1985) and then was systematically verified according to Flora of Iran (Renz, 1978) and Turkey (Renz and Taubenheim, 1984); The Orchid works of Kreutz (1998), Kreutz and Çolak (2009), and Baumann, et al. (2006) have been used for systematic verification species/subspecies status. For the genus *Anacamptis*, the recent monograph of Kretzschmar, et al. (2007) was used, and for the group of *Dactylorhiza romana,* the revision of Pedersen (2006) utilized.

III. Results

The present study deals with two new records of Orchid species for the Flora of Iraq, found in two different sites thanks to the botanical field survey season in 2016. The first one is *A. papilionacea* discovered on Silé waterfall locality (Dinarta area, Dostaka mountain, Duhok governorate), and the second is *D. romana* found on Hariké locality (Gara mountain, Duhok governorate). These two species are considered new records for the Flora of Iraq because of they were never mentioned under any of their synonyms in any previous floristic literatures, that is, Renz (1978), Wood (1985), Kretzschmar, et al. (2007), Baumann, et al. (2006), and Govaerts, et al. (2017).

To accommodate a complete vision about the actual status of these two new recorded species, we have provided and discussed in details our field data and all recent published researches about these two species : Taxonomical, nomenclatural, biological and ecological data (i.e. accepted scientific name, synonyms, infraspecific identification, ecological niche, population size, geographical distribution, and conservation status) thanks to our field data and also all recent published researches about these two Orchid species.

1. *Anacamptis papilionacea* subsp. *schirwanica* (Woronow) H.Kretzschmar, Eccarius and H.Dietr., Orchid Gen. *Anacamptis Orchis Neotinea*, ed. 2: 174 (2007).

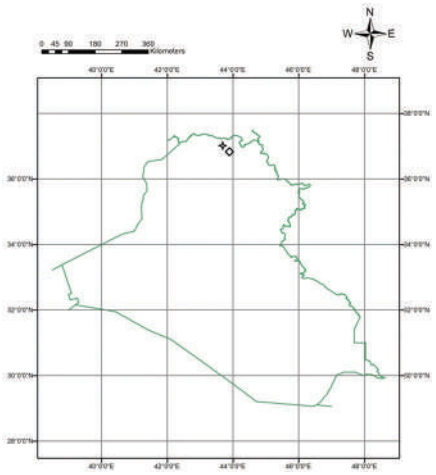

Fig. 1. Location of Orchid sites: Silé waterfall on Dostaka Mountain, Diralok province for *Anacamptis papilionacea* subsp. *schirwanica* (lozenge); and Hariké on Gara Mountain, Akré province for *Dactylorhiza romana* subsp. *georgica* (star), Kurdistan Region of Iraq.

≡ *Orchis schirwanica* Woronow, Izv. Kavkazsk. Muz. 4(4): 263 (1909).
≡ *Orchis papilionacea* subsp. *schirwanica* (Woronow) Soó, Bot. Arch. 23: 36 (1928).
= *Orchis caspia* Trautv. in Trudy Imp. S.-Peterburgsk. Bot. Sada 2: 484 (1873).
= *Orchis papilionacea* var. *bruhnsiana* Gruner in Bull. Soc. Imp. Naturalistes Moscou 4: 453 (1867).
≡ *Vermeulenia papilionacea* var. *bruhnsiana* (Gruner) Szlach., Polish Bot. J. 46: 128 (2001).

A. Type

The lectotypus has been designated by Kretzschmar, et al. (2007). LE, (right specimen - Pict. 17411),02.05.1908, leg. A.Schelkownikov and G.J.Woronow. Origin: Azerbaijan, Scharodilskier ascent in the region Schemajinsk (Gouvemement Baku).

B. General Specific Description

It is a robust plant, having an erect stem (15-30 cm), often with 2-8 lanceolate unspotted leaves. This subspecies is mainly quite stocky with inflorescences that are rich in flowers. Its flowers have a spatula-shaped discreetly spotted crenelated lip.

C. Infraspecific Identification (Fig. 2)

In classical floras (for example, Flora of Turkey and Flora Iranica), this taxon was treated under the genus *Orchis*. Recently, this species has been proposed to be considered in the separated genus *Anacamptis* (Kretzschmar, et al., 2007; Véla and Viglione, 2015), but some others specialists propose to place it in another small genus *Vermeulenia* according to Löve and Löve (1972). Kretzschmar, et al. (2007) reported six subspecies mainly distributed in Mediterranean Region except one in Irano-Anatolian and eastern Caucasian Region *A. papilionacea* subsp. *schirwanica* is given for Azerbaijan and Southeastern of Anatolian Turkey territories (Kretzschmar, et al., 2007; Kreutz, 1998), but its real geographical distribution area remains not exactly delimited. In the Flora of Iraq (Wood, 1985) and all other literatures (Renz, 1978; Renz and Taubenheim, 1984; Kretzschmar, et al., 2007; Kreutz and Çolak, 2009), *A. papilionacea* has never been indicated for Iraq territories. During our botanical field surveys, the researchers found *A. papilionacea* for the first time in Silé waterfall in Akré province. About the precise taxonomical identification, it can be confirmed the subspecies *schirwanica* thanks to the lip shape conform to the plants from Azerbaijan, excluding the subspecies *palaestina*, and the density of inflorescence, excluding the typical subspecies from Italy (Kretzschmar, et al., 2007). Therefore, this observation is the first report for the species in Iraq and consequently also for its subspecies. Actually, its presence in Kurdistan region of Iraq is not really surprising because it belongs to the same mountain chain extending WesternZagros until Southeastern Turkey. Hence, the research finding extents the geographical distribution south-eastward into Iraqi territories, not very far from Iranian border (<100 km). It is why it can reconsider the hypothesis of a potential presence for Iranian territories, previously rejected by Kretzschmar, et al. (2007) "due to a huge distance (>800 km) to the nearest known site" but initially evocated in Flora Iranica, northward in the Alborz mountains (Renz, 1978).

Fig. 2. *Anacamptis papilionacea* subsp. *schirwanica*; (a) Habitat, Silé waterfall locality, south aspect of Dostaka mountain, Akré province (Duhok governorate) Pseudosteppe grassland habitats in middle open Gall oak forest. (b) Habit. (c) Inflorescence. 09 April, 2016. (photos SamiYoussef).

D. Material Examined

Four individuals were collected directly from field (Silé waterfall locality, Akré province), and two specimens among them were deposited in the herbaria of Faculty of Agriculture, University of Duhok, (acronym DPUH). Date of collection: 09/04/2016; Collector Dr. Sami YOUSSEF.

A. papilionacea subsp. *schirwanica* (Woronow) H.Kretzschmar; Akré; herb. Sami Youssef; DPUH no. 3629.

E. Environment and Geographical Distribution

This species has been found at Silé waterfall locality (36°50'43.65" N, 43°53'40.70" E), south exposure of Dostaka mountain, and Akré province Kurdistan Region of Iraq. It occurs at about 875 m. a.s.l. in pseudosteppe grassland habitats in middle open Gall oak (*Quercus aegilops*) on the piedmont of a southern slope. These herbaceous vegetation communities are essentially dominated by herbaceous plants (for example, *Bromus* sp., *Carex* sp., *Hordeum* sp., and *Stipa* sp.) and mainly geophytes species (for example, *Anemone coronaria*, *Poa bulbosa*, *Allium* sp., *Bellevalia* sp., *Muscari* sp., and *Ornithogalum* sp.) which disappear completely during summer. These pseudosteppe forests are characterized by the presence of sparse Gall oak trees and some shrubs (for example, *Rhus coriaria* var. *zebaria, Prunus* sp., *Juniperus oxycedrus* s.l., and *Pistacia khinjuk*). The general climate of this site is Mediterranean continental characterized by a moderate cold and rainy/snowy winter and a hot and completely dry summer Annual rainfall in Akré is around 900/1000 mm, mean minimal temperature of coldest month around 0°C, and mean maximal temperature of hottest month

http://dx.doi.org/10.14500/aro.10261

40°C (Guest and Al-Rawi, 1966; Climate Data for Cities Worldwide, 2017).

F. Conservation Status

In Silé waterfall locality, the researchers found only one small population with a few disperses individuals (<20) occupied a small surface area (<1 hectare). This location is threatened by high anthropogenic activities: It is frequented by a high number of tourists due to its famous and wonderful waterfall. Furthermore, this region is internationally well known by the over-collecting of the "Zebaria sumac fruit" (*R. coriaria* var. *zebaria*) used in divers traditional Kurdish dishes (Shahbaz, et al., 2015). The over-harvesting of the others wild edible plants (such as *Gundelia* sp., *Allium* sp., *Arum* sp., *Echium* sp., and *Rheum* sp.) leads to the degradation of many natural habitats. Consequently, this rare species needs an urgent planning strategy for biological conservation by regional Kurdish authorities.

2. *D. romana* subsp. *georgica* (Klinge) Soó ex Renz &Taubenheim, Notes Roy. Bot. Gard. Edinburgh 41: 271 (1983).

≡ *Orchis mediterranea* subsp. *georgica* Klinge, Trudy Imp. S.-Peterburgsk. Bot. Sada 17(1): 19 (1898).

= *Dactylorchis flavescens* (K.Koch) Verm., Stud. Dactylorch:. 65 (1947).

A. Type

The lectotypus has been designated by Pedersen (2006). Rchb.f., Icon. Fl. Germ. Helv. XIII/XIV: Pl. 62(I), 1851.

B. General Specific Description

It is a robust tuberous plant (15-40 cm high). With Basal leaves lanceolate or narrowly obovate, up to 18 cm long; Inflorescence cylindrical densely flowered; bracts clear bright green, lanceolate, exceeding the flowers; Flowers mainly or only yellow color, rather small; labellum usually longer than broad, to 8 mm broad, shortly 3-lobed toward the apex; Spur narrowly cylindrical, horizontal, or slightly turned upward, slightly ascending, usually shorter than the ovary, around 1.5 longer than the lip.

C. Infraspecific Identification (Fig. 3)

D. romana with both subspecies *georgica* and *romana* has been highlighted their occurrence in Turkey territories (Renz and Taubenheim, 1984), whereas only *D. romana* subsp. *georgica* had been reported for Iranian territories (Renz, 1978). These two subspecies are well distinguished both morphologically and biogeographically: *D. romana* subsp. *romana* is a real Mediterranean element (from Italy to Turkey throughout Balkan Region) and mostly characterized by its rather large flowers with red-to-yellow color, whereas *D. romana* subsp. *georgica* is an Irano-Anatolian and Transcaucasian element (from East Turkey to Turkmenistan throughout Iran) and characterized by its rather small flowers mainly or only yellow color and with shorter spur (Renz, 1978; Renz and Taubenheim, 1984; Delforge, 2005). These

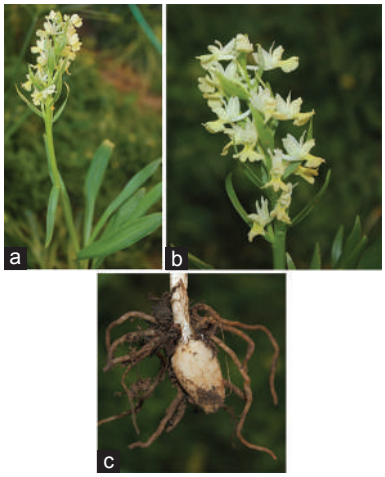

Fig. 3. *Dactylorhiza romana* subsp. *georgica*; Hariké locality, northern aspect of Gara mountain, Diralok province, 16 April 2016. (a) Habit; (b) inflorescence; (c) undivided tubercle (photos Sami Youssef).

two subspecies have never been reported in Kurdistan Region and Iraqi territories (Renz, 1978; Renz and Taubenheim, 1984; Wood, 1985; Kreutz, 1998; Delforge, 2005; Govaerts, et al., 2017). During our botanical field survey in 2016, the researchers found some specimen of *D. romana* for the first time in Hariké locality (Gara Mountain). About the taxonomical identification, we it can be confirm the *D. romana* subsp. *georgica* characterized by its rather small flowers mainly or only yellow color, and its shorter spur around 1.5 longer than the lip (Renz and Taubenheim, 1984; Delforge, 2005). Thus, it is a new record for the Flora of Iraq. Its occurrence in Kurdistan Region of Iraq is not really surprising because already known from Golistan and Azerbaijan provinces in Northwest and North of Iran (Renz, 1978) and even more from Siirt and Bitlis provinces in Southeast of Turkey (Renz and Taubenheim, 1984; Kreutz, 1998) not far from Kurdistan Region border.

D. Material Examined

Four individuals were collected directly from field (Hariké locality, Diarlok province), and one of them was cultivated in Montpellier (South-Eastern France). Date of collection 16/04/2016; Collector Mr. Zerevan Mergye and Dr. Sami Youssef.

E. Environment and Geographical Distribution

This species has been found at Hariké locality (37°01'20.97" N, 43°40'59.21" E) northern slope of Gara Mountain, Diralok province, Kurdistan Region of Iraq. It has been found in open habitat at more or less 969 m. a.s.l. dominated by herbaceous vegetation community marked frequently by the occurrence of diverse dwarf shrub (for example, *Daphne acuminata*, *Lonicera arborea,* and *Astragalus* sp.). It is just situated on the margin of Lebanon Oak (*Quercus libani*) forest zone on a secondary crest with northern exposure. It grows on relatively deep soil with a sufficient water supply in spring. The local climate is globally the same than previously described, but the topoclimate is

characterized by a shadow winter with a persistent snow (at least 1 or 2 months) and a cooler spring and summer.

F. Conservation Status

The observed population comprises only few individuals (<20) in a small surface of much less than one hectare. Consequently, the study can confirm that *D. romana* subsp. *Georgica* is a rare species in locations (only one at Iraq level), occupied surface area and size of population. Furthermore, this location could be potentially threatened by traditional harvesting of the edible plants. Particularly, the real threaten is concerning collecting of the tuberous testicles of Orchid species (for example, *Orchis mascula* and *Orchis anatolica*) by local people to sell it on traditional markets that will be used after made "Saleb" and ice cream "dondurma" in Turkey. By chance, as far as researchers know, this yellow-flowered *Dactylorhiza* is not collected probably because ignoring their identical properties.

IV. Discussion

A. Flowers Field Surveys as a Proxy Toward the New Floristic Paradigm

The floristic surveys as an old scientific concept remain the basic foundation for describing the plant biodiversity of an area and our ability to communicate about them (Heywood, 2001; 2002). It has always received considerable attention from botanists and evolutionary systematicists. However, the "new floristic paradigm" emerged in the recent year is characterized by satisfaction of a wide range of users "taxonomists," high quality outputs data, and accessibility and consistent in its methods and procedures (Heywood, 2002; 2004). This revolution development has actively participated to identify the biological conservation priorities in the megadiverse countries (Heywood, 2004; Victor, et al., 2015). From this new paradigm standpoint, the necessity of completing floristic inventories has become an evident key player to update permanently the existent floras. In this context, the Flora of Iraq, thus far, remains the basic foundation for the plant biodiversity description and to communicate about it. Despite the formidable floristic inventories of the past century (Townsend and Guest, 1966-1985), the status of the Flora of Iraq is outdated and incomplete, and it can be designated as a hotspot of biodiversity but coldspot of knowledge. The main raison for the nonachievement of this flora could be resumed by the chronic instability of the political situation. This has been aggravated by some scientific-personal interest changes in Iraq allowed to unaccomplished the mission of publication the remaining parts (volumes 6 and 7) of the Flora of Iraq (Ghazanfar and McDaniel, 2016). The strong lack in taxonomists and/or naturalists or they lack of autonomy on the field cannot allow filling the gaps of floristic data on unexplored area such as lot of the local mountains (Barzan area, Barwarya Bala, and Nerwayé areas near Turkish border). However, some important advances have been made in the past decade insight of new contribution to the Flora of Iraq For example, divers botanical field surveys carried out and reported several new taxa and new records for Iraq (National Report on Biodiversity in Iraq, 2010; Ahmad, 2013; Véla, et al., 2013; Shahbaz, et al., 2015; Youssef, et al., 2015; Ahmad, 2016; Youssef, et al., 2017). Meanwhile, a lot of taxa remain to be discovered, which is not surprising in view of its geographical situation as a part of Irano-Anatolian hotspot of biodiversity. In regard to this particular situation, the Flora of Iraq needs an urgent completing floristic inventories to provide adequate continual updating data, and gigantic efforts should be realized to modernize the flora toward the new paradigm. In this context, the present study attributes these new data as a continuity of the updating floristic works on Orchid species list occurring in Kurdistan Region (Véla, et al., 2013; Youssef, et al., 2015) and also updating their nomenclature status (accepted names, synonyms…). In contrast, this floristic field surveys contribute to highlight the urgent need to a national program strategies for biodiversity conservation, which will play an important role to find a suitable balance between biodiversity management and decreasing the influence of the increasing anthropogenic activities (for example, over-collecting edible plants).

In this botanical field survey on Orchid species, there were two new records of Orchid species for the Flora of Iraq which was not highlighted previously (Véla, et al., 2013; Youssef, et al., 2015). In this study, both taxa are considered as very rare species, and their localities are under real or potential threaten by the increasing anthropogenic activities. To take advantage of this situation thus, the researchers could organize themselves effectively to play a key role in influencing the decision-making "governments" about the urgent biological conservation priorities.

Acknowledgment

The authors would like to express their deepest gratitude to the University of Duhok for supporting the botanical exploration.

References

Adams, P.B. and Lawson, S.D., 1993. Pollination in Australian orchids: A critical assessment of the literature1882-1992. Australian Journal of Botany, 41, pp.553-575.

Ahmad, S.A., 2013. Eighteen species new to the flora of Iraq. Feddes Repertorium, 124, pp.65-68.

Ahmad, S.A., 2016. Scrophularia kollakii (*Scrophulariaceae*), a new species from Kurdistan, Iraq. Harvard Papers in Botany, 21, pp.93-95.

Arlott, W.W., 1978. *Orchids of Britain and Europe, Britain*. Collins, London.

Baumann, H., Künkele, S. and Lorenz, R., 2006. *Orchideen Europas, Mit Angrenzenden Gebieten*. Eugen Ulmer, Stuttgart.

Christenhusz, M.J. and Byng, J.W., 2016. The number of known plants species in the world and its annual increase. Phytotaxa, 261(3), pp.201-217.

Climate Data for Cities Worldwide, 2017. Available from: https://www.en.climate-data.org. [Last accessed on 2017 May 10].

Cozzolino, S. and Widmer, A., 2005. Orchid diversity: An evolutionary consequence of deception? Trends in Ecology and Evolution, 20(9), pp.487-494.

Delforge, P., 2005. *Guide des Orchidées d'Europe, d'Afrique du Nord et du Proche-Orient.* 3rd ed. Delachaux and Niestlé, Paris.

Dressler, R.L., 1993. *Phylogeny and Classification of the Orchid Family*. Dioscorides Press, Portland, U.S.A.

Ghazanfar, G. and Mcdaniel, T., 2016. Flora of the Middle East: A quantitative analysis and Biogeography of the flora of Iraq. Edinburgh Journal of Botany, 73(1), pp.1-24.

Govaerts, R., Bernet, P., Kratochvil, K., Gerlach, G., Carr, G., Alrich, P., Pridgeon, A.M., Pfahl, J., Campacci, M.A., Holland-Baptista, D., Tigges, H., Shaw, J., Cribb, P., George, A., Kreutz, K. and Wood, J., 2017. World checklist of *Orchidaceae. Facilitated by the Royal Botanic Gardens, Kew*. Available from: http://www.apps.kew.org/wcsp. [Last retrieved on 2017 Sep 29].

Guest, E. and Al-Rawi, A., 1966. *Flora of Iraq, Introduction to the Flora*. Vol. 1. Ministry of Agriculture and Agrarian Reform, Republic of Iraq, Baghdad.

Heywood, V.H., 2001. Floristics and monography: An uncertain future? Taxon, 50, pp.361-380.

Heywood, V.H., 2002. The future of floristics in the mediterranean region. Israel Journal of Plant Sciences, 50 Suppl 1, pp.5-13.

Heywood, V.H., 2004. Modern approaches to floristics and their impact on the region of SW Asia. Turkish Journal of Botany, 28, pp.7-16.

Kasparek, M. and Grimm, U., 1999. European trade in Turkish salep with special reference to Germany. Economic Botany, 53, pp.396-406.

Kretzschmar, H., Eccarius, W. and Dietrich, H., 2007. *The Orchid Genera Anacamptis, Orchis, Neotinea*. EchinoMedia, Bürgel.

Kreutz, C.A.J. and Çolak, A.H., 2009. *Türkiye Orkideleri*. RotaYayınları, İstanbul.

Kreutz, C.A.J., 1998. *Die Orchideen der Türkei*. C.A.J. Kreutz, Landgraaaf, NL.

Kreutz, C.A.J., 2004. New and interesting orchid sites from South-eastern Turkey and remarks to the continual decline of the orchids in this country. Journal Europäischer Orchideen, 36, pp.1045-1059.

Löki, V., Tökölyi, J., Süveges, K., Lovas-Kiss, A., Hürkan, K., Sramkó, G. and Molnár, V., 2015. The orchid flora of Turkish graveyards: A comprehensive field survey. Willdenowia, 45(2), pp.231-243.

Löve, Á. and Löve, D., 1972. Vermeulenia-a new genus of orchids. Plant Biology, 21(5), pp.553-554.

Mittermeier, R.A., Roblesgil, P., Hoffmann, M., Pilgrim, J., Brooks, T., Mittermeier, C.G., Lamoreux, J. and da Fonseca G.A.B., 2004. *Hotspots Revisited Earth's Biologically Richest and Most Endangered Ecoregions*. CEMEX, Mexico City, Mexico.

National Report on Biodiversity in Iraq. (2010), *Ministry of Environment.* Iraq. Available from: http://www.cbd.int/doc/world/iq/iq-nr-04-en.pdf. [Last retrieved on 2017 May 20].

Pedersen, H., 2006. Systematics and evolution of the *Dactylorhiza romana*/*Sambucina polyploid* complex (*Orchidaceae*). Botanical Journal of the Linnean Society, 152(4), pp.405-434.

Ramírez, S.R., Gravendeel, B., Singer, R.B., Marshall, C.R. and Pierce, N.E., 2007. Dating the origin of the *Orchidaceae* from a fossil Orchid with its pollinator. Nature, 448(7157), pp.1042-1045.

Renz, J. and Taubenheim, G., 1984. *Orchidaceae*. In Davis, P.H., editor. *Flora of Turkey and the East Aegean Islands*. Vol. 8. Edinburgh University Press, Edinburgh.

Renz, J., 1978. *Orchidaceae*. In: Rechinger, K.H., editor. *Flora Iranica: Convolvulaceae, Akademische Druck-u.* Vol. 126. Verkagsanstalt Graz, Austria. pp.1-148.

Sezik, E., 2002. Turkish orchids and salep. Acta Pharmaceutica Turcica, 44, pp.151-157.

Shahbaz, S.E., Saleem, J.I. and Abdulrahman, S.S., 2015. *Rhus coriaria* var. zebaria (*Anacaridaceae*), a new variety from Iraq. Nordic Journal of Botany, 33, pp.50-56.

Townsend, C.C. and Guest, E., 1966-1985. *Flora of Iraq*. Vol. 1, 2, 3, 4, 8. The White Friars Press Ltd, Ministry of Agriculture and Agrarian Reform, Republic of Iraq, Tonbridge, Baghdad.

Véla, E. and Viglione, J., 2015. Recent inputs to Lebanese orchid flora and anessay of a national checklist for *Orchidaceae* family. Acta Botanica Gallica-Botany Letters, 162(4), pp.271-285.

Véla, E., Youssef, S. and Mahmood, A., 2013. First survey on orchids (*Orchidaceae*) of Duhok province in Kurdistan region (N-Iraq). Journal Europaïscher Orchideen, 45, pp.235-254.

Victor, J.E., Smith, G.F. and Van Wyk, A.E., 2015. A method for establishing taxonomic research priorities in a megadiverse country. Phytotaxa, 203(1), pp.55-62.

Weston, P.H., Perkins, A.J. and Entwisle, T.J., 2005. More than symbioses Orchid ecology, with examples from the Sydney region. Cunninghamia, 9(1), pp.1-15.

Wood, J.J., 1985. *Orchidaceae*. In: Townsend, C.C. and Guest, E., editors. *Flora of Iraq*, *Monocotyledones, Excluding Gramineae.* Vol. 8. The White Friars Press Ltd, Ministry of Agriculture and Agrarian Reform, Republic of Iraq, Tonbridge, Baghdad.

Youssef, S., Mahmood, A. and Véla, E., 2017. On the genus Sternbergia (Amaryllidaceae) in Iraq. Anales del Jardin Botanico de Madrid, 74(1), p.e053.

Youssef, S., Mahmood, A., Mahdi, H. and Vela, E., 2015. New contribution on orchids (*Orchidaceae*) of Duhok province in Kurdistan region (N-Iraq). Journal Europäischer Orchideen, 47, pp.405-420.

Thermal Effects on Compressive Strength of Local Limestone and Claystone

Rahel K. Ibrahim[1], Nawzat R. Ismail[2] and Hemn M. Omar[2]

[1]Department of Civil Engineering, Faculty of Engineering, Koya University, Danielle Mitterrand Boulevard, Koya KOY45, Kurdistan Region - F.R. Iraq

[2]Department of Geotechnical Engineering, Faculty of Engineering, Koya University, Danielle Mitterrand Boulevard, Koya KOY45, Kurdistan Region - F.R. Iraq

Abstract–Limestone and claystone are widely used in rocky mountainous areas as building materials in Kurdistan region, in particular, the city of Koya. The outbreak of fire in buildings will have a great impact on strengths of building materials. The property performance of these local materials is understudied. This research investigates the impact of high temperature on the physicomechanical properties of limestone and claystone from Fatha Formation in Koya in Kurdistan region of Iraq. For this purpose, cores were taken from intact rocks; their ends were cut by a mechanical saw to obtain a cylindrical shape and immersed in water for 24 h, and then, subjected to physicomechanical tests of specific gravity, water absorption, porosity, and uniaxial compressive strength. For determining the residual compressive strength, the specimens were taken out from water, surface dried, and exposed to high temperatures of 450, and 650°C for 2 h using an electric oven. The results showed that claystone specimens show more stable mechanical properties than the limestone after exposure to high temperatures, and the high temperature causes lightening in color and significant cracks in both materials.

***Index Terms*—Compressive strength, Claystone, Limestone, Kurdistan Region, Thermal effects.**

I. Introduction

Limestone and claystone have many applications in the construction sector. Using these materials as building units in houses, bridges, tunnels, and the renovation of historic structures are some of these applications. The superior physicomechanical properties for these materials and their low cost qualify them for use in the mentioned applications.

Fire causes destructive damages to structures. Cracks, crusts, and spalling were observed in building stone when exposed to fire. It is considered that cracks refer to discontinuities formed by thermal gradients within the rock blocks during the fire (Koca, et al., 2006). Besides the undesired esthetic considerations, cracks may cause serious structural problems to the structures. It is important to investigate the effect of fire and high temperature on the building units, including natural stones. The walls of structures built by these materials must necessarily withstand high temperatures in the fire which causes serious deterioration in strength and stability (Hajpál, 2002).

Ozguven and Ozcelik (2013) investigated the effect of different degrees of temperatures (room temperature, 200°C, 400°C, 600°C, 800°C, and 1000°C) on marble and limestone using the aspects of change in color and whiteness, polish reception, daily physical changes, and pH. Ozguven and Ozcelik (2013) found that, when natural stones are heated to temperatures above 800°C their structure damages and/or changes, the material becomes pours and cracks occur. They also mentioned that natural stones that face this amount of heat under atmospheric conditions generally, crack, fragmentize, spall, and disperse. Sengun (2014) investigated the influence of temperatures ranging from 105°C to 600°C on the physical and mechanical properties of six carbonate rock samples (two marbles, two low-porous limestones, and two high-porous limestones). It was found that the values of bulk density, P-wave velocity, uniaxial compressive strength and modulus of elasticity, tensile strength, and shore hardness decreased to different extents, whereas apparent porosity increased under the influence of heat up to 600°C. The results indicated a maximum decrease of 62–82% in modulus of elasticity and the least reduction of 1.2–2.7% in bulk density of carbonate rocks. Moreover, the uniaxial compressive strength, tensile strength, P-wave velocity, and shore hardness values decreased by 27–51%, 28–75%, 36–69%, and 10–40%, respectively. Besides, increase in apparent porosity values of tested rocks with very high porosity was decreased, whereas the apparent porosity values of low-porous rocks increased up to 10 times of the initial value.

The calcinations of calcite from 800°C may constitute the main effect generated by fire, as both the transformation from

ARO-The Scientific Journal of Koya University
Volume V, No 2(2017), Article ID: ARO.10283, 6 pages
DOI: 10.14500/aro.10283
Received 31 July 2017; Accepted 11 November 2017
Regular research paper: Published 28 November 2017
Corresponding author's e-mail: hemn.omar@koyauniversity.org

http://dx.doi.org/10.14500/aro.10283

calcite to calcium hydroxide and the subsequent hydration of calcium hydroxide involve important volume changes that may alter the internal structure of the stone.

$CaCO_3$ + HEAT → CaO + CO_2↑

CaO + H_2O → $Ca(OH)_2$ + HEAT

The most catastrophic changes occurred in limestone cores, beginning to take place above 600°C due to calcination processes. This process has been previously reported as a result of high temperature in testing stones containing calcite (Török and Hajpál, 2005; Gomez-Heras, et al., 2006).

It is known that fire and high temperatures cause degradation of natural building stones. There are insufficient studies focusing on the effect of high temperature on physicomechanical properties of limestone and claystone building units. The aim of this research is to investigate the effect of high temperature on the limestone and claystone cores were taken from Fatha Formation in Koya/Iraqi Kurdistan region to show the rocks residual strength after the fire.

II. Geological Setting of the Study Area

Koya tectonic lies in the High Folded Zone of Unstable Shelf, and geographically, it is located in the North East (NE) of Iraq. Haibat Sultan anticline is considered as one of the main folds belongs to this zone which is double plunging and asymmetrical anticline. The fold is extending in the direction of North West–South East trends parallel to the Zagros Fault Thrust Zone. The Iraqi Shelf can be divided into five tectono-physiographic zones. The zones are characterized by varying degrees of Neogene structural deformations. Currently, it is generally bounded by major faults which represent deep-seated structural elements. These zones from NE to South West (SW) are as follows: The Thrust Zone, the Folded Zone, the Mesopotamian Basin, and Salman Zone and the Rutbah-Jezira Zone (Buday and Jassim, 1987; Jassim and Goff, 2006). The Fatha Formation is one of the most widespread and economically important formations in Iraqi Kurdistan region. It forms the continuous belt at the foot SW limb of Haibat Sultan Mountain in Koya area. It is from Middle Miocene age, comprises of anhydrite, gypsum, and salt interbedded with limestone and marl (Buday, 1980). The thickness of the formation is greatly variable. In the central parts of the basin, the thickness is up to 900 m, whereas the thickness of the formation in the studied area ranges between 60 and 200 m (Youkhana and Sissakian, 1986; Omer, 2009). The formation represents the deposits of a relatively strong sinking basin, which often had been separated from the open sea by rising ridges (Buday, 1980). It consists of cyclic deposits of claystone and limestone with gypsum beds in lower cycles. Claystone, reddish-brown in color, is of fine particles and highly fractured, which represents the main consistent of the formation (Omer, 2009). In the studied area, the formation comprises cycles of claystone, siltstone, and sandstone with gypsum and limestone bed. Claystones, reddish-brown in color, are fine to very fine grained, and limestone of white-to-grayish color is characterized by the development of joints and fractures. The bedded exist in moderate to well thick beds, which represents the main constituents of the formation. The locations of study samples are bounded by the Universal Transverse Mercator (UTM) grid 3995011 and 3995423 North, 0468319 and 0468973 East, as summarized in Table I and Fig. 1.

III. Materials and Methods

Eighteen outcrop samples of limestone and claystone were taken from three locations of Fatha Formation. The samples were cut by the use of core cutting machine. After cutting, the two circular surfaces of the specimens were straitened by an electrical saw. All the samples were cut to have a cylindrical shape of 7.5 cm in diameter and 14 cm height. The core samples were coded and immersed in a water tank for 24 h (Fig. 2).

To determine the effect of high temperature, the most common method is putting the samples in an oven (Hajpál and Török, 2004; Gomez-Heras, et al., 2009), and to explain the effect of temperatures, different degrees of temperature must be selected. The purpose of this operation is to clearly show what kind of changes occurs at different high temperatures. Samples were exposed to the heat separately starting from gradually 450°C and 650°C and then compared with reference samples at room temperature of 25°C. The oven was brought to the desired high temperature, and then, the samples were taken out from water tank, surface dried, and put in the oven for 2 h. After heating, the samples were taken out from the oven, cooled to room temperature, and then, subjected to compression test with the non-heated samples. The compressive strength tests were carried out according to the Standards American Society for Testing and Materials (2014).

IV. Physicomechanical Properties Results and Discussions

The average values of the specific gravity, water absorption, and porosity determined from the laboratory for limestone and claystone are 2.67, 0.281, and 0.75 and 2.36, 6.28, and 14.97, respectively, as shown in Table II. The results of uniaxial compressive strength and relative compressive strength for limestone and Claystone are shown in Figs. 3 and 4, respectively. The strength trend curves for the both materials before and after exposure to high temperatures are shown in Fig. 5. For relative compressive strength, the strength of non-heated limestone samples was taken as 100%, and the strength for other specimens was related to this strength. The

TABLE I
Locations of Outcrops Samples in the Study Area by Universal Transverse Mercator (UTM)

Location number	Formation	Coordinates (North and East line)
1	Fatha	3995325 N and 0468422 E
2	Fatha	3993775 N and 0469925 E
3	Fatha	3992230 N and 0469575 E

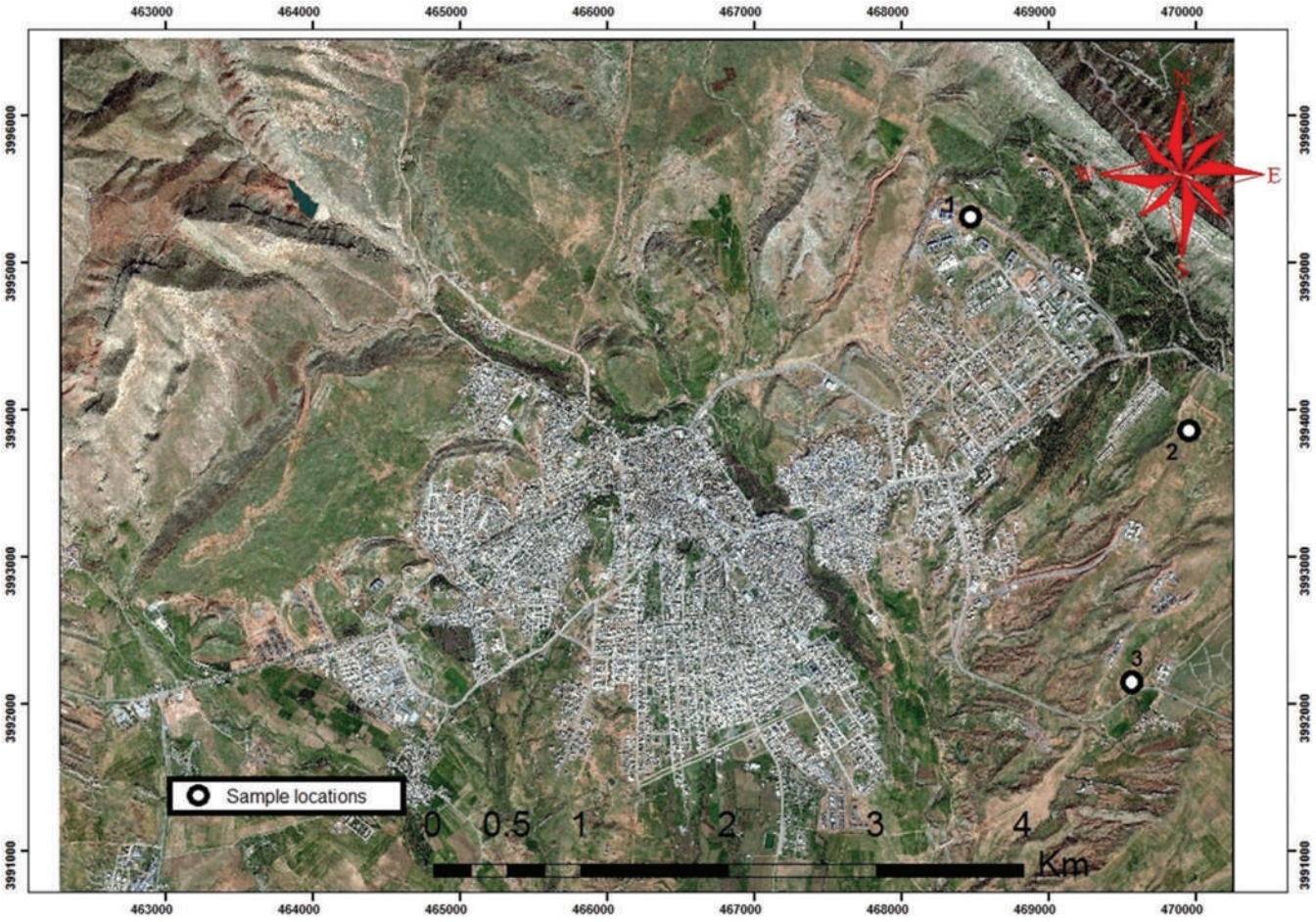

Fig. 1. Satellite Image of Koya City which Indicates the Sample Locations.

Fig. 2. Eighteen Different Core Samples Collection from Limestone and Claystone of Fatha Formation for Laboratory Tests.

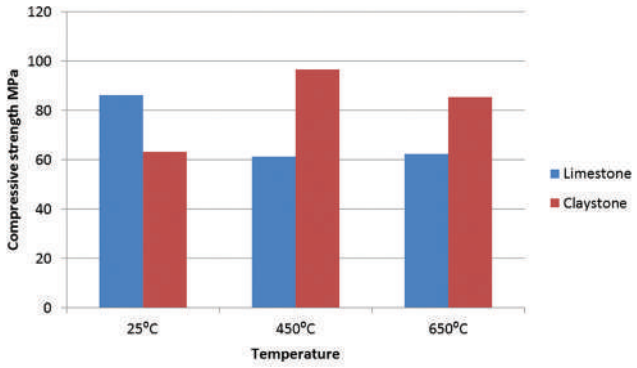

Fig. 3. Compressive Strength for Limestone and Claystone Cores Exposed to Different Temperatures.

average value of compressive strength for limestone ranges from 61.37 to 86.32 MPa, whereas for claystone, the value ranges from 63.17 to 96.6 MPa. The uniaxial compressive strength of limestone and claystone falls within the range of high strength according to New Zealand Geotechnical Society, 2005. Field description of soil and rock, New Zealand: Publication of NZ Geotechnical Society. Statistical models were generated to relate the mechanical properties with the physical properties.

A. Specific Gravity

The specific gravity of a rock is one of its basic properties. It is influenced primarily by the density of the minerals, their content, and amount of void space inside the rock (Bell and Lindsay, 1999). In general, the specific gravity is said to be high when its value exceeds 2.8, and it is usually considered as low when that value is <2.3. The specific gravity stated that the specimens did not show significant changes through laboratory tests. The results of the analyses revealed that the specific gravity displayed little variation and average range from 2.67 to 2.36 for limestone and claystone, respectively, this indicates that limestone has medium value, but claystone has a low value of specific gravity.

http://dx.doi.org/10.14500/aro.10283

TABLE II
RESULTS OF SPECIFIC GRAVITY, WATER ABSORPTION, AND POROSITY OF SAMPLES

Symbol number	Lithology	Saturated surface dry (g)	Weight in water (g)	Dry weight (g)	Specific gravity	Water absorption (W %)	Porosity (n %)
A1	Limestone	751	471	747	2.66	0.535	1.43
A2	Limestone	846	533	845	2.69	0.118	0.32
A3	Limestone	820	516	818	2.69	0.244	0.66
A4	Limestone	907	572	905	2.70	0.220	0.59
A5	Limestone	822	516	820	2.67	0.243	0.65
A6	Limestone	791	491	789	2.63	0.250	0.66
A7	Limestone	853	538	852	2.70	0.117	0.32
A8	Limestone	779	489	776	2.68	0.386	1.03
A9	Limestone	713	447	710	2.67	0.422	1.13
Average					2.67	0.281	0.75
B1	Claystone	736	447	697	2.41	5.595	13.50
B2	Claystone	840	500	783	2.30	7.279	16.76
B3	Claystone	740	451	703	2.43	5.263	12.80
B4	Claystone	749	450	706	2.36	6.090	14.38
B5	Claystone	646	390	606	2.36	6.600	15.63
B6	Claystone	626	376	585	2.34	7.008	16.40
B7	Claystone	721	433	676	2.34	6.656	15.63
B8	Claystone	694	420	654	2.38	6.116	14.59
B9	Claystone	734	441	693	2.36	5.916	15.02
Average					2.36	6.280	14.97

B. Effect of High Temperature on the Compressive Strength of Limestone

The compressive strength and relative compressive strength for limestone cores exposed to different temperatures are shown in Figs. 3 and 4, respectively. Exposing limestone cores to 450°C resulted in a significant decrease in compressive strength, the strength dropped from 86.32 to 61.37 MPa. The compressive strength of cores after exposure to 650°C was 62.27 MPa which remained approximately similar to that of 450°C. The exposure to high temperature resulted in approximately 30% strength reduction with respect to non-heated samples. This phenomenon is highly due to the transformation of calcium carbonate to lime CaO by the effect of high temperature as stated by Koca, et al., 2006. Moreover, the vapor pressure due to temperature rise inside the specimens causes micro and visible cracks which in turn reduce the compressive strength.

Limestone is consisting of calcite. Calcite is a mineral not much harder than a fingernail. Consequently, limestone is soft. It can easily be dissolved when it exposed to a temperature up to 400°C and changes to free lime as found by Yong and Thomas (1999) and Egger (2006).

C. Effect of High Temperature on the Compressive Strength of Claystone

The compressive strength and relative compressive strength results for claystone cores after exposure to high temperatures are shown in Figs. 3 and 4, respectively. The claystone specimens after exposure to 450°C exhibited a considerable increase in compressive strength. The strength rise was around 40%, and it rises from 63.17 MPa for non-heated specimens to 96.6 MPa for those exposed to 450°C. The compressive strength of 85.4 MPa was recorded for claystone cores after exposure to 650°C; this recorded value is around 13% less than the strength of specimens exposed to 450°C but greater than the none-heated specimens by nearly 25%.

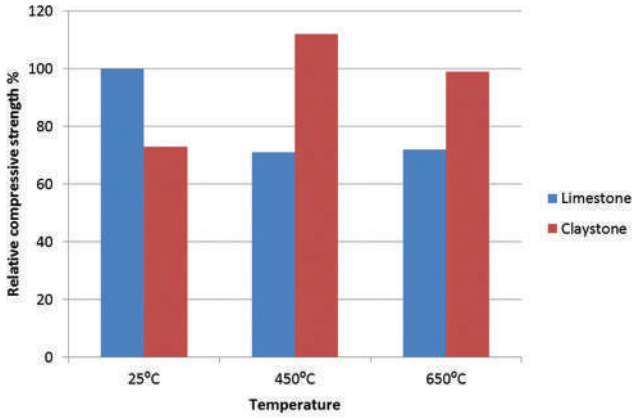

Fig. 4. Relative Compressive Strength for Limestone and Claystone Cores Exposed to Different Temperatures.

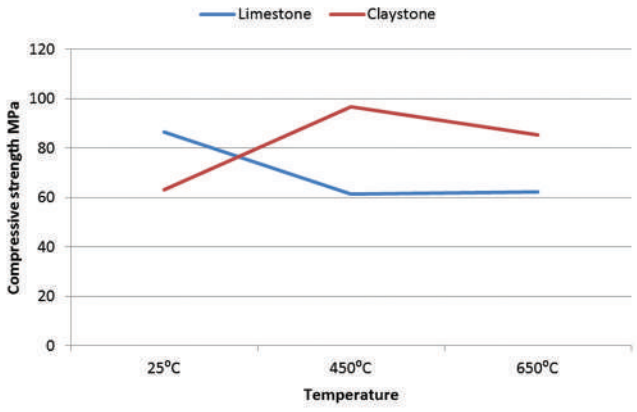

Fig. 5. The Strength Trend Curves for Limestone and Claystone before and after Exposure to High Temperature.

The increase of strength for claystone after exposure to high temperature is attributed to strengthening the bonds of silicate minerals in claystone when exposes to high temperatures. Although some visible cracks were detected on the specimens due to high temperature, the strength was higher than that of non-heated specimen. This phenomenon indicates how strong the bonds become between the silicate minerals after exposure to 650°C. Moreover, the mineralogical decomposition may not occur in claystone, and the high temperature made the particles to be packed together tightly, which by turn resulted in increasing the strength after exposure to high temperature.

D. Porosity Effect on the Compressive Strength

During the process of diagenesis, sediments undergo physical, chemical, mechanical, and mineralogical changes by increasing in temperature and pressure. This increase in temperature and pressure causes loose grained sediments that become tightly packed reducing porosity, essentially squeezing water out of the sediment. Porosity is further reduced by the precipitation of minerals into the remaining pore spaces as stated by Boggs, (2006). A comprehensive study of porosity can provide valuable information to determine whether a given type of natural stone is susceptible to thermal stresses or not (Malaga-Starzec, et al., 2006). The compressive strength results for the limestone and claystone cores after exposure to different temperatures as a function of porosity as shown in Table II.

From the porosity results, it can be observed that limestone samples showed lower porosity than claystone ones. This phenomenon is due to the susceptibility of high clay mineral in claystone for decomposition caused by moisture, an action that increases porosity for the rocks.

The exposure to high temperature causes the moisture in the samples to evaporate. This phenomenon produces a buildup vapor pressure in the samples and causes them to crack which in turn reduces compressive strength. Hence, the higher compressive strength that recorded for claystone than limestone after exposure to high temperature is due to the vapor release caused by the high porosity of the claystone which produces escape path for the vapor pressure to release.

E. Water Absorption at Atmospheric Pressure

Water absorption is a measure of the effective porosity of a stone. The total water absorption value under atmospheric pressure conditions indicates how much water a rock can absorb over 24 h when placed at 3–5 cm below the water level. The water uptake in relation to the dry weight of the sample is mainly influenced by porosity, pore size distribution, and the mineralogical composition of the rock. The water absorption is dependent on the clay minerals present in the rock material which indirectly affects the strength (Mohamad, et al., 2013). Due to the dominance of quartz and clay mineral, the specific gravity of claystone is about 2.36, whereas calcitic limestone rocks have a specific gravity of 2.67. The claystone shows initially over a short period of time very fast water absorption; this can be explained by the information provided by its pore size distribution, that is, the range of pore sizes that allow water to access the open porosity (14.97%). The limestone shows long period of time with slow water absorption to access the ineffective porosity (0.75%).

The results values were obtained are 0.281% and 6.28% for limestone and claystone, respectively. Water absorption values increase in direct proportion with exposure to the temperature of natural stones. Temperature variation and water absorption are parallel characteristics of limestone and claystone samples. This feature, physically, enables to determine the cracks of natural stones.

F. Optical Detections

The exposure to high temperatures caused obvious cracks in both limestone and claystone samples (Fig. 6). Limestone samples were more susceptible for cracking than the claystone ones. By increasing the exposure temperature, the color of the samples became lighter. This phenomenon is highly due to losing moisture and the decomposition of materials at high temperatures.

Fig. 7 shows the limestone sample after exposure to a high temperature of 650°C. From the figure, the decomposition of calcite to free lime can be concluded.

Fig. 6. Cracks in Limestone (a) and Claystone (b) Generated due to High Temperature.

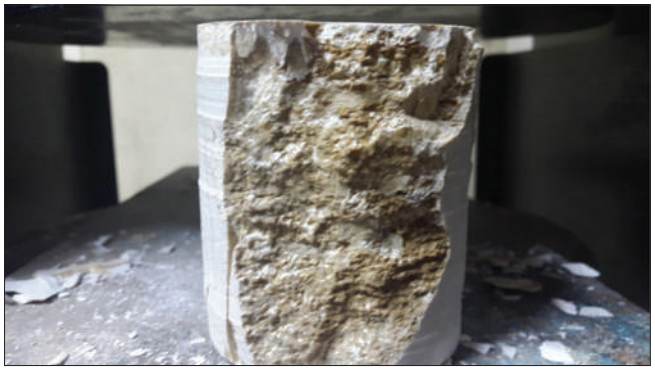

Fig. 7. Limestone Core Sample show Deformation due to Exposure to 650°C.

http://dx.doi.org/10.14500/aro.10283

V. Conclusions

The following conclusions can be drawn from this research:

1. Limestone loses up to 30% of its strength after exposure to high temperatures of 450°C and 650°C.
2. Claystone shows up to 40% strength increase after exposure to 450°C, whereas around 25% increase in strength was recorded after exposure to 650°C.
3. Exposure to high temperatures results in the occurrence of significant cracks and lightening in color for both limestone and claystone building units. Limestone is more susceptible for cracking than the claystone.
4. The strength reduction for limestone after exposure to 450°C is highly due to its low porosity which in turn leads in producing excessive builds up vapor pressure in the samples, whereas in the Claystone samples, the vapor pressure can be released attributable to the high porosity for the rocks.

References

American Society for Testing and Materials., 2014. D7012: 2014 *Standard Test Methods for Compressive Strength and Elastic Moduli of Intact Rock Core under Varying States of Stress and Temperatures.* ASTM, America.

Bell, F.G. and Lindsay, P., 1999. The petrographic and geomechanical properties of some sandstone from the newspaper member of the natal group near Durban. Engineering Geology, 53, pp. 57-81.

Boggs, S Jr., 2006. *Principles of Sedimentology and Stratigraphy, 4th ed.* Pearson Prentice Hall, New Jersey.

Buday, T. and Jassim, S., 1987. *The Regional Geology of Iraq, Vol. 2: Tectonism, Magmatism and Metamorphism*. Publication of GEOSURV, Baghdad.

Buday, T., 1980. *The Regional Geology of Iraq, Vol. 1: Stratigraphy and Paleontology*. Publication of GEOSURV, Baghdad.

Egger, A.E., 2006. *Rocks and Minerals*; *The Silicate Minerals Visionlearing, Vol. EAS-2 (9).* Post, Tweet, United States.

Gomez-Heras, M., McCabe, S., Smith, B.J. and Fort, R., 2009. Impacts of fire on stone-built heritage. Journal of Architecture and Conservation, 15(2), pp. 47-58.

Gomez-Heras, M., Alvarez de Buergo, M., Fort, R., Hajpal, M., Török, A. and Varas, M.J., 2006. Evolution of porosity in hungarian building stones after simulated burning. *International Conference on Heritage, Weathering and Conservation*. Madrid, pp.513-519.

Hajpál, M. and Török, Á., 2004. Mineralogical and colour changes of quartz sandstones by heat. Environmental Geology, 46(3-4), pp.311-322.

Hajpál, M., 2002. Changes in sandstones of historical monuments exposed to fire or high temperature. Fire Technology, 38, pp.373-382.

Jassim, S.Z. and Goff, J.C., 2006. *Geology of Iraq*. Dolin, Prague.

Koca, M.Y., Ozden, G., Yavuz, A.B., Kincal, C., Onargan, T. and Kucuk, K., 2006. Changes in the engineering properties of marble in fire-exposed columns. International Journal of Rock Mechanics and Mining Sciences, 43, pp.520-530.

Malaga-Starzec, K., Akesson, U., Lindqvist, J.E. and Schouenborg, B., 2006. Microscopic and macroscopic characterization of the porosity of marble as a function of temperature and impregnation. Construction and Building Materials, 20, pp.939-947.

Mohamad, E.T., Dan, M.F., Aziz, A.A., Maiye, O.M. and Liang, M., 2013. The effect of moisture content on the strength and anisotropy index of tropically weathered shale. Electronic Journal of Geotechnical Engineering, 18, pp.5967-5979.

Omer, H., 2009. *Primary Geotechnical Assessment of Haibat-Sultan Area and its Suitability for Proposed Tunnel Construction*, M.Sc., Koya University.

Ozguven, A. and Ozcelik, Y., 2013. Investigation of some property changes of natural building stones exposed to fire and high heat. Construction and Building Materials, 38, pp.813-821.

Sengun, N., 2014. Influence of thermal damage on the physical and mechanical properties of carbonate rocks. Arabian Journal of Geosciences, 7(12), pp.5543-5551.

Török, Á. and Hajpál, M., 2005. Effect of temperature changes on the mineralogy and physical properties of sandstones, a laboratory study. Restoration of Building and Monuments, 11(4), pp.211-218.

Yong, R.N. and Thomas, H.R., 1999. Geoenvironmental Engineering: Ground Contamination: Pollutant Management and Remediation. *British Geotechnical Society Geoenvironmental Engineering Conference*. Thomas Telford, London.

Youkhana, R. and Sissakian, V., 1986. Stratigraphy of shaqlawa-koisanjaq area. Journal of the Geological Society of Iraq, 19(3), pp.137-154.

Three-dimensional Image Segmentation using Tissue-like P System

Salah I. Yahya[1,2,3], Rafaa I. Yahya[3,4], Bisan Al-Salibi[3], Ghada K. Al-Khafaji[3,5] and Siti Mariyam Shamsuddin[3]

[1]Department of Software Engineering, Faculty of Engineering, Koya University, Danielle Mitterrand Boulevard, Koya KOY45, Kurdistan Region – F.R. Iraq

[2]Department of Computer Science and Engineering, School of Science and Engineering, University of Kurdistan Hewler, Erbil, Kurdistan Region – F.R. Iraq

[3]UTM Big Data Center, Ibnu Sina Institute for Scientific and Industrial Research, Universiti Teknologi Malaysia, UTM Skudai, Malaysia

[4]Department of Computer, Collage of Science, University of Al-Mustansiriyah, Baghdad, F.R. Iraq

[5]Department of Computer, College of Science, University of Baghdad, Baghdad, F.R. Iraq

***Abstract*– Membrane computing (MC), which abstracts computational models from the structure and functioning of biological cells or population of cells in tissues, has served as a rich framework for handling many problems. Various types of P systems have been proposed in the literature to perform edge-based and region-based segmentation of two-dimensional digital images. However, less attention has been paid to the segmentation of three-dimensional (3D) medical images. Hence, the main contribution of this paper is to propose a tissue-like P system for segmenting 3D medical images. To the best of our knowledge, this is the first work that practically adapts MC for 3D images. Experimental results demonstrate the efficiency of the proposed approach in segmenting 3D images, and it has the potential to be used in real-world applications.**

***Index Terms*–Membrane computing, Region-based image segmentation, Three-dimensional images, Tissue-like P systems.**

I. Introduction

Membrane computing (MC) has emerged as a recent branch of natural computing, which is mainly based on the assumption that the flow of metabolites within the compartmental architecture and functioning of biological cells can be interpreted as a flow of information for computations (Paun, 2002). The computational devices in MC are known as P systems in honor of their initiator, Paun and Rozenberg (2002). More importantly, P systems are massively parallel and distributed computing models processing multisets of objects based on predefined evolution rules in a nondeterministic manner. Due to the inherent parallelism, MC has the ability of solving NP-complete problems in polynomial or often in linear time and this feature has been shown extensively in the literature. The basic ingredients of a typical P system model consist of (1) membrane structure, (2) a set of evolution rules, and (3) multisets of objects. The main novelty of MC relies on the fact that membrane systems look at the whole cell as a computing device. They are defined as systems consisting of a hierarchical arrangement of membranes delimiting regions, which represent various compartments of a cell, and with each region having associated rules, which represent different biochemical processes taking place inside each compartment (Bernardini and Gheorghe, 2005). Basically, MC devices or P systems constitute three different models of computing devises depending on the particular features of the cell which are as follows: (1) Cell-like P systems (inspired from the structure of the cell), (2) tissue-like P systems (inspired from organization of cells in tissue), and (3) spiking neural-like membrane systems - inspired from the way neurons are linked in neural nets (Paun and Prez-Jimnez, 2006).

In this paper, tissue-like P system is used for segmentation of three-dimensional (3D) images. MC has applications in many fields including digital image analysis (Alsalibi, et al., 2015) and optimization (Alsalibi, et al., 2014; Alsalibi Venkat and Al-Betar, 2017).

This paper is organized as follows: The related work is presented in Section II. Section III provides a basic definition of tissue-like P system. Section IV describes the use of tssue-like P system for automatic region-based segmentation of 3D images as well as presents the methodology of segmentation with MC using P-lingua, and Section V concludes the paper and suggests some directions for the future work.

ARO-The Scientific Journal of Koya University
Volume V, No. 2(2017), Article ID: ARO.10316, 8 pages
DOI: 10.14500/aro.10316
Received 18 October 2017; Accepted 28 November 2017
Regular research paper: Published 08 December 2017
Corresponding author's e-mail: salah.ismaeel@koyauniversity.org

 http://dx.doi.org/10.14500/aro.10316

II. Related Work

The fundamental objective of digital image processing is to extract meaningful information from images without human assistance. Segmentation is an important task of image processing for satellite and medical images (Somasundaram and Alli, 2011). Technically speaking, in computer vision (Shapiro and Stockman, 2001), segmentation is the process of partitioning a digital image into multiple segments (sets of pixels), aiming to simplify or modify the representation of an image to be more expressive and easier to analyze and understand. Image segmentation is typically used to locate objects and boundaries (lines and curves) in images. More precisely, image segmentation is the process of assigning a label to every pixel in an image such that pixels with the same label share certain visual characteristics.

Recently, MC techniques have been used in solving problems arising from digital images. Image segmentation has been addressed extensively in the literature. For example, the authors (Christinal, et al., 2009; Yahya, et al., 2016) presented a tissue-like P systems to improve the standard edge-based segmentation method using MC rules. Christinal, et al. (2010) presented a MC rule framework to solve the threshold problem using cell-like P system, wherein the solution has been reached in linear time depending on the number of pixels of the input image. Similarly, Reina-Molina, et al. (2010) presented a new segmentation approach based on a tissue-like P system with the use of MC rules with multiple auxiliary cells for solving segmentation problem. Diaz-Pernil, Reina-Molina, and Carnero (2010) proposed a new software tool for performing a segmentation of two-dimensional (2D) digital images based on MC platform. However, they did not explain in detail the technical aspects of implementing the tool. The authors (Christinal, et al., 2011) developed a tissue-like P system (using MC rules) to design a region-based segmentation algorithm in a constant number of steps. In their approach, 4-adjacency relation between pixel's neighborhoods has been adopted for 2D digital images where 6-adjacency relation between voxel neighborhoods has been used for 3D digital images. Sheeba, et al. (2011) proposed a tissue-like P system algorithm to enhance morphological segmentation methods in medical image. Christinal, et al. (2012) proposed bio-inspired MC through tissue-like P system (MC rules) to perform a parallel color segmentation of images using a threshold method. Yang, et al. (2013) proposed a novel membrane algorithm (tissue-like P system) to develop region-based segmentation. Along with this line, Peng, et al. (2012) proposed a novel threshold segmentation approach using cell-like P system (membrane algorithm) to improve threshold segmentation. Daz-Pernil, et al. (2013) presented a novel device architecture called CUDATM to implement tissue-like P system MC rules for segmentation of images with gradient-based edge detection. Furthermore, Peng, et al. (2014) proposed a novel segmentation by adaptive traditional region-based color segmentation method using tissue-like P system (membrane algorithm). Isawasan, et al. (2014) developed a tissue-like P system using MC rules to segment hexagonal images, wherein the segmentation has been done in 7 steps. Peng, et al. (2014) proposed a novel method using cell-like P system (membrane algorithm) to solve the optimal multilevel thresholding problem. Yahya, et al. (2015) presented region-based segmentation with tissue-like P system rules that implement a simple artificial image with a more detailed illustration of how P system works furthermore, where different color relations have been explored to show the effect of color on the segmentation results. Interestingly, a new research line has been recently launched in which MC has been adopted to solve several problems relating to digital imagery. For example, region-based segmentation of 2D and 3D images have been investigated. However, the main drawback of their approach is that the image has been manually codified in the tissue simulator.

In the work of Christinal, et al. (2009), P systems have been linked to computational topology with digital images where this development paved way for a new and promising line of research. Christinal, et al. (2009) designed a collection of tissue-like P systems that used the communication rules of MC to perform edge-based segmentation. This communication entails the discovery of adequate different region boundaries among the input images. The experiment was conducted such that the artificial 2D and 3D images, using 4-adjacency and 26-adjacency, respectively, have been employed. Experiments show that results were obtained in a fixed number of 9 and 26 steps pertaining to 2D and 3D images, respectively. Furthermore, in the work of Christinal, et al. (2011), a tissue-like P system was proposed with the use of MC rules for the design of an edge-based segmentation algorithm in a constant number of steps. In their work, 4-adjacency relationships between neighboring pixels were adopted for 2D digital images. They proved that only 9 steps were sufficient to get an edge-based segmentation for a 2D image. In addition, 26-adjacency relationships between voxel neighborhoods were implemented for 3D digital images. They theoretically proved that 26 steps are required to get an edge-based segmentation for a 3D image. However, no practical examples have been provided. Meanwhile, the main weakness of their method is the fact that the image has been manually codified in the tissue simulator. This leads to a lack of efficiency in favor of expressiveness. For a comprehensive review of image segmentation using MC, interested readers are referred to Yahya, et al. (2017).

Thus, in this paper, we present a dynamic software using P-lingua for edge-based segmentation of 3D digital images based on the segmentation rules presented by Christinal, et al. (2011). Basically, edge-based segmentation is performed based on membrane computing and implemented in P-lingua with real medical images which are loaded automatically in the system. P-lingua is an official programing language for MC that offers a general syntactic framework that could define a unified standard for MC, covering a broad variety of models (Daz-Pernil, et al., 2009).

III. Tissue-like P System

Tissue-like P system was introduced by Martín-Vide, et al. (2003). The structure of tissue-like P system is organized as

a graph representing all the communication channels existing between interacting cells as can be seen in Fig 1. The set of interconnections is dynamic, and in the course of the evolution of the system, it can possibly change whosesoever a new communication way is established or another one is closed (Bianco, 2007). From the computational perspective, the essential characteristic of tissue-like P system is that membranes do not have electrical charges as in the cell-like P systems. Typically, the form of tissue-like P systems model with the input of degree q is a tuple.

$\Pi=(\Gamma, \Sigma, \varepsilon, W_1, \ldots, W_q, (R_1), \ldots, (R_q), i\Pi, o\Pi)$

Where

1. Γ is a finite alphabet, whose symbols are called objects;
2. $\Sigma \subset \Gamma$ is the input alphabet;
3. $\varepsilon \subseteq \Gamma$ is the list of objects in the environment, each one in arbitrarily infinite copies;
4. μ is the membrane structure;
5. M_i is a set of strings over Γ representing the multisets of objects associated with the membrane i, $1 \leq i \leq q$ at the initial configuration;
6. R_i is a finite set of communication rules of the following form: $(i, u/v, j)$, for $i, j \in \{0, 1, 2, \ldots, q\}$, $i = j$, $u, v \in \Gamma *$
7. $o\Pi \in \{0, 1, 2, \ldots, q\}$ refers to the output cell;
8. $i\Pi \in \{1, 2, \ldots, q\}$ refers to the input cell.

In the typical framework of MC, each cell is viewed as a computing unit working in a maximally parallel and nondeterministic way. The configuration is an instantaneous description of the P system at a particular moment, where a sequence of computation steps can be applied in a parallel manner to obtain a new configuration. A computation is said to be successful if it halts, reaching a specific configuration where no more rules can be applied to the current objects. With a halting computation, the associated output can be codified by the content of the output membrane.

IV. Tissue-like P System for Automatic Segmentation of 3D Images

Edge-based approaches rely on common patterns in intensity values within a cluster of neighboring pixels. The cluster is referred to as the region, and the goal of segmentation algorithm is to group regions according to their anatomical or functional roles (Siddiqui and Richhariya, 2013). The main aim of edge-based segmentation is to use image characteristics to map individual pixels in an input image to set of pixels called regions that might correspond to an object (Zhao, et al., 2008). Segmentation in digital imagery has several interesting features which makes it suitable for mechanisms inspired by nature. One of them is that it can be solved in a parallelized and localized manner. Regardless of how large is the picture, the segmentation process can be simultaneously performed in different local areas of the picture. Another interesting feature is that the basic required information can be easily encoded by different bioinspired representations.

In this paper, automatic edge-based segmentation will be applied to 3D images (.nrrd) rather than typical 2D (.png) images. To automatically load the images in the system, the segmentation rules will be written using P-lingua programing language. Furthermore, to deal with 3D images automatically, P- lingua will be linked to MATLAB to enable the processing of 3D images. P-LinguaCore4 library will be also integrated to handle P-lingua input files and check possible programing errors, both lexical/syntax and semantics (Frisco, et al., 2014). This library is used to implement MC with edge-based segmentation of 3D images.

Different from the 2D segmentation, in 3D segmentation, the input data will be voxels of the type C {i, j, k}, where c is the color of the voxel and i, j, and k are the three coordinates of that voxel. The edge-based segmentation of the 3D digital image problem can be formulated as follows: Given a digital 3D image with voxels of (possibly) different colors, obtain the boundaries of regions in that image. The solution of this problem can be described with several steps as follows:

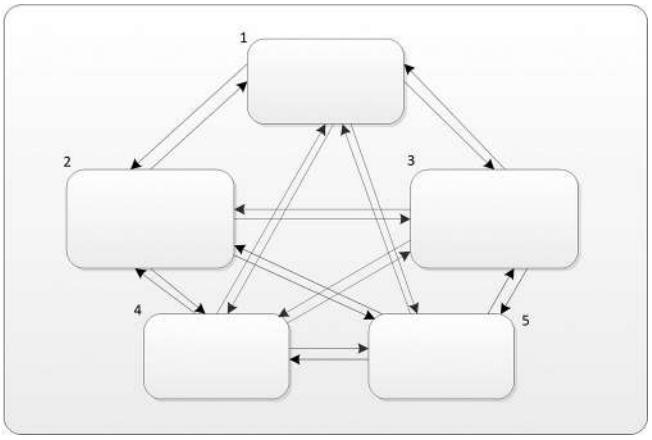

Fig. 1. The membrane structure of a tissue-like P system

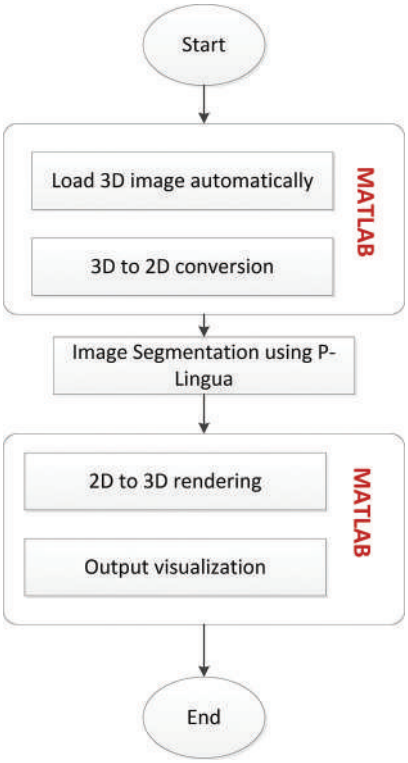

Fig. 2. Flowchart of three-dimensional image segmentation procedure

http://dx.doi.org/10.14500/aro.10316

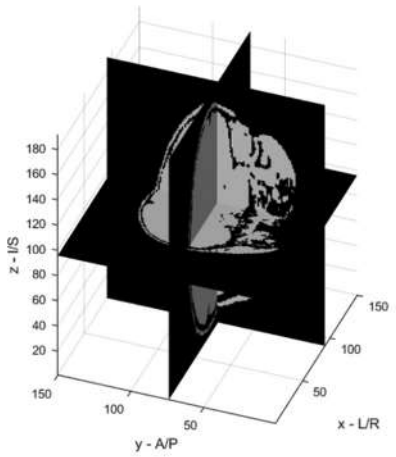

Fig. 3. Input three-dimensional (3D) image (3D slice)

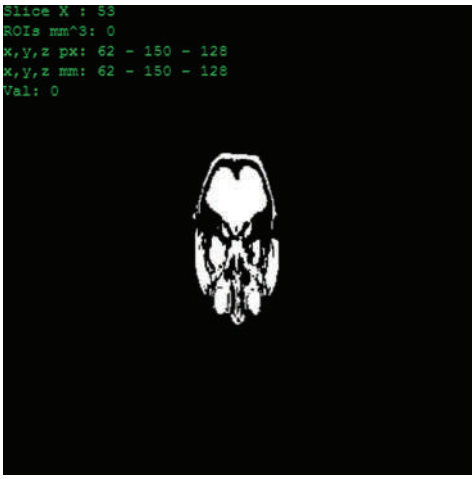

Fig. 4. Input three-dimensional image (horizontal slice)

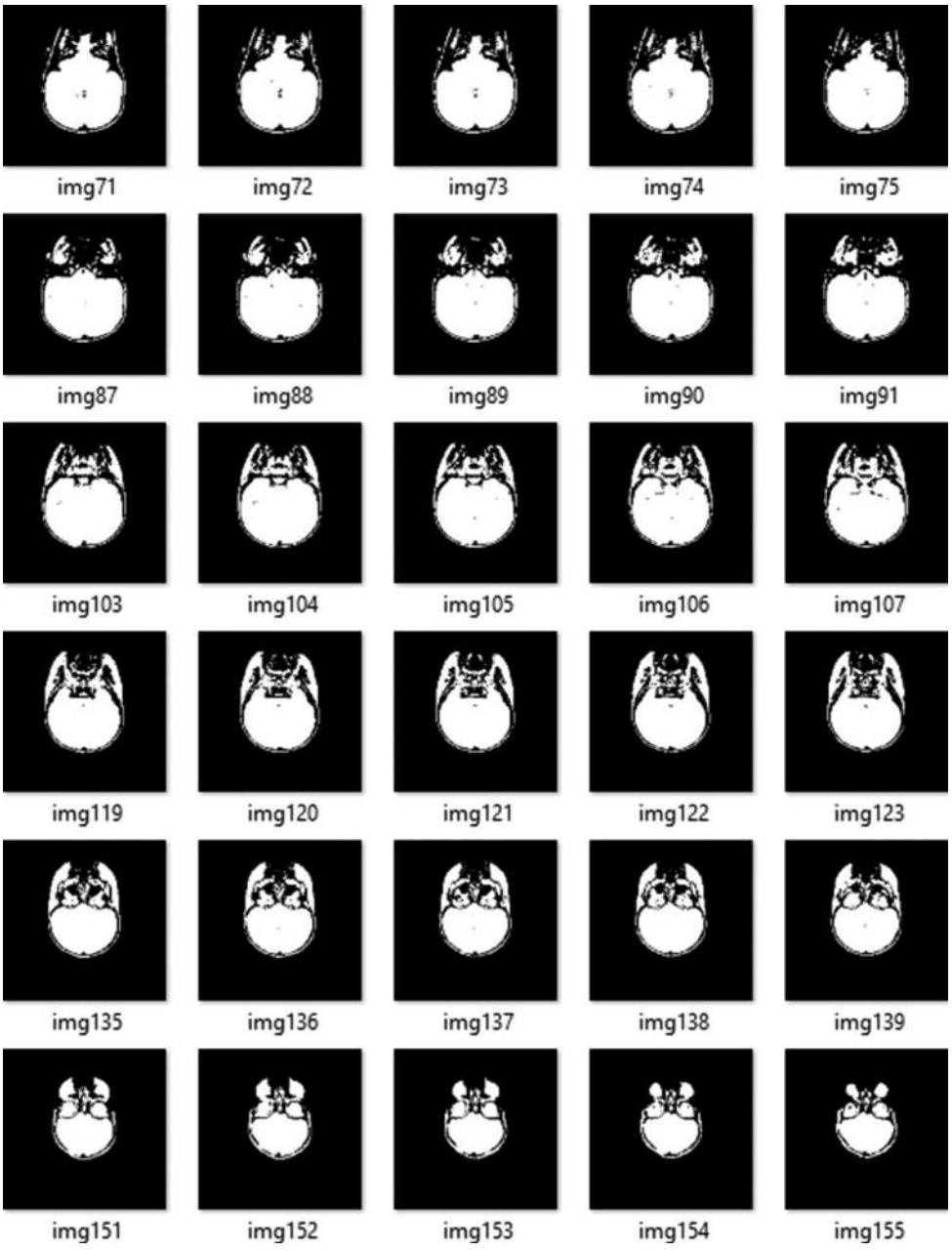

Fig. 5. Part of the obtained two-dimensional slices

- First marking voxels: Here, mark some of the voxels which belong to a boundary between two regions (border voxels).
- Second marking voxels: We add voxels adjacent to two edge voxels with the same color as them and adjacent to other voxel with a different color to the edge voxels.
- Output stage: The system sends to the environment all the marked voxels. This stage works in parallel to the previous steps.

Another procedure of solving the 3D image segmentation problem is to convert the 3D image into a set of 2D slices. In this case, the 3D segmentation problem will be simplified to the 2D segmentation case. After segmenting all the slices, it will be combined and rendered back to the 3D shape. This procedure will be illustrated in the following section.

A. Methodology of the Proposed Work

As mentioned previously, the tissue-like P system rules will be implemented sing P-lingua to segment the 3D images. Fig. 2 shows the steps of performing the segmentation using P-lingua and MATLAB software.

B. Load the 3D Image Automatically

In the first step of the work, the 3D image with type (.nrrd) will be automatically loaded and processed by MATLAB software using "NRRDREAD" function. Examples of the 3D input image are shown in Figs. 3, and 4. Fig. 3 represents the vertical slice of the combined 3D image.

C. 3D to 2D Conversion

Here, the MATLAB processes the 3D image using "NRRDREAD" command which reads the image volume

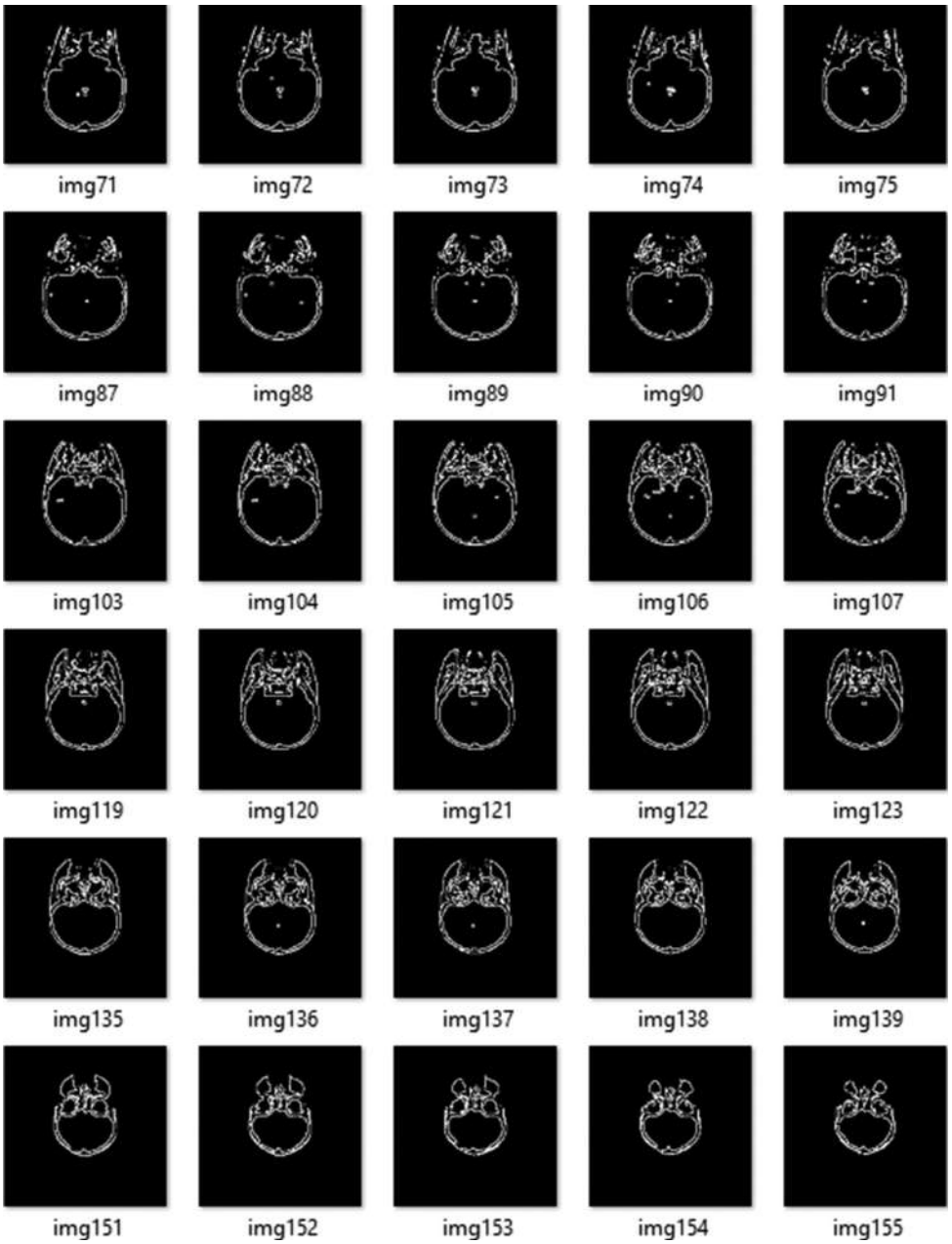

Fig. 6. Part of the segmented two-dimensional slices (edge-based segmentation)

 http://dx.doi.org/10.14500/aro.10316

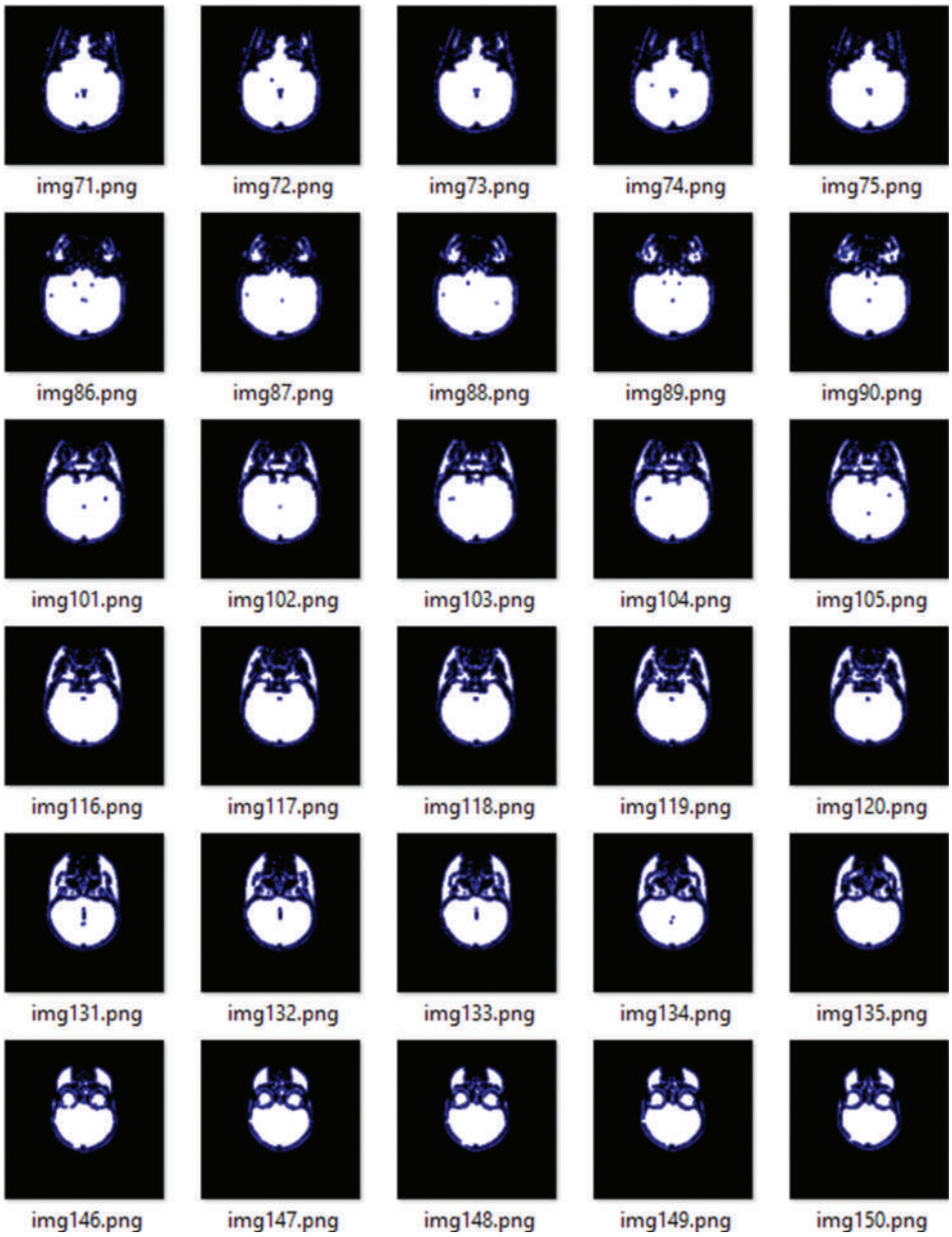

Fig. 7. Part of the obtained two-dimensional slices (region-based segmentation)

and its associated metadata from the NRRD-format file specified by the FILENAME. In this case, the 3D image will be converted into *m* 2D slices to simplify the segmentation process and to be able to use the P-lingua segmentation rules. Note that the number of slices *m* corresponds to the *z* dimension of the 3D image. The result of this step is shown in Fig. 5.

D. Image Segmentation using P-Lingua

Typically, in the standard P-Lingua syntax format, the pixels should have color and coordinates. Basically, the color and the coordinates of each pixel will be read and converted to P-lingua syntax. The standard syntax is to indicate the color of the pixel followed by curly brackets that contain the coordinate of the associated pixel, which in turn will be written into the.txt file. For example, in B{x,y}, x and y are the coordinates of the black pixel in the image, whereas in W{x,y}, x and y are the white pixel.

In this paper, the segmentation rules adopt the rules of MC used by Christinal, et al., 2011. The rules are written in the P-lingua format and saved in a text file. After loading the images, the images will be automatically codified as an input and concatenated to the rules file to the final form .PLI file. This file is now ready to be executed.

If the image contains two colors which are white and black, then if the four adjacencies are considered, the segmentation rules will be as follows:

$[W_{i,j}, B_{i,j}]1 \leftrightarrow [Wx_{i,j}, B_{i,j+1}]0$
$[W_{i,j}, B_{i,j-1}]1 \leftrightarrow [Wx_{i,j}, B_{i,j-1}]0$
$[W_{i,j}, B_{i+1,j}]1 \leftrightarrow [Wx_{i,j}, B_{i+1,j}]0$
$[W_{i,j}, B_{i-1,j}]1 \leftrightarrow [Wx_{i,j}, B_{i-1,j}]0$
$[Wx_{i,j}, W_{i,j+1}, Wx_{i+1,j+1}, B_{i+1,j}]1 \leftrightarrow [Wx_{i,j}, Wx_{i,j+1}, Wx_{i+1,j+1}, B_{i+1,j}]0$

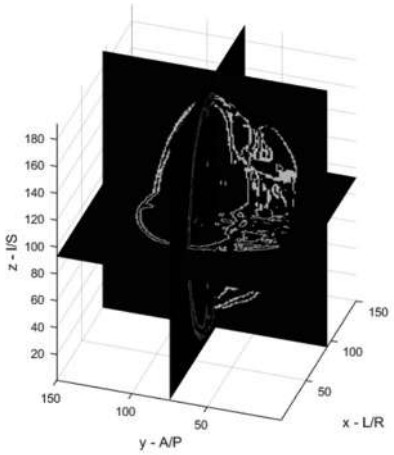

Fig. 8. The segmented three-dimensional image

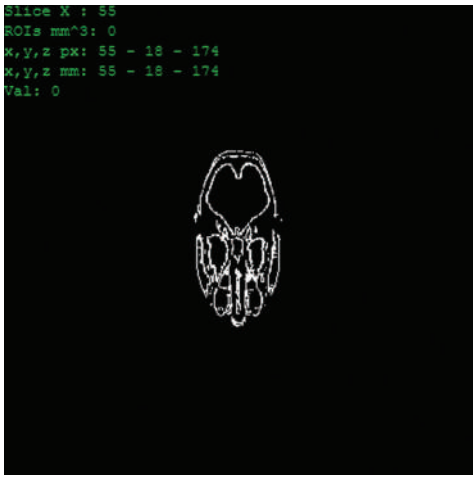

Fig. 9. Horizontal slice of the segmented three-dimensional images

$[Wx_{i,j}, W_{i\text{-}1,j}, Wx_{i\text{-}1,j+1}, B_{i,j+1}]1 \leftrightarrow [Wx_{i,j}, Wx_{i\text{-}1,j}, Wx_{i\text{-}1,j+1}, B_{i,j+1}]0$
$[Wx_{i,j}, W_{i,j+1}, Wx_{i\text{-}1,j+1}, B_{i\text{-}1,j}]1 \leftrightarrow [Wx_{i,j}, Wx_{i,j+1}, Wx_{i\text{-}1,j+1}, B_{i\text{-}1,j}]0$

Once the images have been segmented using MC into one of two cells, the output can be read from any of these cells as needed. There are two types of segmentation strategies regarding the philosophy of reading the output from a chosen cell. Cell one contains the input image that has had its boundary pixels sent to cell two so that it contains only the regions of the image. If the output is read from cell one, region-based segmentation is obtained. If the output is read from cell two, edge-based segmentation is obtained and visualized. Cell two contains the border and edge pixels.

The result of segmentation of the 2D slices is shown in Fig. 6 for edge-based segmentation and Fig. 7 for region-based segmentation.

E. 2D to 3D Rendering

To work with color images in P-Lingua, a relatively many rules will be required to test all possibilities of color relationships between pixels, which in turn will impose high computational overhead of the proposed approach and makes it impractical for real-time applications. To address this limitation, the color images will be converted into binary (black and white) images. The binarization will reduce not only the number of required rules but also the computational time required to achieve the segmentation.

Therefore, the input image will be converted into binary format with only black and white pixels to simplify the segmentation rules and speed up the execution. Binarization refers to the process in which each pixel in an image is converted into one bit with the value of one or zero depending on the specified threshold value of all pixels. If the pixel value is greater than the particular threshold value, then the pixel will be converted to one; otherwise, it will be zero. A binary image is a digital image with only two possible values for each pixel (black or white). In the proposed method, the average RGB value of each pixel is computed and then compared with the threshold value which is set to 128. If it is greater than the threshold, then the pixel will be converted to white; otherwise, it will be black.

Once all the 2D slices are being segmented using P-lingua, step-D, those images will be combined to form the segmented 3D image as shown in Figs. 8 and 9.

V. Conclusion

Segmentation has special characteristics which enables it to be suitable for methods of natural computing. However, for those techniques to be more effective and practical in real applications, a suitable software tool is of great importance. In this paper, MC software was presented as a tool for automatically segmenting 3D images using P-lingua programing language and MATLAB. The proposed software is able to deal with images of different sizes and has the potential of becoming a helping tool for dealing with large medical images. According to the literature of related work pertaining to image segmentation using MC, the majority of work has been focused on 2D images, but very less attention has been paid to 3D images. Hence, the contributions of the paper as can be summarized as follows: First, the input image has been codified automatically by linking P-lingua with the Java platform. Second, the proposed approach can deal with 3D images of different sizes. However, there are still some drawbacks of the proposed approach which need to be addressed thoroughly. One of the major limitations of our approach is that the proposed approach has been only simulated using a sequential architecture which in turn does not exploit the massive parallelism inherited in P systems. In our future work, to fully make use of the MC parallelism, a parallel architecture such as CUDA™ speedups over the serial implantation will be used to gain higher performance.

References

Alsalibi, B., Venkat, I., Subramanian, K.G., Lutfi, S. and Wilde, P.D., 2015. The impact of bio-inspired approaches towards the advancement of face recognition. ACM Computing Surveys, 48(1), p.5.

Alsalibi, B., Venkat, I., Subramanian, K.G. and Christinal, H.A., 2014. A Bio-Inspired Software for Homology Groups of 2d Digital Images. Asian Conference on Membrane Computing ACMC 2014, Coimbatore, pp.1-4.

Alsalibi B., Venkat I. and Al-Betar M., 2017. A membrane-ins*pired bat algorithm to recognize faces in unconstrained scenario*s. Engineering Applications of Artificial Intelligence, 64, pp.242-260.

Bianco, L., 2007. Membrane Models of Biological Systems, (Doctoral Dissertation, Ph.D. Thesis, University of Verona). In: Bernardini, F. and Gheorghe, M., editors. 2005. *Membrane Systems for Molecular Computing and Biological Modelling*. University of Sheffield. Ph.D. Thesis.

Christinal, H.A., Daz-Pernil, D. and Jurado, P.R., 2009. Segmentation in 2D and 3D image using tissue-like P system. *In:* Progress in Pattern Recognition, Image Analysis, Computer Vision, and Applications. Springer. Berlin, Heidelberg. pp.169-176.

Christinal, H.A., Daz-Pernil, D. and Real, P., 2011. Region-based segmentation of 2D and 3D images with tissue-like P systems. Pattern Recognition Letters, 32(16), pp.2206-2212.

Christinal, H.A., Diaz-Pernil, D., Gutierrez-Naranjo, M.A. and Perez-Jimenez, M.J., 2010. Thresholding of 2D images with cell-like P systems. Romanian Journal of Information Science and Technology (ROMJIST), 13(2), pp.131-140.

Christinal, H.A., Diaz-Pernil, D., Jurado, P.R. and Selvan, S.E., 2012. Color Segmentation of 2D images with thresholding. Ecofriendly Computing and Communication Systems, 305, pp.162-169.

Daz-Pernil, D., Berciano, A., Pena-Cantillana, F. and GutiRrez-Naranjo, M.A., 2013. Segmenting images with gradient-based edge detection using membrane computing. Pattern Recognition Letters, 34(8), pp.846-855.

Daz-Pernil, D., Perez-Hurtado, I., Perez-Jimenez, M.J. and Riscos-Nunez, A., 200*9. A P-lingua programming environment for* membrane computing. Membrane Comp[ut]ing, 5391, pp.187-203.

Diaz-Pernil, D., Reina-Molina, R. and Carnero, J., 2010. A bio-inspired software for segmenting digital images. In: Bio-Inspired Computing: Theories and Applications (BIC-TA). 2010 IEEE 5th International IEEE Conference.

Frisco, P., Gheorghe, M. and Prez-Jimnez, M.J., 2014. *Applications of Membrane Computing in Systems and Synthetic Biology.* Springer, Cham, Switzerland.

Isawasan, P., Venkat, I., Subramani, K., Khader, A., Oman, O. and Christinal, H., 2014. *Region-Based Segmentation of Hexagonal Digital Images using Membrane Computing.* 2014 Asian Conference on Membrane Computing (ACMC).

Martín-Vide, C., Paun, G., Paros, J. and Rodríguez-Patón, A., 2003. Tissue P systems. Theoretical Computer Science, 296(2), pp.295-326.

Paun, G., 2002. *Membrane Computing*. Springer, Heidelberg. pp.1-6.

Paun, G. and Prez-Jimnez, M.J., 2006. Membrane computing: Brief introduction, recent results and applications. Biosystems, 85(1), pp.11-22.

Paun, G. and Rozenberg, G. 2002. A guide to membrane computing. Theoretical Computer Science, 287(1), pp.73-100.

Peng, H., Wang, J. and Prez-Jimnez, M.J., 2014. Optimal multi-level thresholding with membrane computing. *Digital Signal Processing 37, pp.53-64.*

Peng, H., Yang, Y., Zhang, J., Huang, X. and Wang, J., 2012. Image thresholding with cell-like P systems. In: Proceedings of the 10th Brainstorming Week on Membrane Computing. University of Seville, Spain.

Peng, H., Yang, Y., Zhang, J., Huang, X. and Wang, J., 2014. A region-based color image segmentation method based on P systems. Romanian Journal of Information Science and Technology, 17(1), pp.63-75.

Reina-Molina, R., Carnero, J. and Diaz-Pernil, D., 2010. Image segmentation using tissue-like P systems with multiple auxiliary cells. Image-A, 1(3), pp.143-150.

Shapiro, L. and Stockman, G.C., 2001. *Computer Vision*. 1st ed. Prentice Hall, Pearson.

Sheeba, F., Thaburaj, R., Nagar, A.K. and Mammen, J.J., 2011. *Segmentation of Peripheral Blood Smear Images Using Tissue-Like P Systems*. Bio-Inspired Computing: Theories and Applications (BIC-TA), 2011 6th International Conference.

Siddiqui, F.K. and Richhariya, V., 2013. An efficient image segmentation approach through enhanced watershed algorithm. Computer Engineering and Intelligent Systems, 4(6), pp.1-7.

Somasundaram, P. and Alli, P., 2011. A review on recent research and implementation methodologies on medical image segmentation. Journal of Computer Science, 8(1), pp.170-174.

Yahya, R.I., Hasan, S., George, L.E. and Alsalibi, B. 2015. Membrane computing for 2D image segmentation. International Journal Advance Soft Computer Applications, 7(1), pp.35-50.

Yahya, R.I., Shamsuddin, S.M., Hasan, S. and Yahya, S.I., 2016. Tissue-like P system for segmentation of 2D hexagonal images. ARO-The Scientific Journal of Koya Un*iversity, 4(1), pp.35-42.*

*Yahya, R.I., Shamsuddi*n, S.M., Yahya, S.I., Hasan, S., Al-Salibi, B. and Al-Khafaji, G.H., 2017. Image segmentation using membrane computing: A literature survey. Bio-inspired Computing Theories and Applications. Vol. 681. Springer, China. pp.314-335.

Yang, Y., Peng, H., Jiang, Y., Huang, X. and Zhang, J., 2013. A Region-based image segmentation method under P systems. Journal Information Computer Science, 10(10), pp.2943-2950.

Zhao, Y., Liu, J., Li, H. and Li, G., 2008. Improved Watershed Algorithm for Dowels Image Segmentation. *In: Intelligent Control and Automation.* 7th World Congress on WCICA 2008.

General Information

Aro's Mission: Aro seeks to publish those papers that are most influential in their fields or across fields and that will significantly advance scientific understanding. Selected papers should present novel and broadly important data, syntheses, or concepts. They should merit the recognition by the scientific community and general public provided by publication in Aro, beyond that provided by specialty journals.

We welcome submissions from all fields of natural science and technology, and from any source. We are committed to the prompt evaluation and publication of submitted papers. Aro is published biannually; selected papers are published online ahead of print.

Submission

Manuscripts should be submitted by the correspondent authors of the manuscript via the on-line submission page. Regardless of the source of the word-processing tool, only electronic Word (.doc, .docx, .rtf) files can be submitted on-line. There is no page limit. Only online submissions are accepted to facilitate rapid publication and minimize administrative costs. Submissions by any other one but the authors will not be accepted. The submitting author takes responsibility for the paper during submission and peer review. If for some technical reason submission through the email is not possible, the author can contact aro.journal@koyauniversity.org for support. Before submitting please check Aro's guide to authors thoroughly to avoid any delay in the review and publication process.

Authors are explicitly responsible for the language of their texts. Paper should be submitted in a well written in understandable English. Authors should not expect the editor or editorial board to rewrite their paper. Prior to submission, authors should have their paper proofread by a possible academic native speaker of English.

- Submit the Article with contact Information
- File name should be your article tittle
- Don't submit your article in multiple journal, we are taking only minimum time for review process. please don't waste our time
- Once the paper is accepted, it can't be withdrawn
- Please follow publication ethics and regulation
- Avoid plagiarism and copied material
- Strictly Follow Aro's Template

Terms of Submission

Papers must be submitted on the understanding that they have not been published elsewhere and are not currently under consideration by another journal or any other publisher. Aro accepts original articles with novel impacts only. Post conference papers are not accepted "as is", however, regular papers on the same topic but with a different title can be submitted. The new paper should contain significant improvements in terms of extended content, analysis, comparisons with popular methods, results, figures, comments, etc. Please do not forget that the publication of the same or similar material in Aro constitutes the grounds for filing of an (auto) plagiarism case.

The submitting author is responsible for ensuring that the article’s publication has been approved by all the other co-authors. It is also the authors’ responsibility to ensure that the articles emanating from a particular institution are submitted with the approval of the necessary institution. Only an acknowledgement from the editorial office officially establishes the date of receipt. Further correspondence and proofs will be sent to the author(s) before publication unless otherwise indicated. It is a condition of submission of a paper that the authors permit editing of the

paper for readability. All enquiries concerning the publication of accepted papers should be addressed to aro.journal@koyauniversity.org.

Peer Review

All manuscripts are subject to peer review and are expected to meet standards of academic excellence. Submissions will be considered by an editor and "if not rejected right away" by peer-reviewers, whose identities will remain anonymous to the authors.

Guide to Author

We welcome submissions from all fields of science and from any source. We are committed to the prompt evaluation and publication of submitted papers. Selected papers are published online ahead of print. Authors are encouraged to read the instructions below before submitting their manuscripts. This section arranged into an overview speedy guidelines below and more detailed at the bottom section of this page

Manuscript Preparation

Submitting your manuscript will be in two stages namely before final acceptance and after.

Stage one:

At the first stage manuscript needs to be prepared electronically and submitted online via the online submission page in a Word (.doc, .docx, .rtf) format of one column double-spaced page, Times New Roman font type, and 12 p font size. A pdf version of the submitted manuscript should be submitted too. All authors' names, affiliations, e-mail addresses, and mobile phone numbers should be typed on a cover page, indicating the correspondent author.

Stage two:

- File type: MS-Word version 2003 or later.
- Format: The preferred format of the manuscript two-column template with figures and captions included in the text. This template can be downloaded via the following link. Please follow instructions given in the template; http://aro.koyauniversity.org/about/submissions#onlineSubmissions
- Text: All text is in Times New Roman font. The main text is 10-point, abstract is 9-point font and tables, references and captions are 8-point font.
- Figures: Figures should be easily viewed on a computer screen.

Units of Measurement

Units of measurement should be presented simply and concisely using System International (SI) units.

Title and Authorship Information

The following information should be included;

- Paper title.
- Full author names.
- Affiliation.
- Email addresses.

Abstract

The manuscript should contain an abstract. The abstract should be self-contained and citation-free and should not exceed 200 words.

Introduction

This section should be succinct, with no subheadings.

Materials and Methods

This part should contain sufficient detail so that all procedures can be repeated. It can be divided into subsections if several methods are described.

Results and Discussion

This section may each be divided by subheadings or may be combined.

Conclusions

This should clearly explain the main conclusions of the work highlighting its importance and relevance.

Acknowledgements

All acknowledgements (if any) should be included at the very end of the paper before the references and may include supporting grants, presentations, and so forth.

References

References must be included in the manuscript and authors are responsible for the accuracy of references. Manuscripts without them will be returned. Aro is following Harvard System of Referencing. (Learn how to import and use Harvard Styling in your Microsoft Office by following this link: http://bibword.codeplex.com/releases/view/15852)

Preparation of Figures

Upon submission of an article, authors are supposed to include all figures and tables in the PDF file of the manuscript. Figures and tables should be embedded in the manuscript. Figures should be supplied in either vector art formats (Illustrator, EPS, WMF, FreeHand, CorelDraw, PowerPoint, Excel, etc.) or bitmap formats (Photoshop, TIFF, GIF, JPEG, etc.). Bitmap images should be of 300 dpi resolution at least unless the resolution is intentionally set to a lower level for scientific reasons. If a bitmap image has labels, the image and labels should be embedded in separate layers.

Preparation of Tables

Tables should be cited consecutively in the text. Every table must have a descriptive title and if numerical measurements are given, the units should be included in the column heading. Vertical rules should not be used.

Copyright

ARO Reviewer/Associate Editor Application Form

Aro is a scientific journal of Koya University (p-ISSN: 2410-9355, e-ISSN: 2307-549X) which aims to offer a novel contribution to the study of Science. The purpose of Aro is twofold: first, it will aim to become an ongoing forum for debate and discussion across the sciences and Engineering. We hope to advance our problem solving capacity and deepen our knowledge regarding a comprehensive range of collective actions. Second, Aro accepts the challenges brought about by multidisciplinary scientific areas and aspires to expand the community of academics who are able to learn from and help to produce advances in a variety of different disciplines.

The Journal is seeking reviewers who can provide constructive analysis of papers thus enhancing overall reputation of the Journal. If any expert is interested in participating of the review process, we highly encourage you to sign up as a reviewer for our Journal and help us improve our presence in domain of your expertise. Appropriate selection of reviewers who have expertise and interest in the domain relevant to each manuscript are essential elements that ensure a timely, productive peer review process. We require proficiency in English.

How to apply

To apply for becoming a reviewer of Aro, please submit the application form by following the link:
http://aro.koyauniversity.org/user/register
To apply for becoming a member of the Editorial Board of Aro, please submit the application form by following the link: http://aro.koyauniversity.org/pages/view/AEB

Both Associate Editor and Reviewers should specify their areas of research and expertise. Applicants must have a doctorate (or an equivalent degree), and if Master degree they need to have significant publishing experience. Please note that;

- You will need to write your full official name.
- Please provide an email which reflects your official name, such as nameOne.NameTwo@... , or your institute's official email.
- All data need to be written in English.

Note: For more information, kindly visit the following websites:

1. Aro.koyauniversity.org.
2. http://libweb.anglia.ac.uk/referencing/harvard.htm.
3. http://bibword.codeplex.com/releases/view/15852.

INDEXING


THOMSON REUTERS
Emerging Sources Citation Index
WEB OF SCIENCE™


Crossref


OCLC
WorldCat


PRESERVED IN
LOCKSS


INDEXED IN
DOAJ


Google
Scholar


SHERPA
RoMEO


ROAD
DIRECTORY
OF OPEN ACCESS
SCHOLARLY
RESOURCES


ResearchGATE
scientific network

ARO THE SCIENTIFIC JOURNAL OFFICE
KOYA UNIVERSITY PARK
DANIELLE MITTERRAND BOULEVARD
KOYA KOY45
KURDISTAN REGION - F.R. IRAQ

ONLINE-ISSN: 2307-549X
PRINT-ISSN: 2410-9355

ARO
The Scientific Journal of Koya University

KOYA UNIVERSITY

Koya University is a young University established in 2003 and it is located in the city of Koya (Koysinjaq), short distance to the East of regional capital city of Erbil (Arbil, Hewlêr) in Kurdistan Region of Iraq. It is on the foothills of beautiful High Mountain. Its campus has been carefully laid out to embrace the beautiful mountainous nature. The Koya University has a Faculty system which enhances the interactions between similar academic fields. Today, Koya University has four Faculties: Engineering, Science and Health, Humanity and Social Science, and Education in addition to the School of Medicine, which all consist of twenty-five scientific departments in different fields, such as Petroleum Engineering, Geotechnical Engineering, Software Engineering, Physics, Chemistry, Clinical Psychology, Social Science, Medical Microbiology and Sport Education.

ARO-The Scientific Journal of Koya University is a biannual journal of original scientific research, global news, and commentary in the areas of Science and Technology. ARO is a Peer-reviewed Open Access journal with CC BY-NC-SA 4.0 license. It provides immediate, worldwide and barrier-free access to the full text of research articles without requiring a subscription to the journal, and has no article processing charge (APC). ARO Journal seeks to publish those papers that are most influential in their fields or across fields and that will significantly advance scientific understanding. ARO Journal is a member of ROAD and Crossref agencies and has got ESCI, DOAJ seal, SHERPA/RoMEO deposit policy, and LOCKSS archiving policy.